UNIVERSITY OF CALGARY

Flow of Newtonian and non-Newtonian Fluids in Porous Media : The Viscous Fingering Instability

by

Brajesh Kumar Singh

A THESIS

SUBMITTED TO THE FACULTY OF GRADUATE STUDIES

IN PARTIAL FULFILMENT OF THE REQUIREMENTS FOR THE

DEGREE OF MASTER OF SCIENCE

DEPARTMENT OF CHEMICAL AND PETROLEUM ENGINEERING

CALGARY, ALBERTA

MARCH, 2000

ABSTRACT

In a porous medium, the viscous fingering is a phenomenon associated with displacement processes involving two fluids of different mobility ratios. The growth, pattern, and propagation of these fingers during the displacement process have a strong impact on the fractional recovery of the process. In some practical applications the fluids involved are non-Newtonian and can lead to interfacial dynamics that are different from those commonly observed in the case of Newtonian fluids.

The present study focuses on the effects of the shear-thinning character of the fluids on the stability of miscible displacements in a two-dimensional Hele-Shaw cell. To model the rheological behavior of the fluids, we used the Carreau model which involves two dimensionless parameters De and n. Three different combinations of Newtonian and non-Newtonian fluids have been considered: a Newtonian fluid displacing another Newtonian fluid, a non-Newtonian fluid displacing a Newtonian fluid, and a Newtonian fluid displacing a non-Newtonian fluid.

In this study we adopted an approach that combines linear stability analyses and nonlinear simulations. Linear stability analyses using the quasi-steady-state-approximation (QSSA) are performed to predict the growth rate of the perturbations in the flow. The resulting eigenvalue problems are solved numerically to obtain the complete spectrum of unstable wavenumbers. A parametric study is presented to investigate the effects of the rheological parameters on the stability of the displacement processes under consideration.

The Hartley transform based spectral method technique has been used tosimulate the non-linear evolution of the interfacial instability. The shear-rate dependent viscosity of the non-Newtonian fluids led to new interfacial dynamics and ramified pattern formations.

Apart from the fingering mechanisms observed in the case of a Newtonian displacement process, new fingering mechanisms such as side-branching, diagonal fingering, and trailing lobe detachment are reported in the case of a non-Newtonian fluid displacing a Newtonian fluid. The shear-thinning effects of the non-Newtonian fluids leading to the new viscous fingering patterns are investigated in detail in terms of the values of the dimensionless parameters De and n.

A study of the mixing length of the displacement process which gives a good idea of the front advancement and the broadening of the mixing zone, is also presented.

ACKNOWLEDGEMENTS

I take this opportunity to express my gratitude, regards and sincere thanks to my thesis supervisor Dr. Jalel Azaiez for his able guidance and support throughout the course of this work.

I would also like to express my sincere thanks to my course instructors : Dr. Ayodeji Aderopo Jeje, Dr. Caroline Hyndmann, and Dr. Celine Bellehumeur for their valuable guidance and help during my course work here.

I would like to thank secretaries of the Dept. of Chemical & Petroleum Engineering for their help, cooperation and good humor.

I am very much indebted to all of my fellow graduate students for their help and making my stay here enjoyable.

Brajesh Kumar Singh

March, 2000
University of Calgary.

CONTENTS

LIST OF FIGURES

NOMENCLATURE

A	Aspect ratio
b	Hele-Shaw thickness
c	Concentration
D	Dispersion coefficient
De	Parameter similar to Deborah number
g	Acceleration due to gravity
k	Permeability
k_x, k_y	Wavenumbers in x and y direction
L	Hele-Shaw length
M	Mobility ratio
n	Power-law index
N_x, N_y	Grid size in x and y direction
p	Pressure
Pe	Peclet number
Q	Volumetric flow rate
R	Log of viscosity ratio
t	Time
t_0	Base state time
u	Macroscopic velocity vector
U	Uniform displacing velocity
W	Hele-Shaw width
σ	Growth rate of disturbances
μ	Viscosity
μ_0	Zero shear viscosity
ω	Vorticity

ψ Streamfunction

$\dot{\gamma}$ Shear rate

δ Magnitude of disturbances

CHAPTER 1

INTRODUCTION

1.1 General

The flow of non-Newtonian fluids through porous media has become increasingly important because of its major application in Enhanced Oil Recovery (For a review of some of the early developments in this area see Homsy 1987). In this field, both experiment and theory have undergone a rapid development in the recent years. The sweep efficiency, which is defined as "the fraction of reservoir area contacted by a displacing fluid to the reservoir area behind the displacement front", is restricted by an interfacial instability phenomenon termed *viscous fingering*. This occurs when a less viscous fluid displaces a more viscous fluid, and has many important applications in secondary and tertiary oil recovery, filtration, hydrology, and fixed bed regeneration. Both Newtonian and non-Newtonian fluids may be involved in these processes.

The flow of Newtonian fluids through porous media has been extensively studied and there is a great wealth of experimental and numerical work on this topic which started in early 1960. On the other hand the flow of non-Newtonian fluids in porous media did not receive as much attention as their Newtonian counterparts, even though this type of flow is of increasing interest to scientists and engineers as the use of polymeric materials grows. Polymer solutions, which are non-Newtonian fluids, are used in the form of emulsions, foams, gels etc., to improve the oil recovery. Consequently, there is a need for the adequate understanding of the rheological effects of non-Newtonian fluids in oil displacement mechanisms.

Beside the practical application, the flow of non-Newtonian fluids in porous media is a subject of fluid mechanics of intrinsic fundamental interest. An understanding of the physics of the flow of non-Newtonian fluids in porous media may reveal to be helpful in improving our current understanding of the flow instability in Newtonian displacements.

Instability and viscous fingering are associated with both miscible and immiscible displacements. In the case of immiscible displacements, capillary forces at interface between oil and water prohibit the complete recovery of oil from a reservoir. Eliminating the capillary forces by injecting large amounts of an inexpensive displacing material that is miscible with the oil promises to achieve high recovery [Zimmerman and Homsy, 1991]. The efficiency of miscible displacements is greatly determined by the amount of instability between displacing and displaced fluids.

It has been shown [Pascal, 1992] that non-Newtonian displacing fluids of shear thinning behavior may eliminate the viscous fingering effect. Many experimental and theoretical investigations have been conducted to determine rheological models, or correlation of apparent viscosity with flow properties for a given non-Newtonian fluid [Abou-Kassem et al., 1995]. Shear-thinning non-Newtonian fluids are characterized by the fact that their viscosity is a decreasing function of the shear rate. However, it is practically impossible to determine the distribution of the shear rate in a microscopic sense within a porous medium, and the rheological models developed in fluid mechanics for non-Newtonian fluids cannot be easily applied to porous media. In this work, an average shear rate based on the average or macroscopic flow velocity, is used to characterize the non-Newtonian flow behavior. We address the problem of the rheological implications of the shear-thinning nature of the displacing and displaced fluids on the oil displacement mechanisms in a rectilinear Hele-Shaw cell. We will also limit the study to the case of miscible displacements, where the instability is driven by the viscosity contrast. In miscible displacements, unlike immiscible displacements, there is no interface and hence a single-phase Darcy's law holds throughout the domain.

For Newtonian fluids the viscosity variation results from variations in the concentration of a chemical component in the fluid, while in the case of non-Newtonian fluids the viscosity is a function of concentration and shear rate. This feature of shear rate dependent viscosity, is responsible for the large difference between the Newtonian and non-Newtonian fluid dynamics.

In what follows, we give brief definitions of the common terms associated with the flow through porous media, that we will be using in this study :

- **Porosity**

Porosity, is a measure of the pore space and is defined as the ratio of pore volume to the total volume of a given sample of material. This is also known as the 'total' porosity of a porous media. There is another term called 'effective' porosity, which refers only to that part of the pore space which is available to fluid flow. There are several methods available in literature for the measurement of both the total and the effective porosity of a porous medium [see M. Muskat, 1947].

- **Permeability**

Permeability is a measure of the ease with which fluids pass through a porous medium. It is a property of the medium, and is independent of the density and viscosity of the fluid. The permeability k, appears in Darcy's law relating the pressure drop to the flow rate :

$$\frac{\partial p}{\partial x} = -\frac{\mu}{k}\frac{Q}{A}, \tag{1.1}$$

where Q is the volume of fluid discharged per unit time through a cross section area A, μ is the viscosity of the fluid, and $\partial p/\partial x$ is the pressure gradient in the direction of the flow.

A natural material is commonly assumed to be homogeneous and isotropic with respect to permeability, and most of the analytical work with single-phase flow of fluids universally assume that permeability is constant with respect to time [Roger et al., 1969].

- **Mobility**

There is theoretical and experimental evidence for the occurrence of macroscopic instabilities in the displacement of one viscous fluid by another through a porous medium. This frontal instability is strongly dependent on the mobility ratio, MR. The mobility of a fluid in a porous media is defined as the ratio of the permeability of the media to the fluid viscosity :

$$M = \frac{k}{\mu}. \tag{1.2}$$

The mobility ratio for two fluids is defined as :

$$MR = \frac{M_2}{M_1} = \frac{(k/\mu)_2}{(k/\mu)_1}, \tag{1.3}$$

where subscripts 1 and 2 refer to the displacing and displaced fluid respectively.

If the mobility ratio is unity or less than one, the displacement is stable and the sweep efficiency is maximum. On the other hand, when the mobility ratio is greater than one, the more mobile displacing fluid will finger through the less mobile displaced one making the flow unstable. The mobility ratio can be improved by the use of high viscosity polymer solutions as displacing fluids. Thus the use of low mobility polymer solutions, which are non-Newtonian fluids, may increase the displacement efficiency in reservoirs [Savins, 1969].

1.2 Hele-Shaw Flows

Considering the complexity of the flow through porous media, researchers have tended to study this type of flow instability in simpler, somewhat more idealized model systems such as the Hele-Shaw cell. The Hele-Shaw model is an analogue of the porous medium, and is used extensively to study and describe the two-dimensional features of the flow, *depth-averaged* over the thickness.

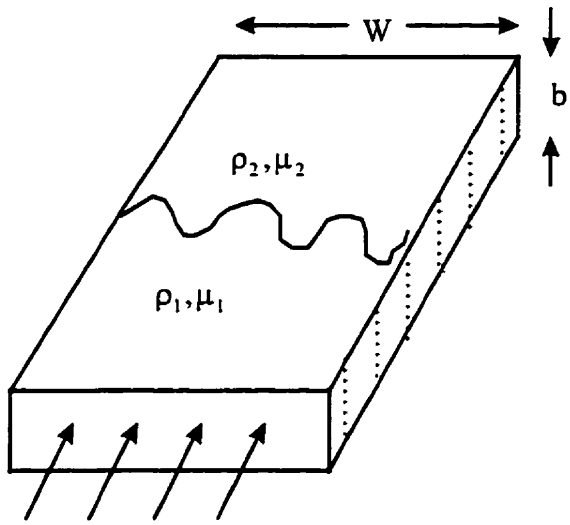

Fig. 1.1 Schematic of a Hele-Shaw flow.

The dimensions are as shown in the Fig. 1.1, where b represents the thickness of the cell and W its width. The flow takes place through the small gap b, with a depth averaged velocity U. Then the two-dimensional governing equations are the continuity equation and Darcy's law :

$$\nabla \cdot \bar{\mathbf{u}} = 0, \tag{1.4}$$

$$\nabla \cdot \bar{p} = -\frac{\mu}{b^2/12}\bar{\mathbf{u}} + \rho \mathbf{g}, \tag{1.5}$$

where $\bar{\mathbf{u}}$ is the macroscopic velocity vector, and $\bar{p}$ is the macroscopic pressure. This flow satisfies Darcy's law equation (1.5) with an equivalent permeability of $b^2/12$, and is valid in the limit of low-Reynolds-number flow, and $b/W \to 0$. Thus, the Hele-Shaw flow

is analogous to a two-dimensional incompressible flow in porous media. The Hele-Shaw flow is of fundamental interest and can be very useful in studying various aspects of flow through a porous medium.

1.3 Mechanisms of Viscous Fingering

Consider a miscible displacement in a homogeneous porous medium, characterized by a constant permeability k. This flow can be modeled by a Hele-Shaw flow as shown in Fig. 1.1. The flow involves the displacement of a fluid of viscosity μ_2 and density ρ_2 by a second fluid of viscosity μ_1 and density ρ_1. It is the variation of these properties across the front that leads to the development of the instability [Homsy, 1987].

The following reasoning is made in order to understand the mechanism of instability. From Fig. 1.1 the pressure force $(p_1 - p_2)$ on the displaced fluid as a result of a displacement δx of the interface from equation (1.5) is :

$$(p_1 - p_2) = \left[(\mu_2 - \mu_1)U / k + (\rho_1 - \rho_2)g\right]\delta x . \qquad (1.6)$$

If the net pressure force is positive, any small displacement will amplify leading to an instability. Thus, a combination of unfavorable density and/or viscosity ratios can make the flow unstable. Depending upon the signs of viscosity difference ($\Delta\mu$), and density difference ($\Delta\rho$) one can be either stabilizing or destabilizing. For example, consider a downward vertical displacement of a dense, viscous fluid by a lighter, less viscous one. Which means we have :

$$(\mu_2 - \mu_1) > 0, \text{ and } (\rho_1 - \rho_2) < 0,$$

in this case the viscosity is destabilizing, while the gravity force is stabilizing, leading to a critical velocity above which the flow is unstable :

$$u_c = (\rho_2 - \rho_1)gk/(\mu_2 - \mu_1). \qquad (1.7)$$

In this work we have considered a two-dimensional horizontal displacement, where gravity force is absent and the instability is driven by the viscosity contrast only.

1.4 Proposed Objectives

In this work, the instability of miscible displacements in porous media is considered. The aim of this work is to study the instability for both Newtonian and non-Newtonian fluids by modeling this process and conducting numerical simulations. This work was taken up with the following objectives :

1. To derive a mathematical model of the process for the following cases :
   - a non-Newtonian fluid displacing a Newtonian fluid,
   - a Newtonian fluid displacing a non-Newtonian fluid.
2. Carry out a linear stability analysis of this problem for the different combinations of the fluids mentioned above.
3. Develop a numerical scheme based on a combination of *spectral* and *finite difference* methods, and conduct nonlinear numerical simulations of the problem.
4. Study and compare the initial growth rate obtained from the linear stability for the different cases under consideration.
5. Study the results and analyze the fingering patterns to explain the effects of shear-thinning on the instability.
6. Compare the results with other numerical studies as well as with available experimental observations.

1.5 Outline of this work

In chapter 2 a comprehensive review of the literature on fluid flow through porous media is given. This includes both simulation and experimental studies. The Literature review is divided into three major sections. The first section deals with the results of previous experimental studies, while the second section is devoted to linear stability analysis. The

third section covers nonlinear simulations. Both miscible and immiscible displacements have been covered in all the three sections, however more emphasis has been put on miscible displacements.

In chapter 3, a brief introduction of the generalized Newtonian model is given and the equation for the shear-thinning Carreau model is presented. A detailed mathematical formulation of the problem along with the appropriate boundary and initial conditions is given, followed by the proper scaling of the problem. The governing equations and their development are presented for the three different types of displacements - (a) Newtonian fluid displacing Newtonian fluid (b) Non-Newtonian fluid displacing Newtonian fluid, and (c) Newtonian fluid displacing non-Newtonian fluid.

Chapter 4 is devoted to the linear stability analysis of the problem. The details of the derivation of the linearized equations are given for the three cases under consideration, followed by a description of the numerical method used to solve the eigenvalue problems. Stability characteristics are presented and discussed in terms of the effects of the different parameters on the flow instability.

Chapter 5 contains the description of the numerical technique used for the simulation of nonlinear viscous fingering in miscible displacements. A brief review of the Fourier and Hartley transforms is given followed by the numerical algorithm used. The nonlinear simulation results, their discussion and comparison are presented. A detailed description of the different types of mechanisms, their physical interpretation, and new mechanisms observed is presented.

Finally, in chapter 6 we summarize the major conclusions of this study and give recommendations for future work.

CHAPTER 2

LITERATURE REVIEW

In this chapter, a detailed discussion of the previous studies related to displacements in porous media is presented. Major topics include, linear stability analysis, non-linear simulations, and experimental studies. Both miscible and immiscible displacements involving Newtonian and non-Newtonian fluids have been covered. A chronological analysis of these studies reveals that the 1960s saw a growing deal of interest among scientists and engineers in this problem. This interest was in part triggered by the potential for application in Enhanced Oil Recovery (EOR) projects foreseen during this period. A very comprehensive review of the published literature dealing with fluid displacement processes is given by Homsy (1987). This covers most of the early work in linear stability analysis, non-linear simulations, and experiments for both miscible and immiscible displacements.

2.1 Experimental work

In this section, a review of the experimental studies dealing with both miscible and immiscible displacements of Newtonian and non-Newtonian fluids is given.

2.1.1 Newtonian fluids

Viscous fingering of miscible Newtonian fluids was first addressed by Hill (1952). Based on experimental observations, he qualitatively explained the instability by the difference of the driving pressure of a small perturbation at the interface. Slobod & Caudle (1952) used the X-ray shadowgraph technique to measure the sweep efficiency. The X-ray shadowgraph plates showed the fingering patterns during the displacements conducted at

different viscosity ratios. These patterns were reported to be affected by the displacement velocity and the viscosity ratios. Van Meurs (1957), used visual observation techniques to study the mechanism of flow processes in a three dimensional transparent model.

Saffman and Taylor (1958) studied the stability of an interface between two immiscible fluids. These authors conducted experiments in a Hele-Shaw cell using an air-glycerin system and presented the results in the form of nonlinear fingers. They characterized the instability in terms of a parameter λ, defined as the ratio of the width of finger to the spacing of fingers. Blackwell et al. (1959) studied miscible displacements by performing a number of experiments in porous media. In this work, the authors focused on the effects of the mobility ratio and the system geometry on the displacement efficiency. From the results of his experiments, Habermann (1960) concluded that it is viscous fingering rather than reservoir heterogeneity that controls the miscible displacements. Benham et al. (1963) used aluminium sulphate solution to displace an aqueous glycerine solution in their experiments to observe the factors that affect the fingering behavior.

Slobod and Thomas (1963) carried out experimental studies of fingering in porous media and reported the effects of the rate of displacement and mobility ratio on the size and shape of the fingers. They used the X-ray absorption technique to visualize fingering patterns in porous media. Perkins et al. (1965) used the same technique and concluded that the fingers spread and change their lateral scales with time. In the case of immiscible displacements, Perkins & Johnston (1969) showed from their packed bed experiments that immiscible dispersion coefficients are proportional to the interstitial velocity and the product of the bead diameter and inhomogeneity factor. Wooding (1969) performed experiments in Hele-Shaw cell, and studied gravity-driven fingering. His results showed similar fingering patterns to those reported by Slobod and Thomas (1963). Sarma (1986) carried out experimental study of the viscous fingering in miscible displacements in a porous medium as a function of different parameters. Fingering patterns of cyclohexane displacing glycerol solution are shown in Fig. 2.2.

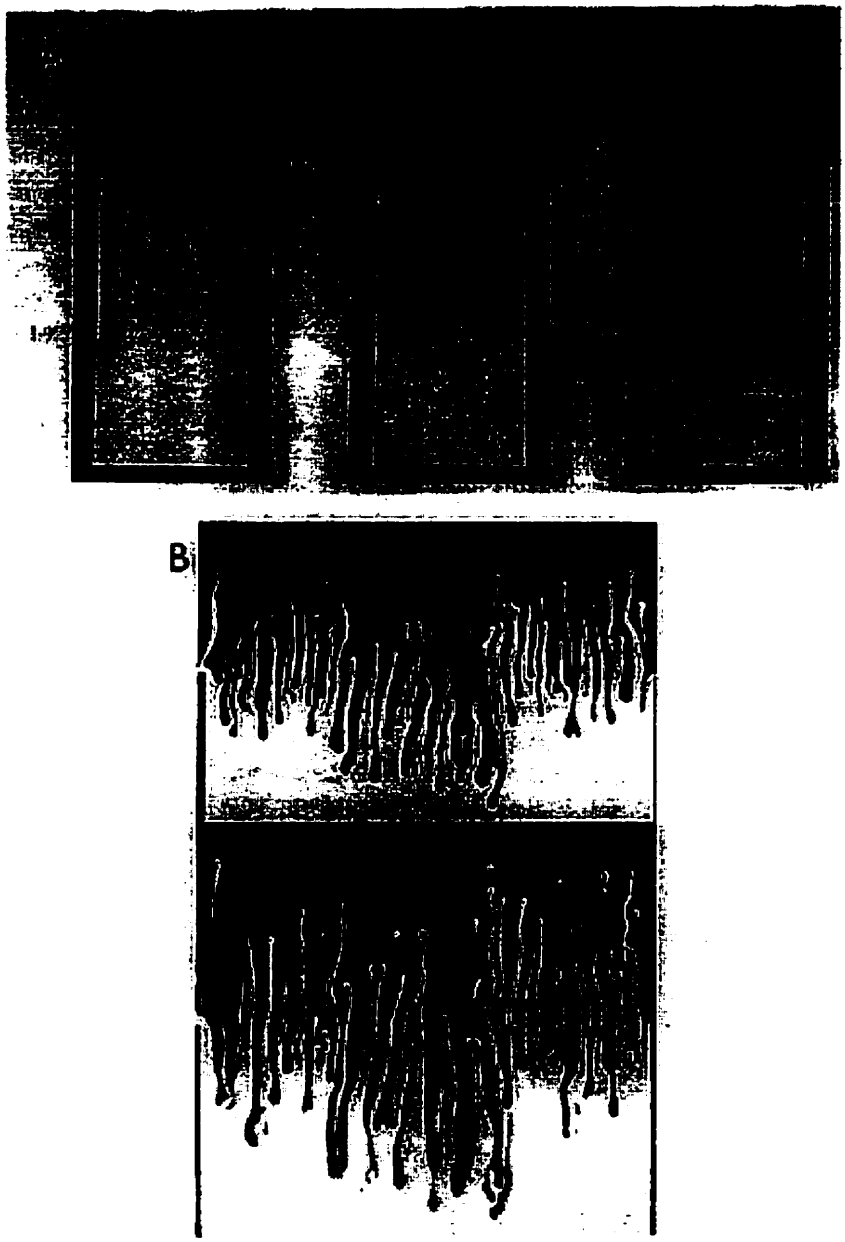

Fig.2.1 Experimental observations of fingering in gravity-driven miscible displacements in Hele-Shaw cell (Wooding, 1969). (A) nonlinear fingering at moderate Peclet number, (B) tip splitting at high Peclet number. Different frames represent time sequence.

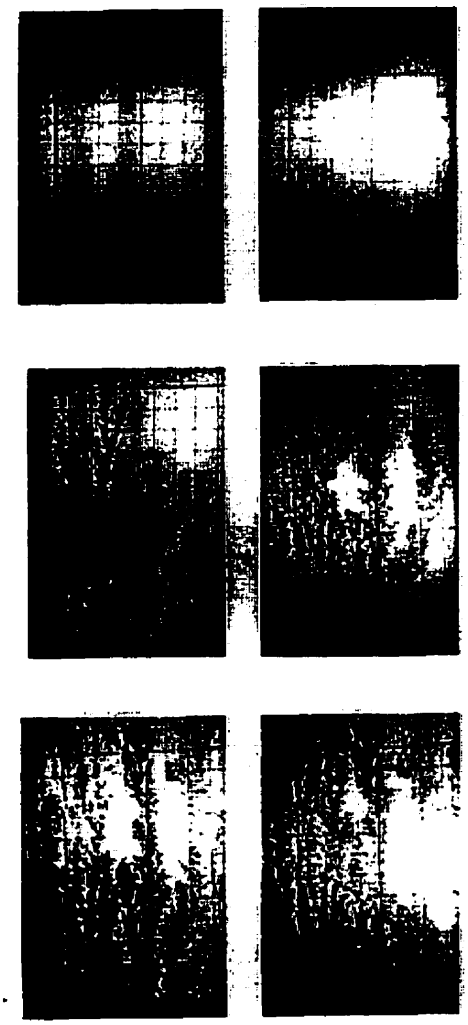

Fig.2.2 Experimental observations of viscous fingering due to viscosity contrast in a miscible displacement. Cyclohexane displacing glycerol solution (Sarma, Powder Tech. 48, 1986).

(i)

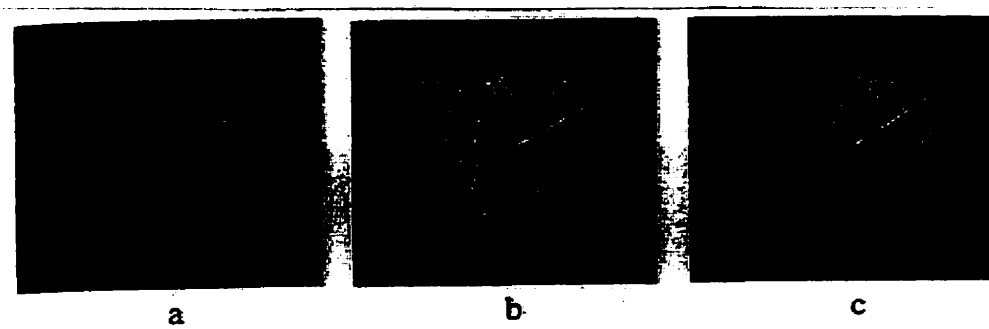

(ii)

Fig.2.3 Experimental observations of viscous fingering patterns in a radial Hele-Shaw cell (Kawaguchi et al., Physica D 105, 1997).

(i) Air displacing Glycerol solution; (ii) Air displacing hydroxypropyl methyl cellulose (HPMC) solution.

2.1.2 Non-Newtonian fluids

Marshall et al. (1967) & Dauben et al. (1967) conducted experiments to study the flow of viscoelastic fluids in packed beds. Lee et al. (1968) concluded from their experiments using pseudoplastic fluids in a Hele-Shaw model that the shear-thinning displacing fluids cause more instability than Newtonian displacing fluids of comparable viscosity. However, in general polymers are more viscous than Newtonian fluids which can decrease the mobility ratio substantially and thus decrease the instability [Savins, 1969].

Several experimental studies have been performed in Hele-Shaw cell to understand the drastic change in fingering patterns from Newtonian to non-Newtonian fluids. Daccord et al. (1985, 1986) were the first to perform fingering experiments of polymer solutions in axial and radial Hele-Shaw cells. In these experiments, the displacement of a non-Newtonian fluid by a Newtonian fluid was considered, and the authors observed very ramified fingering patterns. It was observed that the fingering pattern which develops at the interface, branches repeatedly in a manner which suggests the growth of a fractal. They also concluded that shear-thinning fluids show more tendency for growth on the tips of the fingers than in the bulk. Allen and Boger (1988) presented the results of experiments conducted in a Hele-Shaw cell for different types of fluid : Newtonian, shear-thinning, and ideal elastic. They concluded that shear-thinning fluids exhibit increased interfacial instability, and the fingering patterns are totally different from those of Newtonian fluids at the same flow conditions. However, elastic properties have a negligible effect on the macroscopic development of viscous fingers.

Smith et al. (1992) performed experiments in radial Hele-Shaw cell using solutions of polystyrene in dioctyl phthalate as the non-Newtonian fluid, and observed the onset of instability earlier than in the case of Newtonian fluids. Bonn et al. (1995), performed viscous fingering experiments in a Hele-Shaw cell for immiscible displacements and studied the finger width as a function of the finger tip velocity. In this study they

considered two cases : surfactants system, and polymers system. In the latter case, a shear-thinning polymer solution was taken as the displaced fluid and compressed air as the displacing fluid. For low velocities, narrow, pointed fingers are formed, while for higher velocities blunt and wider fingers were observed. The effects of surface tension on the finger form was studied by adding the surfactants. Comparing with the results for the polymers, they concluded that a local change in surface tension does not alter the finger form considerably.

Recently, Kawaguchi et al. (1997) compared the fingering patterns in polymer and Newtonian solutions by performing radial Hele-Shaw experiments. Aqueous solutions of hydroxypropyl methyl cellulose (HPMC) was used as a non-Newtonian fluid and aqueous solutions of glycerol as a Newtonian fluid. In the case of air displacing Newtonian glycerol solution, uniform fingers with tip splitting were observed, while the case of air displacing HPMC solution exhibited a morphological transition of highly branched pattern with multiple tip splitting.

2.2 Linear stability analysis

This linear stability analysis section is again divided into two subsections dealing with Newtonian displacements and displacements involving non-Newtonian fluids.

2.2.1 Newtonian fluids

The linear stability analysis of viscous fingering was first studied by Chouke et al. (1959). These authors carried out an analytical study based on a linear perturbation analysis of the fingering phenomenon for immiscible liquid-liquid displacements in porous media. They used a piston-like displacement model for which they presented a solution to predict the dynamic response to a perturbation of the displacing fluid front. By including the effects of surface tension at the interface, they reported a cutoff and a most dangerous

wavenumber of the instability. They also performed experiments in a Hele-Shaw model consisting of two parallel plates spaced a short distance apart. Their theoretical results and experimental findings for displacements in Hele-Shaw models were found to be in agreement.

In a subsequent study, Perrine (1961) stated that the effect of diffusion must be considered for miscible displacements, later it was found out by Tan & Homsy (1986) that his solution of the linear stability equations was erroneous. Wooding (1962) attempted to treat the stability of a time-dependent base state for gravity driven instabilities. He considered the problem as an initial value problem and expressed the growth rate of disturbances into Hermite polynomials. By analyzing a one-term truncation, he concluded that corresponding to the dispersive widening of the concentration profile, the cutoff wavelength shifts with time to larger values. Ultimately all disturbances must decay if dispersion is given an infinite time to act.

Schowalter (1965) carried out the linear stability of a system in which fingering is driven by both density and viscosity variations. He assumed a constant mass flux to get a steady base state, which is limited to some specific problems only. Heller (1966) studied the stability of miscible displacements with diffusion, and derived a nonhomogeneous second-order eigenvalue problem, that describes the evolution of the perturbations. Since there should not be any nonhomogeneity in linear stability theory, his form of the equations is questionable. In all these studies, the authors have recognized the importance of including dispersion effect, which leads to the difficulties by making the base state time dependent. Peters and Flock (1981) used a piston-like displacement model as a basis for studying the stability of immiscible displacements in water-wet porous media. From the stability theory, they obtained a dimensionless number to predict the onset of the instability in immiscible displacements.

Tan and Homsy (1986) performed a detailed theoretical analysis of the stability of miscible displacements in porous media for a rectilinear flow. These authors made the quasi-steady-state (QSSA) approximation to predict the growth rate of the disturbances and compared the results with initial value calculations. It was found that both theories were in good agreement except for the very short time when the base state changes rapidly and makes the QSSA invalid. A linear stability analysis of miscible displacement for a radial source flow in porous media, was later conducted by Tan and Homsy (1987). In this study, these authors presented the results for growth constant as a function of the mobility ratio and the Peclet number, and concluded that there is a critical Peclet number above which the displacement becomes unstable.

Hickernell and Yortsos (1986) studied the stability of the miscible displacement process in absence of physical dispersion. They showed that the growth rate of the perturbations depends on the logarithmic spatial derivative of the viscosity profile. Yortsos and Zeybek (1988) extented the linear stability theory to the case of velocity-dependent anisotropic dispersion. They found a small wavelength instability for short times. Manickam and Homsy (1993) studied the effect of nonmonotonic viscosity profile on the stability of miscible displacements and found that a nonmonotonic viscosity profile can be stable even when the end-point viscosity ratio is unfavorable. From the parametric study, they concluded that in the case of a nonmonotonic viscosity profile the diffusion has a destabilizing effect on the flow.

Rogerson and Meiburg (1993) studied the effects of tangential shear on the stability of the miscible displacements by including tangential velocity components to the interface. They concluded that, the tangential shear gives rise to a different nonlinear dynamics, and increases the stability of the miscible displacement processes, which does not seem to be in agreement with the results of their nonlinear simulations. From their nonlinear simulations with tangential shearing, new mechanisms of instability e.g. diagonal fingering, and side-finger instability were observed making the flow more unstable.

While, in the case of immiscible fluids, these authors reported that the growth rate of waves is unaffected by the presence of tangential velocity components and surface tension has the effect of stabilizing the flow.

2.2.2 Non-Newtonian fluids

The stability analysis of displacements involving non-Newtonian fluids has received very limited attention. Pascal (1988) considered the radial displacement of a shear-thinning (power-law) fluid by another shear-thinning fluid in porous media. In this work, the author neglected the importance of the surface tension effects in the immiscible displacement of a non-Newtonian fluid in Hele-Shaw cell. Wilson (1990) performed a linear stability analysis of the flow of purely elastic and purely shear-thinning non-Newtonian fluids in a rectilinear Hele-Shaw cell. He studied the immiscible displacements and concluded that the fractal nature of the patterns is due to the elastic nature and the presence of the interfacial tension. Recently, Sader et al. (1994) presented an analysis of immiscible displacement of a purely shear-thinning fluid by a low-viscosity Newtonian fluid in a radial Hele-Shaw cell. These authors attempted to quantify the mechanisms involved in the formation of ramified fractal patterns. As opposed to Wilson, they have attributed the fractal pattern formation purely to the shear-thinning nature of the non-Newtonian fluid. They argued that Wilson (1990) considered a case which is uncommon in experimental situations, and his results are inconsistent with experimental observations [Nittmann et al. 1986, Van Damme et al. 1987, 1988]. From the results of their linear stability analysis, these authors concluded that decreasing the power law index increases the growth rate of the perturbations, making the tip of the fingers more unstable, thus one sees more tip splitting and fractal patterns. As it will be discussed later, our results are in full agreement with the analysis of Sader et al. (1994) for a purely shear-thinning fluid.

2.3 Nonlinear simulations

In this section, we will present a review of exciting studies dealing with nonlinear simulations. First we will summarize simulations dealing with a Newtonian fluid displacing another Newtonian fluid. Second nonlinear simulations involving non-Newtonian fluids will be discussed.

2.3.1 Newtonian fluids

Koval (1963) and Todd et al. (1972) applied one-dimensional models to study viscous fingering in Newtonian displacements, and their model predictions were in agreement with some experimental observations. However, these one-dimensional models are incapable of explaining the mechanisms of the evolution of fingers. Later Fayers (1988) developed a one-dimensional model with some adjustable parameters in it. With these adjustable parameters, it was possible to describe the two-dimensional geometry and depth-averaged concentration of fingers.

A detailed numerical simulation of the full problem is required to understand the nonlinear phenomena of viscous fingering. In the earliest studies, most of the simulations were done using the finite difference technique. Peaceman et al. (1962) used this approach and generated finger patterns by introducing small perturbations in the permeability. Christie and Bond (1987) used the same finite difference scheme with a fine grid size and performed simulations for large values of the Peclet number and the mobility ratio. They found a reasonable agreement between their computations and the experiments of Blackwell et al. (1959).

In another study, Glimm (1983) investigated the effects of converging and diverging geometry by the use of interface-tracking technique. Two conditions were used to initiate fingering: random initial conditions and permeability variations, and similar results were obtained. Farmer (1985) used the moving point technique to study fingering in linear

geometry and compared his results with an analytic solution for the single-finger case obtained by Jacquard and Seguir (1962).

Tan and Homsy (1987) modeled a two-dimensional flow system and conducted numerical simulations using spectral methods to study the fingering mechanisms. In this study, these authors considered an isotropic dispersion in all the simulations. They successfully simulated the nonlinear viscous fingering and explained certain mechanisms such as spreading and shielding, by which the fingers evolve in time. The tip splitting mechanism was first time observed in their simulations. Christie (1989) developed a finite difference scheme to simulate the instability in porous media flows. His two-dimensional model accounts for anisotropic dispersion, heterogeneous permeability, and gravitational effects and is based more on empirical fingering models. Araktingi and Orr (1990) used a different technique, in which they track a set of fluid particles that disperse according to a random walk. The ensemble-average properties over several realizations compare well with the experiments of Blackwell et al (1959).

The numerical simulations of Tan and Homsy (1987) were extended by Zimmerman and Homsy (1991) to include the effects of anisotropic dispersion. They considered dispersion to be velocity dependent and studied the effects of anisotropy on the evolution of viscous fingers. A new finger interaction mechanism called coalescence was observed in their simulations with anisotropic dispersion. Later, Zimmerman and Homsy (1992) found that the coalescence mechanism is also observed in isotropic simulations with high Peclet number. Zimmerman and Homsy (1992) also simulated miscible displacements in a three-dimensional system and did not observe any new physical mechanisms. They suggested from their three-dimensional simulation results that two-dimensional simulations are sufficient enough to capture the nonlinear interactions of viscous fingers. Further, Tan and Homsy (1992) carried out simulations including the effects of permeability heterogeneity. Bacri et al. (1992) performed the first three-dimensional experiments involving miscible displacements and confirmed some of the findings of the

above simulation studies. More recently, Manickam and Homsy (1993) investigated the effects of nonmonotonic viscosity profile on the nonlinear evolution of viscous fingering. These authors concluded from their simulations that the nonmonotonicity in the viscosity profile gives rise to reverse fingering, in which the displaced fluid fingers through the displacing fluid.

The effect of tangential shearing was included in the nonlinear miscible flow simulations by Rogerson and Meiburg (1993), by including a tangential velocity components at the interface. Tangential shearing not only affected the wavelength and growth of the fingers, but also their shape and orientation. In addition to the finger interaction mechanisms reported in earlier studies, new mechanisms of diagonal fingering and secondary side-finger instability, resulting from the presence of tangential shearing and gravity, were observed.

2.3.2 Non-Newtonian fluids

The subject of flow of non-Newtonian fluids in porous media is relatively new. Most of the studies of viscous fingering in non-Newtonian polymer solutions have been done experimentally. Pressure transient theory of flow of non-Newtonian power-law fluids in porous media was developed by Odeh & Yang (1979), and Ikoku & Ramsey (1979). Numerical methods were used to simulate the power fluid flow by McDonald (1979), and Vongvuthipornchai & Raghvan (1987). Wu et al. (1991, 1992) have done both analytical and numerical simulations for the immiscible displacements involving Newtonian and non-Newtonian fluids.

In recent studies, porous medium has been represented in terms of equivalent lattice models, converting the problem into an analogous problem of resistor networks. Sorbie et al. (1989) numerically simulated the flow of a Carreau fluid using the network model.

Sahimi and Yortos (1990) used effective medium theory (EMT), based on the network models to study the various aspects of power-law fluid flow in porous media.

An alternative approach was first suggested by Paterson (1984) to treat viscous fingering as a fractal phenomenon. According to Nittmann et al. (1985), in diffusion limited aggregation (DLA) processes, the pattern grows by particles diffusing from a distant source and randomly sticking onto the growing aggregate. Thus a random tenuous pattern develops with preferentially developing tips and short side branches.

There is a limited number of theoretical studies on the flow of non-Newtonian fluids in porous media addressing the nonlinear fingering evolution. However, there are some recent studies, on the power-law flow characterization through porous media. Pascal (1983) presented a theoretical development for the nonsteady flow of power-law fluids with a yield stress, and studied the effect of the rheological parameters on the flow behavior through a porous medium. The problem was formulated in terms of several dimensionless groups and the rheological parameters are associated with these groups. The flow behavior was analyzed by means of these dimensionless group values.

In a study of the flow of a shear-thinning polyacrylamide solution through sinusoidal capillaries, Huzarewicz et al. (1991) reported that the product of the friction factor and Reynolds number fR_e, remains constant at low values of Reynolds number. Shah and Yortsos (1995) derived a macroscopic power-law by the use of homogenization theory (see Bensoussan et al., 1978). It was confirmed by the use of the homogenization theory that the flow of power-law fluids can be described by pore network models, in which the solution of the flow problems is simplified by representing the porous media as networks of capillaries.

In a recent study, Yu-Shau Wu and Karten Pruess (1997) have developed a three-dimensional integral finite difference simulator (TOUGH2) for single and multi-phase

flow of non-Newtonian fluids in porous media. These authors presented the results of two case studies: the displacement of a Newtonian fluid by a power-law fluid and the displacement of a Bingham fluid by a Newtonian fluid. They verified the model results with analytical solutions for both single-phase and two-phase flow problems.

2.4 Summary

From the above review of the displacement processes in porous media it was observed that in the case of displacements involving non-Newtonian fluids, ramified viscous-fingering patterns exhibiting fractal characteristics are obtained. In most of the experimental studies [8,13,27,36,37,55], the non-Newtonian fluids involved appear to be predominantly shear-thinning. Therefore, it can be concluded that the severe fingering in these fluids is predominantly caused by the shear-thinning behavior. It is clear from the above literature review that there have been many theoretical and nonlinear simulation studies in the field of Newtonian displacements. However, very little research has been done regarding the modeling and simulation of the non-Newtonian fluid flow in porous media. The mechanisms of instability at the interface involving non-Newtonian fluids and the physics behind their development have not been examined before in the literature. This motivates the present study, in which we decided to model the flow of shear-thinning fluids in Hele-Shaw cell and carry out the nonlinear simulations to help understand the formation of ramified patterns. The simulations results will help understand and analyze the effects of rheological parameters on the viscous-fingering patterns.

CHAPTER 3

THEORETICAL DEVELOPMENT

The subject of flow of non-Newtonian fluids is a subdivision of rheology. In this chapter the rheological equations of state are presented for the generalized Newtonian model and emphasis is placed on the Carreau-Yasuda model. First, the formulation is presented for the displacements involving Newtonian fluids and then the model development is presented for the two different cases of a non-Newtonian fluid displacing a Newtonian fluid, and a Newtonian fluid displacing a non-Newtonian fluid.

3.1 Model Formulation

The pattern of the flow through porous media is complex and at the microscopic scale, not amenable to a rigorous solution of the Navier-Stokes equations. A simplified and useful approach is to consider the fluid motion on a macroscopic scale while still retaining the artifice of a continuum. The macroscopic fluid properties and flow characteristics such as density, velocity, and pressure, can still be thought of as point quantities and continuous. This macroscopic approach is commonly used and forms the basis for most analyses of flow through porous media. The well known Darcy's law for flows through porous media is based on this approach.

A schematic of the two-dimensional Hele-Shaw flow system is shown in Fig. 3.1. The length, width, and thickness of the cell are L, W, and b respectively, where b is taken to be much smaller than W. An incompressible fluid is injected from the left-hand side with a uniform velocity U. Phase I is the displacing fluid, and phase II is the displaced fluid. The transport of the solute is characterized by the convection-diffusion equation. The

problem is formulated for a rectilinear Hele-Shaw cell, with the following appropriate assumptions :

- Both fluids are incompressible.
- The medium is homogeneous and has a constant permeability k.
- Dispersion is isotropic throughout the medium.
- The inertial forces are neglected.
- Both fluids are neutrally buoyant
- Gravity is neglected.

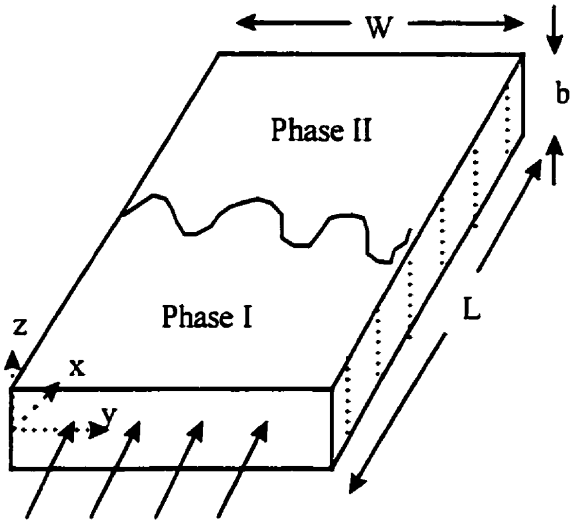

Fig. 3.1 Schematic of the Hele-Shaw flow system.

3.1.1 Basic Equations : Newtonian fluid displacing Newtonian fluid

Consider the two-dimensional displacement in which two incompressible, Newtonian fluids of different viscosities are separated by an interface. Here the x axis is in the direction of the flow and y axis is parallel to the interface.

The conservation of mass is expressed in the form of the continuity equation :

$$\nabla \cdot \mathbf{u} = 0. \tag{3.1}$$

For a very slow flow in a Hele-Shaw cell, the inertial forces are neglected in comparison to the viscous forces and the equation of motion becomes :

$$-\nabla \cdot \tau = \nabla p. \tag{3.2}$$

In the above equations, $\mathbf{u} = (u, v)$ is the velocity vector, p is the pressure, and τ is the stress tensor. For closely spaced plates, where the main shear is in the z direction the above equation can be rewritten in the x and y directions as :

$$-\frac{\partial}{\partial z}\left(-\mu \frac{\partial u}{\partial z}\right) = \frac{\partial p}{\partial x}, \quad \text{and} \quad -\frac{\partial}{\partial z}\left(-\mu \frac{\partial v}{\partial z}\right) = \frac{\partial p}{\partial y}. \tag{3.3}$$

If the viscosity μ is constant, the expression for u after integration becomes :

$$u = \frac{b^2}{2\mu}\left(\frac{z^2}{b^2} - \frac{1}{4}\right)\frac{\partial p}{\partial x}, \tag{3.4}$$

or

$$u = -6\left(\frac{z^2}{b^2} - \frac{1}{4}\right)\bar{u}, \tag{3.5}$$

where $\bar{u}$ is the depth-averaged velocity in the x direction given by :

$$\begin{aligned} \bar{u} &= \frac{\int_{-b/2}^{b/2} u\,dz}{\int_{-b/2}^{b/2} dz} \\ &= -\frac{b^2}{12\mu}\frac{\partial p}{\partial x}. \end{aligned} \tag{3.6}$$

A similar relation is obtained for the velocity component in the y direction. Equation (3.6) is similar to Darcy's law for porous media with an equivalent permeability of $b^2/12$, and can be rewritten as :

$$\bar{u} = -\frac{k}{\mu}\frac{\partial p}{\partial x}. \tag{3.7}$$

Thus, the Hele-Shaw flow is analogous to two-dimensional incompressible flow in porous media. In all what follows, the bars will be dropped and the two dimensional depth-averaged velocity will be denoted by $\mathbf{u} = (\bar{u}, \bar{v})$.

For a miscible displacement, the viscosity is a function of the concentration, and concentration is taken to obey a convective-diffusion equation :

$$\frac{\partial c}{\partial t} + \mathbf{u} \cdot \nabla c = \nabla \cdot D \nabla c, \tag{3.8}$$

where D is the dispersion coefficient, and c is the solvent concentration. In general, the viscosity is a function of the concentration, and will be written as :

$$\mu = \mu(c). \tag{3.9}$$

3.1.2 Boundary Conditions

The above set of equations are solved with the appropriate initial and boundary conditions. The boundary conditions we use are :

Streamwise direction
$$\begin{array}{l} at\ x = 0;\ \ u = U, v = 0, c = c_1 \\ at\ x = L;\ \ u = U, v = 0, c = 0 \end{array}, \tag{3.10}$$

Transverse direction
$$(\mathbf{u}, c)(x, 0, t) = (\mathbf{u}, c)(x, W, t), \tag{3.11}$$

where W is the size of the Hele-Shaw cell in the y direction.

At the far left end, the concentration of phase I is c_1, while at the right end it is zero, which is equivalent to saying that phase II is solvent free.

The boundary conditions in the streamwise direction state that the concentration and velocity at the boundaries are unaffected by the instability which is true because we stop the simulation before the fingered front reaches the other boundary $x = L$. Equation (3.11) is the periodic condition in the transverse direction. This periodic condition has also been used in the simulations of Tan and Homsy (1988). This is restrictive but useful

in studying the fingering patterns by applying spectral methods which require periodic boundary conditions.

The initial conditions we used are :

$$\text{at t} = 0 \qquad \begin{aligned} &u = U, v = 0 \quad \forall(x,y), \\ &c = c_0(x,y,t=0) \quad \forall(\text{x},\text{y}), \end{aligned} \tag{3.12}$$

which means a constant linear velocity in the x direction and a given two-dimensional distribution of the concentration at time zero. This initial concentration profile needs a detailed discussion which will be presented in chapter 5 dealing with the numerical scheme.

The problem description is complete once the viscosity-concentration relationship $\mu(c)$ is specified. In practice, the viscosity-concentration relationship is complicated and changes with the choice of the fluids. Here, for numerical convenience we have chosen an exponential variation of viscosity with concentration :

$$\frac{d\ln(\mu/\mu_1)}{d(c/c_1)} = -Const\,. \tag{3.13}$$

This type of profile has also been used in earlier simulation works [Zimmerman and Homsy, 1991 and Tan and Homsy, 1988]. However, any other general relationship can also be easily incorporated in the simulations.

3.1.3 Scaling

A proper scaling of the system is required to model the fingering. Although there is an obvious characteristic geometric length L, and a characteristic time scale L/U, we are interested more with the diffusive effects. Thus we scale all lengths by the diffusive length D/U and all times by the diffusive time D/U^2 . Since the permeability k of the medium is constant, it can be included in the viscosity itself. In all the remainder of this

study, the symbol μ will be used to represent the ratio of the viscosity and permeability μ/k, and will be referred to as "viscosity". The viscosity is scaled by the viscosity of the displacing fluid μ_1, and the pressure by the characteristic pressure $\mu_1 D$. With these scalings, the dimensionless quantities are :

$$\hat{\mathbf{x}} = \frac{(x,y)}{D/U}\ ;\quad \hat{\mathbf{u}} = \frac{\mathbf{u}}{U};\quad \mathbf{t}^* = \frac{t}{D/U^2},$$
$$c^* = \frac{c}{c_1};\quad \mu^* = \frac{\mu}{\mu_1};\quad p^* = \frac{p}{(\mu_1 D)/k}. \tag{3.14}$$

For convenience, the system is studied in a reference moving with a constant velocity U.

$$\begin{aligned}\mathbf{x}^* &= \hat{\mathbf{x}} - \mathbf{i}t^* \\ \mathbf{u}^* &= \hat{\mathbf{u}} - \mathbf{i}\end{aligned}, \tag{3.15}$$

where $\mathbf{i}$ is the unit vector in the x direction. After scaling, the equations and the boundary conditions become :

$$\nabla \cdot \mathbf{u}^* = 0, \tag{3.16}$$

$$\nabla p^* = -\mu^*\left(\mathbf{u}^* + \mathbf{i}\right), \tag{3.17}$$

$$\frac{\partial c^*}{\partial t^*} + \mathbf{u}^* \cdot \nabla c^* = \nabla^2 c^*, \tag{3.18}$$

$$\frac{d\left(\ln \mu^*\right)}{dc^*} = -R. \tag{3.19}$$

Streamwise direction
$$\begin{aligned} &at\ x^* = -t^*;\ u^* = 0, v^* = 0, c^* = 1, \\ &at\ x^* = LU/D - t^*;\ u^* = 0, v^* = 0, c^* = 0. \end{aligned} \tag{3.20}$$

Transverse direction
$$\left(u^*, v^*, c^*\right)\left(x^*, 0, t^*\right) = \left(u^*, v^*, c^*\right)\left(x^*, WU/D, t^*\right). \tag{3.21}$$

Based on the above scaling, the dimensionless viscosity is related to the dimensionless concentration through the equation :

$$\mu^* = e^{R(1-c^*)}. \tag{3.22}$$

In order to account for the geometry, two dimensionless parameters are introduced as :

$$P_e = \frac{LU}{D} \text{ and } A = \frac{L}{W}, \tag{3.23}$$

where P_e is the Peclet number for mass transfer and A is called the aspect ratio. The Peclet number has been defined based on the length of the domain and represents the ratio of the convective forces over diffusive forces. The parameter A, determines the number of fingers in the transverse direction which will be seen from the simulation results. In all what follows, for convenience, the asterisks will be dropped from the dimensionless variables. The boundary conditions can be rewritten in terms of the above defined parameters as :

$$\begin{aligned} &at\ x = -t;\ \ u = 0, v = 0, c = 1 \\ &at\ x = P_e - t;\ \ u = 0, v = 0, c = 0 \end{aligned} \tag{3.24}$$

and

$$(u, v, c)(x, 0, t) = (u, v, c)(x, P_e / A, t). \tag{3.25}$$

3.1.4 Vorticity and streamfunction formulation

It has been found by several workers that it is more convenient and efficient to work in terms of vorticity and streamfunction than the pressure and velocity field. So the problem is formulated in terms of the streamfunction and vorticity defined in the usual manner :

$$u = \frac{\partial \psi}{\partial y}, \quad v = -\frac{\partial \psi}{\partial x}, \tag{3.26}$$

$$\omega = \frac{\partial v}{\partial x} - \frac{\partial u}{\partial y}. \tag{3.27}$$

The streamfunction ψ and the vorticity ω are related by the following relation :

$$\nabla^2 \psi = -\omega, \tag{3.28}$$

where ∇^2 is the Laplacian operator.

The convection-diffusion equation written in terms of the streamfunction is :

$$\frac{\partial c}{\partial t} + \frac{\partial \psi}{\partial y}\frac{\partial c}{\partial x} - \frac{\partial \psi}{\partial x}\frac{\partial c}{\partial y} = \nabla^2 c\,. \tag{3.29}$$

Taking the curl of equation (3.17), we get :

$$\mu\left(\frac{\partial v}{\partial x} - \frac{\partial u}{\partial y}\right) = (u+1)\frac{\partial \mu}{\partial y} - v\frac{\partial \mu}{\partial x}, \tag{3.30}$$

or

$$\mu\omega = \frac{d\mu}{dc}\left(\frac{\partial \psi}{\partial x}\frac{\partial c}{\partial x} + \frac{\partial \psi}{\partial y}\frac{\partial c}{\partial y} + \frac{\partial c}{\partial y}\right), \tag{3.31}$$

or

$$\begin{aligned}\omega &= \frac{d\ln\mu}{dc}\left(\frac{\partial \psi}{\partial x}\frac{\partial c}{\partial x} + \frac{\partial \psi}{\partial y}\frac{\partial c}{\partial y} + \frac{\partial c}{\partial y}\right)\\ &= -R\left(\frac{\partial \psi}{\partial x}\frac{\partial c}{\partial x} + \frac{\partial \psi}{\partial y}\frac{\partial c}{\partial y} + \frac{\partial c}{\partial y}\right),\end{aligned} \tag{3.32}$$

which is the vorticity formation equation, and shows that vorticity is produced by the concentration gradients not perpendicular to the flow.

3.2 Non-Newtonian fluids

For most industrial applications, shear rate dependent viscosity is the most important property of the non-Newtonian fluids. Since for some fluids the viscosity can change by a factor of 10, 100, or even 1000, clearly such an enormous change cannot be ignored in fluid flow problems.

For an incompressible Newtonian fluid, the shear stress τ is related to the shear rate $\dot{\gamma}$ by the equation :

$$\tau = -\mu\dot{\gamma}\,, \tag{3.33}$$

where, μ is called the viscosity of the fluid and is constant for a given temperature and pressure. The shear rate $\dot{\gamma}$ is defined as ∇u.

The above Newton's law of viscosity is modified for the shear rate dependent viscosity, and the expression for an incompressible generalized Newtonian fluid becomes :

$$\tau = -\mu(\dot{\gamma})\dot{\gamma} \,, \tag{3.34}$$

where μ is a function of $\dot{\gamma}$. Depending on the nature of variation of the apparent viscosity $\mu(\dot{\gamma})$ with the shear rate $\dot{\gamma}$, the fluid is categorized as shear-thinning or shear-thickening. For a shear-thinning fluid, also sometimes referred to as pseudo-plastic fluid, the apparent viscosity decreases with the shear rate $\dot{\gamma}$. A shear-thickening fluid, also sometimes referred to as dilatant, the apparent viscosity increases with the shear rate $\dot{\gamma}$.

Many empiricisms are available for the expression of $\mu(\dot{\gamma})$ based on experimental data analyses. The well known "power-law" model [Bird et al., 1987] is given as :

$$\mu = K\dot{\gamma}^{n-1} \,, \tag{3.35}$$

in which n is called the power-law index, and K is a consistency factor with units of $P_a.s^n$. The power-law model is a widely-used empiricism in engineering work, because a variety of flow problems have been solved analytically for this.

In this work, we have chosen the well known Carreau-Yasuda Model [Bird et al., 1987] to describe the shear-thinning behavior of the non-Newtonian fluid. This model has flexibility to fit a wide variety of experimental data representing the variation of the viscosity μ with shear rate $\dot{\gamma}$. This model has proven to be useful for numerical simulations in which one needs an analytical expression for the non-Newtonian viscosity curve. The model is expressed as :

$$\frac{\mu - \mu_\infty}{\mu_\circ - \mu_\infty} = \left[1 + (\lambda\dot{\gamma})^a\right]^{(n-1)/a} \,, \tag{3.36}$$

where $\mu_\circ$ is the zero shear viscosity, μ_∞ is the infinite-shear-rate viscosity, λ is a time constant, n is the power-law exponent which describes the slope of the $\mu(\dot{\gamma})$ curve (refer to Fig. 3.2), and a is a dimensionless parameter that describes the transition from the

zero-shear-rate region to the power-law region. For many polymer solutions and melts, good fits are obtained for $\mu_\infty = 0$ and $a = 2$. Then equation (3.36) becomes :

$$\mu = \mu_\circ \left[1 + (\lambda\dot{\gamma})^2\right]^{(n-1)/2}, \tag{3.37}$$

which is referred to as Carreau equation. For a power-law exponent n = 1, the model represents the behavior of a Newtonian fluid.

Since the main shear in the Hele-Shaw cell occurs in the direction perpendicular to the plates, the average shear rate can be estimated as the fluid velocity divided by the plate spacing :

$$\bar{\dot{\gamma}} = \frac{V}{b}, \tag{3.38}$$

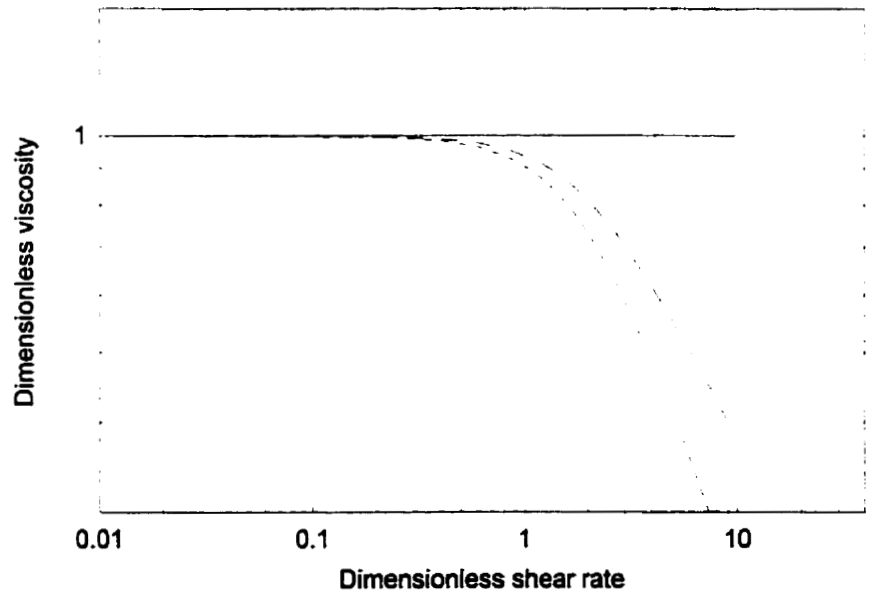

Fig. 3.2 Plot of (μ/μ_0) versus $(\lambda\dot{\gamma})$ for the shear-thinning Carreau model.

where, $$V^2 = u^2 + v^2. \tag{3.39}$$

The expression for the non-Newtonian fluid viscosity becomes :

$$\mu = \mu_0 \left[1 + (D_e V)^2\right]^{(n-1)/2}, \tag{3.40}$$

where D_e is a dimensional parameter similar to the Deborah number, and is defined as :

$$D_e = \frac{\lambda U}{b}. \tag{3.41}$$

3.2.1 Non-Newtonian fluid displacing Newtonian fluid

Consider a system where a shear-thinning fluid with an apparent viscosity $\mu_1(\dot{\gamma})$ is displacing a Newtonian fluid of viscosity μ_2 (see Fig. 3.3). As mentioned earlier in this chapter, we have chosen a generalized Newtonian fluid model known as the Carreau model to study the flow of non-Newtonian fluids. This model represents a shear-thinning fluid behavior, for which the viscosity decreases with increasing shear rate.

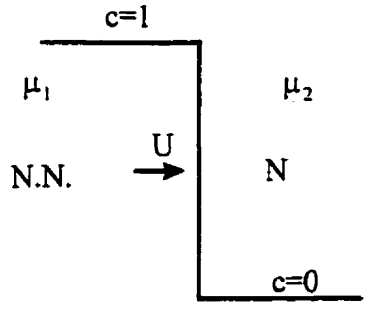

where N → Newtonian

and NN → Non-Newtonian

Fig. 3.3 Schematic of the flow system: non-Newtonian fluid displacing Newtonian fluid.

The viscosity of the non-Newtonian displacing fluid is given by the Carreau model :

$$\mu_1 = \mu_0 \left[1 + (D_e V)^2\right]^{(n-1)/2},$$

where μ_o is the zero shear viscosity of the shear-thinning fluid. The viscosities of both fluids are scaled with the zero shear viscosity of the non-Newtonian fluid, leading to the following expression of the dimensionless viscosities :

$$\mu_1^* = \left[1+(D_e V)^2\right]^{(n-1)/2}, \tag{3.42}$$

and

$$\mu_2^* = \frac{\mu_2}{\mu_0}. \tag{3.43}$$

Assuming a dimensionless viscosity-concentration profile of the form :

$$\mu = A\exp\{R_{ST}(1-c)\}, \tag{3.44}$$

from the above expressions, we have :

at c=1;

$$\mu = A = \mu_1^* = \left[1+(D_e V)^2\right]^{(n-1)/2}, \tag{3.45}$$

at c=0;

$$\mu = A\exp(R_{ST}) = \mu_2^* = \frac{\mu_2}{\mu_0}. \tag{3.46}$$

From equations (3.46) and (3.47), we get :

$$R_{ST} = -\left(\frac{n-1}{2}\right)\ln\left[1+(D_e V)^2\right] + R, \tag{3.47}$$

where the parameter R has been defined as :

$$R = \ln\left(\frac{\mu_2}{\mu_0}\right). \tag{3.48}$$

Substituting the values of A and R_{ST} in equation (3.44), the expression for the viscosity becomes :

$$\mu = e^{R(1-c)}\left(1+D_e{}^2V^2\right)^{c(n-1)/2}. \tag{3.49}$$

For De = 0 or n = 0, the above expression reduces to the viscosity-concentration relation for the case of a Newtonian fluid displacing another Newtonian fluid.

For the non-Newtonian case, the fluid velocity cannot be solved explicitly in terms of pressure gradient ∇p. We make an assumption by neglecting the viscosity variation in the z direction in equation (3.3), which means that the condition

$$\frac{\partial \mu}{\partial z} << \frac{\mu}{z} \tag{3.50}$$

has to be satisfied [D. Bonn et al., 1995]. With this assumption, Darcy's law equation (3.7) remains valid :

$$u = -\frac{k}{\mu(V^2)}\frac{\partial p}{\partial x} \text{ and } v = -\frac{k}{\mu(V^2)}\frac{\partial p}{\partial y}, \tag{3.51}$$

where μ is a function of $V^2 = u^2 + v^2$.

After scaling, equation (3.51) can be written as :

$$\nabla p^* = -\mu^*(V^2)\left[\mathbf{u}^* + \mathbf{i}\right], \tag{3.52}$$

which is similar to equation (3.17) for the Newtonian case. Taking the curl of the above equation, we get :

$$\mu\omega = \frac{d\mu}{dc} N + 2\frac{\partial \mu}{\partial V^2} M, \tag{3.53}$$

or

$$\omega = \frac{d \ln \mu}{dc} N + 2\frac{\partial \ln \mu}{\partial V^2} M, \tag{3.54}$$

where N and M are nonlinear terms given as :

$$N = -v\frac{\partial c}{\partial x} + u\frac{\partial c}{\partial y} + \frac{\partial c}{\partial y}, \tag{3.55}$$

$$M = (u+1)^2\frac{\partial u}{\partial y} - v^2\frac{\partial v}{\partial x} + (u+1)v\left(\frac{\partial v}{\partial y} - \frac{\partial u}{\partial x}\right). \tag{3.56}$$

From equation (3.49) for the viscosity, we have :

$$\frac{\partial \ln \mu}{\partial c} = -R + \left(\frac{n-1}{2}\right)\ln\left(1 + D_e{}^2 V^2\right), \tag{3.57}$$

and
$$\frac{\partial \ln \mu}{\partial V^2} = c\left(\frac{n-1}{2}\right)\left(\frac{D_e^{\,2}}{1+D_e^{\,2}V^2}\right). \tag{3.58}$$

After substituting equations (3.57) and (3.58), the expression for the vorticity becomes :

$$\omega = c(n-1)\left(\frac{D_e^{\,2}}{1+D_e^{\,2}V^2}\right)M - RN + \left(\frac{n-1}{2}\right)\ln\left(1+D_e^{\,2}V^2\right)N. \tag{3.59}$$

The above expression for the vorticity reduces to that of a Newtonian fluid displacing another Newtonian fluid when n = 1 or De = 0. The non-linear term M containing the products of the velocity and its gradients can be simplified for the slow motion flow by neglecting the non-linear terms. With this assumption, equation (3.56) becomes :

$$M = \frac{\partial u}{\partial y}. \tag{3.60}$$

This assumption was verified by comparing the results of the simulations with and without non-linear terms, which will be presented in the next chapter. Although, there were no significant differences between the results of the two cases, in all the simulations non-linear terms were included to obtain the accurate results.

3.2.2 Newtonian fluid displacing non-Newtonian fluid

In this case, a Newtonian fluid is chosen to displace a non-Newtonian fluid in a Hele-Shaw cell. From Fig. 3.4, the displaced fluid is again a non-Newtonian fluid of shear-thinning nature, with an apparent viscosity $\mu_2(\dot{\gamma})$. The model is formulated following the same approach as in the case of a non-Newtonian fluid displacing a Newtonian one. The viscosity of the non-Newtonian displaced fluid is :

$$\mu_2 = \mu_0\left[1+(D_eV)^2\right]^{(n-1)/2}.$$

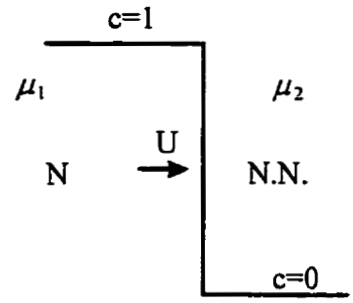

Fig. 3.4 Schematic of the flow system: Newtonian fluid displacing non-Newtonian fluid.

In this case the viscosities are scaled with the viscosity of the displacing fluid μ_1:

$$\mu_1^* = 1, \text{ and } \mu_2^* = \frac{\mu_0}{\mu_1}\left[1+(D_e V)^2\right]^{(n-1)/2}. \tag{3.61}$$

Using equation (3.44) for the concentration-viscosity profile, we have :

at c=1; $$\mu = A = 1, \tag{3.62}$$

at c=0; $$\mu = A\exp(R_{ST}) = \frac{\mu_0}{\mu_1}\left[1+(D_e V)^2\right]^{(n-1)/2}, \tag{3.63}$$

which leads to the following expression for R_{ST}:

$$R_{ST} = \left(\frac{n-1}{2}\right)\ln\left[1+(D_e V)^2\right] + R, \tag{3.64}$$

where the parameter R has been defined as :

$$R = \ln\left(\frac{\mu_0}{\mu_1}\right). \tag{3.65}$$

Therefore the expression for viscosity becomes :

$$\mu = e^{R(1-c)}\left(1+D_e{}^2V^2\right)^{(1-c)(n-1)/2}. \tag{3.66}$$

Again for De = 0 or n = 1, the above expression reduces to the Newtonian case. From the above equation (3.66) for the viscosity, we get :

$$\frac{\partial \ln \mu}{\partial c} = -R - \left(\frac{n-1}{2}\right) \ln\left(1 + D_e^{\,2} V^2\right), \tag{3.67}$$

and

$$\frac{\partial \ln \mu}{\partial V^2} = (1-c)\left(\frac{n-1}{2}\right)\left(\frac{D_e^{\,2}}{1 + D_e^{\,2} V^2}\right). \tag{3.68}$$

Hence from equation (3.54) the expression for the vorticity becomes :

$$\omega = (1-c)(n-1)\left(\frac{D_e^{\,2}}{1 + D_e^{\,2} V^2}\right) M - RN - \left(\frac{n-1}{2}\right) \ln\left(1 + D_e^{\,2} V^2\right) N, \tag{3.69}$$

where M and N are non-linear terms as expressed earlier. To verify, again the above expression for vorticity reduces to the case of a Newtonian displacing Newtonian fluid for De = 0 or n = 1.

3.3 Summary

We conclude this chapter by summarizing the above developed equations for the three different cases under consideration. The streamfunction and vorticity relation equation (3.28), and convective-diffusion equation (3.29) are common to all the three cases under consideration and are given as :

$$\nabla^2 \psi = -\omega, \tag{3.70}$$

$$\frac{\partial c}{\partial t} + \frac{\partial \psi}{\partial y}\frac{\partial c}{\partial x} - \frac{\partial \psi}{\partial x}\frac{\partial c}{\partial y} = \nabla^2 c. \tag{3.71}$$

The vorticity formation for the three different cases is :

- Newtonian fluid displacing another Newtonian fluid

$$\omega = -R\left(\frac{\partial \psi}{\partial x}\frac{\partial c}{\partial x} + \frac{\partial \psi}{\partial y}\frac{\partial c}{\partial y} + \frac{\partial c}{\partial y}\right), \tag{3.72}$$

- Non-Newtonian fluid displacing Newtonian fluid

$$\omega = c(n-1)\left(\frac{D_e^{\,2}}{1 + D_e^{\,2} V^2}\right) M - RN + \left(\frac{n-1}{2}\right) \ln\left(1 + D_e^{\,2} V^2\right) N, \tag{3.73}$$

- Newtonian fluid displacing non-Newtonian fluid

$$\omega = (1-c)(n-1)\left(\frac{D_e^{\,2}}{1+D_e^{\,2}V^2}\right)M - RN - \left(\frac{n-1}{2}\right)\ln\left(1+D_e^{\,2}V^2\right)N, \quad (3.74)$$

where N and M are :

$$N = -v\frac{\partial c}{\partial x} + u\frac{\partial c}{\partial y} + \frac{\partial c}{\partial y}, \quad (3.75)$$

$$M = (u+1)^2\frac{\partial u}{\partial y} - v^2\frac{\partial v}{\partial x} + (u+1)v\left(\frac{\partial v}{\partial y} - \frac{\partial u}{\partial x}\right). \quad (3.76)$$

CHAPTER 4

LINEAR STABILITY ANALYSIS

This chapter deals with the linear stability analysis of the problem of viscous fingering in a rectilinear Hele-Shaw cell. First the linear stability concept is presented followed by the formulation of the problem for purely Newtonian displacements. Theoretical development of equations for the other two cases of a Non-Newtonian fluid displacing a Newtonian fluid, and a Newtonian fluid displacing a non-Newtonian fluid is given in Appendix A.

The quasi-state state approximation (QSSA) is applied to determine the growth of the disturbances. Applying the QSSA reduces the partial differential equations to ordinary differential equations, which is an eigenvalue problem and can be solved using appropriate numerical schemes. Finally, a brief description of the numerical method used to solve the resulting eigenvalue problem is presented followed by the results obtained and their discussion.

4.1 Basic concepts

Hydrodynamic stability has been recognized as one of the central problems of fluid mechanics. In general, instability occurs because there is some disturbance of the equilibrium of the external forces, inertia, and viscous forces of a fluid. In the case of viscous fluids, the viscosity has complicated effects of diffusing momentum. This can make the flow unstable, while the same flow of an inviscid fluid may be stable. Any small disturbance may either die away, persist as a disturbance of the same magnitude, or

grow so much that the basic flow becomes unstable. Such disturbances are called *stable*, *neutrally stable*, and *unstable* respectively [Drazin and Reid, 1989].

In linear stability analysis, we consider a steady base flow and assume that the equations of motion and boundary conditions may be linearized for sufficiently small disturbances. The second and higher order terms in the perturbed equations are neglected in comparison with the first order terms. Thereby a linear homogeneous system of partial differential equations and boundary conditions is obtained. The linearized equations have coefficients that may vary in space but not in time since the base flow is steady. In general the solution of the system can be expressed as real parts of integrals of components, each component varying exponentially with time like $e^{\sigma t}$, where the real part of σ is called the growth rate of the disturbance. The resulting linear problem is an eigenvalue problem which can be solved to determine σ [Drazin and Reid, 1989].

A small disturbance of the base flow will in general excite all modes. If the growth rate is positive ($\sigma > 0$) for a mode, then the corresponding disturbance will amplify, growing exponentially with time leading to nonlinear instability. If the growth rate is identically zero ($\sigma = 0$), the mode is said to be neutrally stable, and if it is negative ($\sigma < 0$) it is said to be stable. Thus if $\sigma > 0$ for at least one mode then the flow is unstable. The objective of linear stability analysis is to determine under which circumstances the flow is unstable.

4.2 Newtonian displacements

Consider a three-dimensional rectilinear Hele-Shaw cell, as shown in Fig. 3.1. First we consider the case of a Newtonian fluid displacing another Newtonian fluid, and derive the linearized equations that govern the stability of the flow.

4.2.1 Basic Equations

The governing equations of the problem are similar to those in chapter 3, and are generalized to the three-dimensional system. The governing equations are as given below in a dimensionless form :

$$\frac{\partial u}{\partial x} + \frac{\partial v}{\partial y} + \frac{\partial w}{\partial z} = 0 , \tag{4.1}$$

$$\frac{\partial p}{\partial x} = -\mu(u+1) , \tag{4.2}$$

$$\frac{\partial p}{\partial y} = -\mu v , \tag{4.3}$$

$$\frac{\partial p}{\partial z} = -\mu w , \tag{4.4}$$

$$\frac{\partial c}{\partial t} + u\frac{\partial c}{\partial x} + v\frac{\partial c}{\partial y} + w\frac{\partial c}{\partial z} = \frac{\partial^2 c}{\partial x^2} + \frac{\partial^2 c}{\partial y^2} + \frac{\partial^2 c}{\partial z^2} , \tag{4.5}$$

$$\mu = \mu(c) = \exp R(1-c) . \tag{4.6}$$

At the base state, the above set of equations reduce to :

$$\bar{u} = \bar{v} = \bar{w} = 0 , \tag{4.7}$$

$$\frac{\partial \bar{p}}{\partial x} = -\bar{\mu} , \tag{4.8}$$

$$\frac{\partial \bar{c}}{\partial t} = \frac{\partial^2 \bar{c}}{\partial x^2} , \tag{4.9}$$

$$\bar{\mu} = \bar{\mu}(\bar{c}) = \bar{\mu}(x,t) . \tag{4.10}$$

It is clear that the base state is time dependent, which enters through the time dependence of concentration. The base state concentration is known from the solution of equation (4.9), and is given as :

$$\bar{c}(x,t) = \frac{1}{2}\left[1 - erf\left(x/\sqrt{4t}\right)\right], \tag{4.11}$$

where the error function is defined as :

$$erf(x) = \frac{2}{\sqrt{\pi}} \int_0^x e^{-\theta^2} d\theta . \tag{4.12}$$

4.2.2 Stability analysis

In order to conduct the linear stability analysis of the problem, small disturbances are induced into the system at the base state :

$$c(x,y,z,t) = \bar{c}(x,t) + c'(x,y,z,t), \tag{4.13}$$

$$p(x,y,z,t) = \bar{p}(x,t) + p'(x,y,z,t), \tag{4.14}$$

$$\mu(x,y,z,t) = \bar{\mu}(x,t) + \mu'(x,y,z,t), \tag{4.15}$$

$$u = \bar{u} + u',\ v = \bar{v} + v',\ w = \bar{w} + w', \tag{4.16}$$

where primed quantities represent small disturbances from the base state denoted by the bars. These values are substituted into the system of equations, and the resulting linearized set of equations governing small disturbances is :

$$\frac{\partial u'}{\partial x} + \frac{\partial v'}{\partial y} + \frac{\partial w'}{\partial z} = 0 , \tag{4.17}$$

$$\frac{\partial p'}{\partial x} = -\mu' - \bar{\mu} u' , \tag{4.18}$$

$$\frac{\partial p'}{\partial y} = -\bar{\mu} v' , \tag{4.19}$$

$$\frac{\partial p'}{\partial z} = -\bar{\mu} w' , \tag{4.20}$$

$$\frac{\partial c'}{\partial t} + u' \frac{\partial \bar{c}}{\partial x} = \frac{\partial^2 c'}{\partial x^2} + \frac{\partial^2 c'}{\partial y^2} + \frac{\partial^2 c'}{\partial z^2} , \tag{4.21}$$

$$\frac{1}{\bar{\mu}} \frac{d\mu'}{dc'} = -R . \tag{4.22}$$

Darcy's law component equations (4.18), (4.19), and (4.20) can be written in a vector notation as :

$$\nabla p' = -\bar{\mu} \mathbf{v}' - \mu' \mathbf{i} . \tag{4.23}$$

Taking the curl of equation (4.23) gives :

$$\frac{\partial w'}{\partial y} - \frac{\partial v'}{\partial z} = 0, \tag{4.24}$$

$$\frac{\partial \mu'}{\partial z} - \bar{\mu}\frac{\partial w'}{\partial x} - w'\frac{\partial \bar{\mu}}{\partial x} + \bar{\mu}\frac{\partial u'}{\partial z} = 0, \tag{4.25}$$

$$\bar{\mu}\frac{\partial v'}{\partial x} + v'\frac{\partial \bar{\mu}}{\partial x} - \bar{\mu}\frac{\partial u'}{\partial y} - \frac{\partial \mu'}{\partial y} = 0. \tag{4.26}$$

Differentiating Eqs. (4.25) and (4.26) with respect to z and y respectively, along with the use of equation (4.17) gives :

$$\frac{\partial^2 \mu'}{\partial z^2} - \bar{\mu}\frac{\partial^2 w'}{\partial x \partial z} - \frac{\partial \bar{\mu}}{\partial x}\frac{\partial w'}{\partial z} + \bar{\mu}\frac{\partial^2 u'}{\partial z^2} = 0, \tag{4.27}$$

and

$$-\bar{\mu}\left(\frac{\partial^2 u'}{\partial x^2} + \frac{\partial^2 u'}{\partial y^2}\right) - \bar{\mu}\frac{\partial^2 w'}{\partial x \partial z} + \frac{\partial \bar{\mu}}{\partial x}\frac{\partial v'}{\partial y} - \frac{\partial^2 \mu'}{\partial y^2} = 0. \tag{4.28}$$

After subtracting equation (4.28) from equation (4.27), we get :

$$\bar{\mu}\left(\frac{\partial^2 u'}{\partial x^2} + \frac{\partial^2 u'}{\partial y^2} + \frac{\partial^2 u'}{\partial z^2}\right) + \frac{\partial \bar{\mu}}{\partial x}\frac{\partial u'}{\partial x} = -\frac{\partial^2 \mu'}{\partial y^2} - \frac{\partial^2 \mu'}{\partial z^2}. \tag{4.29}$$

Since the coefficients of the equations are independent of y and z, the perturbations can be decomposed into Fourier components in the y and z directions :

$$f'(x,y,z,t) = f(x,t)\exp(ik_y y)\exp(ik_z z). \tag{4.30}$$

The above linearized equations can be written in terms of only the concentration disturbance c' and the streamwise velocity u' by eliminating p', v', and w'. The two disturbance functions u' and c' are written in the form :

$$(u', c') = (\phi, \psi)\exp(ik_y y)\exp(ik_z z), \tag{4.31}$$

where k_y, k_z are the disturbance wavenumber in the y and z direction respectively, and ϕ, ψ are functions of x and t only. We define the wavenumber k as :

$$k^2 = k_y^{\,2} + k_z^{\,2}. \tag{4.32}$$

After substituting the expression for u', c' into Eq. (4.21), we get the first differential equation :

$$\frac{\partial \psi}{\partial t} - \frac{\partial^2 \psi}{\partial x^2} + k^2 \psi = -\frac{\partial \overline{c}}{\partial x}(x,t)\phi\,, \tag{4.33}$$

now substituting for the velocity perturbation in equation (4.29) and using equation (4.22), we get :

$$\frac{\partial^2 \phi}{\partial x^2} + \frac{1}{\overline{\mu}}\frac{\partial \overline{\mu}}{\partial x}(x,t)\frac{\partial \phi}{\partial x} - k^2\phi = k^2 \frac{1}{\overline{\mu}(x,t)}\frac{d\mu'}{dc'}\psi\,, \tag{4.34}$$

which is the second differential equation of the system.

4.2.3 Quasi-steady-state approximation

The Quasi-steady-state approximation (QSSA) is applied to determine the stability of the flow. Using this approximation, one assumes that the small perturbations change in time much faster than the base state, allowing to treat the base state as if it were steady by freezing it at a time t_0. This approximation has been applied by many workers and was first stated by Heller (1966). Although it is difficult to justify a priori, it can be explained by looking at the rate of change of the base state under consideration, $\partial \overline{c}/\partial t$, which decreases as $t^{-3/2}$ with time and smears out diffusively in time. Thus for time t > 0, the QSSA is expected to hold. More rigorous justification can be obtained from the initial value calculations, as shown by Tan & Homsy (1986).

When applying the QSSA, the base state solution is frozen at time t_0, and assumed to be steady. The coefficients of Eqs. (4.33) and (4.34) are defined as :

$$(\phi, \psi)(x,t) = (\phi, \psi)(x,t_0)\exp\left[\sigma(t_0)t\right], \tag{4.35}$$

where, σ is the quasistatic growth rate. Here, it has been assumed that the disturbances grow exponentially with time. Substituting the above expression (4.35) into equations (4.33) and (4.34) and simplifying gives :

$$\left(\sigma(t_0) - \frac{d^2}{dx^2} + k^2\right)\psi = -\frac{d\bar{c}}{dx}(x,t_0)\phi, \tag{4.36}$$

and $$\left(\frac{d^2}{dx^2} + \frac{1}{\bar{\mu}}\frac{d\bar{\mu}}{dx}(x,t_0)\frac{d}{dx} - k^2\right)\phi = \frac{k^2}{\bar{\mu}(x,t_0)}\frac{d\mu'}{dc'}\psi. \tag{4.37}$$

Using equation (4.22) the above equation (4.37) becomes :

$$\left(\frac{d^2}{dx^2} - R\frac{d\bar{c}}{dx}(x,t_0)\frac{d}{dx} - k^2\right)\phi = -k^2 R\psi. \tag{4.38}$$

With the use of QSSA, the partial differential equations have been reduced to ordinary differential equations forming an eigenvalue problem where σ appears as the eigenvalue. The growth rate depends on the wavenumber k, and varies with the value of the constant time t_0.

4.3 Numerical Solution

The linear stability analysis equations are summarized below for the three different cases under consideration. First equation is common to all the three cases :

$$\left(\sigma(t_0) - \frac{d^2}{dx^2} + k^2\right)\psi = -\frac{d\bar{c}}{dx}(x,t_0)\phi, \tag{4.39}$$

and the second differential equation for the three different cases is :

- a Newtonian fluid displacing another Newtonian fluid

$$\left(\frac{d^2}{dx^2} - R\frac{d\bar{c}}{dx}(x,t_0)\frac{d}{dx} - k^2\right)\phi = -k^2 R\psi. \tag{4.40}$$

- a Non-Newtonian fluid displacing a Newtonian fluid

$$\left(\frac{d^2}{dx^2}+A\frac{d\bar{c}}{dx}(x,t_0)\frac{d}{dx}-k^2(1+B\bar{c})\right)\phi = Ak^2\psi\,. \tag{4.41}$$

- a Newtonian fluid displacing a non-Newtonian fluid

$$\left(\frac{d^2}{dx^2}+C\frac{d\bar{c}}{dx}(x,t_0)\frac{d}{dx}-k^2\left(1+B(1-\bar{c})\right)\right)\phi = Ck^2\psi\,. \tag{4.42}$$

A finite difference method is used to solve the above eigenvalue problem, consisting of a system of two coupled ordinary differential equations. The finite difference technique has advantage over other methods, since by using this method complete spectrum of the eigenvalues can be obtained. A nonuniform geometric mesh is used which is very fine near the origin where the concentration gradients are large, and spacing increases geometrically with the distance from the origin. Both eigenfunctions ϕ and ψ are discretized using this technique, and the computation domain is chosen wide enough to capture all the eigen-solutions.

By discretizing the set of ordinary differential equations, the problem reduces to an algebraic eigenvalue problem. A second-order central difference formula is used for the space derivatives. Eigenfunctions are set equal to zero at the boundaries, which are the two boundary conditions being used. The discretized equations are given blow :

The first common equation to all the three cases is :

$$\left[\frac{2}{h_{i+1}(h_i+h_{i+1})}\right]\psi_{i+1}-\left[\frac{2}{h_ih_{i+1}}+k^2-\sigma\right]\psi_i+\left[\frac{2}{h_{i+1}(h_i+h_{i+1})}\right]\psi_{i-1}=\frac{d\bar{c}}{dx}\phi_i\,, \tag{4.43}$$

and the second generalized equation is given below :

$$\begin{aligned}&\left[\frac{2}{h_{i+1}(h_i+h_{i+1})}-F_1\frac{d\bar{c}}{dx}\frac{h_i}{h_{i+1}(h_i+h_{i+1})}\right]\phi_{i+1}-\left[\frac{2}{h_{i+1}h_i}-F_1\frac{d\bar{c}}{dx}\frac{h_i-h_{i+1}}{h_{i+1}h_i}+F_2\right]\phi_i\\&+\left[\frac{2}{h_i(h_i+h_{i+1})}+F_1\frac{d\bar{c}}{dx}\frac{h_{i+1}}{h_i(h_i+h_{i+1})}\right]\phi_{i-1}=-k^2F_1\psi_i\,,\end{aligned} \tag{4.44}$$

where the coefficients F_1 and F_2 are as defined below for the three different cases :

- a Newtonian fluid displacing another Newtonian fluid

$$F_1 = R; \text{ and } F_2 = k^2. \tag{4.45}$$

- a Non-Newtonian fluid displacing a Newtonian fluid

$$F_1 = R - \left(\frac{n-1}{2}\right)\ln\left(1+D_e^2\right), \tag{4.46}$$

and
$$F_2 = k^2\left[1+\bar{c}\left(\frac{n-1}{2}\right)\frac{2D_e^2}{1+D_e^2}\right]. \tag{4.47}$$

- a Newtonian fluid displacing a non-Newtonian fluid

$$F_1 = R + \left(\frac{n-1}{2}\right)\ln\left(1+D_e^2\right), \tag{4.48}$$

and
$$F_2 = k^2\left[1+(1-\bar{c})\left(\frac{n-1}{2}\right)\frac{2D_e^2}{1+D_e^2}\right]. \tag{4.49}$$

A standard 'rg' subroutine is used to solve for the eigenvalues and eigenvectors of the resulting matrix. This subroutine reduces the general real matrix into an upper Hessenberg form in order to solve for the eigenvalues. This 'rg' subroutine is a part of the eigensystem subroutine package 'eispack' available on the Netlib repository on the web. For a domain size of 50, a 80-point mesh converges quickly with the appropriate geometric spacing. The discrete eigenvalues are insensitive to the width of the domain, if the domain is chosen large enough to accommodate the decaying eigenfunctions. Among the set of discrete eigenvalues obtained, the maximum value corresponds to the maximum growth rate for a given wave number. We report only the value of the largest growth rate, since for a given values of the parameters it dominates all other modes.

4.4 Results

Results of the linear stability analysis are presented. First we present the linear stability results for Newtonian displacements and compare with the results of previous studies. Next, we discuss the results obtained for the two different combinations of non-Newtonian fluid displacing Newtonian fluid and Newtonian fluid displacing non-Newtonian fluid.

4.4.1 Newtonian displacements

In Fig. 4.1 dispersion relation is plotted for R = 3 at different times. Since for a given wavenumber, there is a discrete set of eigenvalues, only the maximum value of σ is plotted for which the flow is inherently unstable. It is also seen from figure 4.1 that for a given time, the growth rate is positive for a certain range of wavenumbers and is maximum at a particular value known as the most dangerous wavenumber, k_m. The most dangerous mode and the cutoff wavenumber shift to longer wavelengths with time.

From Fig. 4.2 we see that the magnitude of the growth rate is maximum in the beginning (t = 0) and decreases with time, which is expected since the dispersion acts to spread the profile and the base state changes slowly with time. All these results are in good agreement with those of Tan and Homsy (1986), for a Newtonian fluid displacing another Newtonian fluid. In order to study the effect of mobility ratio on instability, we have shown the instability characteristics for a different mobility ratio, MR = 7.4 (R = 2) in figure 4.3. By comparing the results of Fig. 4.1 and Fig. 4.3, it is clear that the general features and the trends remain the same, only the magnitude of the growth rate increases with the mobility ratio.

It is found that the most dangerous mode k_m is proportional to R, and the maximum value of the growth rate σ_m is proportional to R^2. This observation matches well with the results of Tan and Homsy (1986).

4.4.2 Non-Newtonian fluid displacing Newtonian fluid

Here the case of a non-Newtonian fluid displacing a Newtonian fluid is considered. To study the effects of shear-thinning on the flow stability, we compare the results with the Newtonian displacements for different values of the rheological parameters in the model. For R = 3 and n = 0.2, the effect of the parameter De is shown in Fig 4.4 at time, t = 0.1. As seen from the figure, by increasing De, the growth rate increases making the flow more unstable. The most dangerous mode and the cutoff wavenumber shift to smaller wavelengths with increasing De. For De = 0, the growth rate curve coincides with the Newtonian displacement curve. This is in agreement with the Carreau model, which reduces to the Newtonian model for De = 0.

Fig. 4.5 shows the effect of the power-law index parameter n. It is observed that, a decrease in the parameter leads to a more unstable flow. Again, the most dangerous mode and the cutoff wavenumber shift to smaller wavelengths by decreasing the value of n. This destabilizing effect associated with a decrease in n can also be explained mathematically, in terms of the effective viscosity ratio of the two fluids. Since by decreasing the value of n, the viscosity of the shear-thinning displacing fluid decreases much rapidly leading to higher instability. Again, for n = 1, the curve represents the Newtonian growth rate.

In Fig. 4.9 (a), the most dangerous mode k_m is plotted against the R for a non-Newtonian fluid displacing Newtonian fluid, with parameter values of De = 0.6 and n = 0.2. The most dangerous mode is found to be proportional to R as seen from the figure. From Fig. 4.10 (a) it is concluded that the maximum growth rate of the disturbances σ_m varies as R^2.

4.4.3 Newtonian fluid displacing non-Newtonian fluid

Another combination consisting of a Newtonian fluid displacing a non-Newtonian fluid is studied, and in this case two different trends are observed. Fig. 4.6 shows instability characteristics for R = 3 and n = 0.4, and for different values of De varying between 0.2 and 0.6. From the figure, we see that the growth rate of the disturbances increases slightly for small increments in De, and is always greater than that of a Newtonian displacement. However, there is virtually no significant change in the most dangerous mode, and only a small increase in the cutoff wavenumber. For the same values of R and n, a different trend is observed when flow instability is examined for larger values of the parameter De as shown in Fig. 4.7. The growth rate decreases with increasing De, and becomes less than that of a Newtonian displacement after a certain critical value of the Deborah number ($De_c = 4$, in Fig). It is also seen that both the most dangerous mode and the cutoff wavenumber shift to longer wavelengths. These findings can also be explained in terms of the arguments of viscosity ratios. Since initially the viscosity of the non-Newtonian displaced fluid is higher than the viscosity of the Newtonian fluid, the flow is unstable, and the small increase in De is not enough to decrease the viscosity of the shear-thinning fluid considerably. Thus the growth rate of the disturbances increases with De. Whereas, for large increments in the De (by order of one), the viscosity of the shear-thinning fluid decreases much rapidly making the flow more stable. The effect of the parameter n on the growth rate is plotted in Fig. 4.8. Again a small decrease in n leads to an increase in the growth rate, however there is no significant shift in the cutoff wavenumber and most dangerous mode.

The variation of the most dangerous mode k_m with R is shown in Fig. 4.9 (b) for the case of a Newtonian fluid displacing a non-Newtonian fluid. Again the most dangerous mode varies linearly with R, however, there is a decrease in the magnitude in comparison with the case of a non-Newtonian fluid displacing a Newtonian fluid. In the next Fig. 4.10 (b),

the variation of the maximum growth rate with R^2 follows the same trend observed in the case of a non-Newtonian fluid displacing a Newtonian fluid.

4.5 Summary

The linear stability results of Newtonian displacements agree very well with the results of Tan and Homsy (1986). Results show that any displacement with unfavorable viscosity contrast ($\mu_1 < \mu_2$) is always unstable. We have seen that in the case of a non-Newtonian fluid displacing a Newtonian fluid, the presence of the shear-thinning behavior has a destabilizing effect. The effect of the parameter De and the power-law index n was investigated and it was found that the growth rate of the disturbances increases with decrease in n, and with an increase in De. In the other case of a Newtonian fluid displacing a non-Newtonian fluid the shear-thinning fluid exhibits a stabilizing effect. From the above analysis, we conclude that the presence of a shear thinning fluid in the displacement process, gives rise to quite different interfacial dynamics. There is a need for full nonlinear simulations to obtain the deep understanding and complete details of the flow processes.

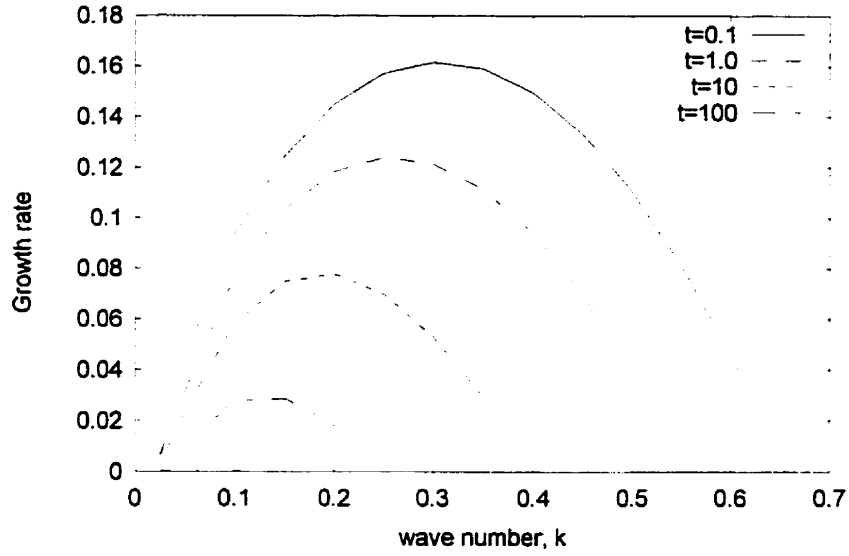

Fig. 4.1 Instability characteristics for R = 3, Newtonian fluid displacing Newtonian fluid.

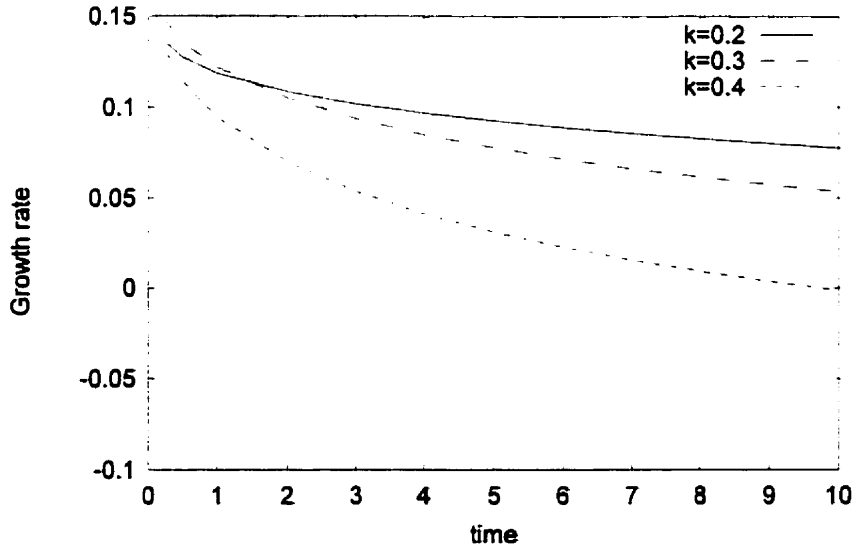

Fig. 4.2 Instability characteristics (growth rate σ vs. time t_0) for R = 3, Newtonian fluid displacing Newtonian fluid.

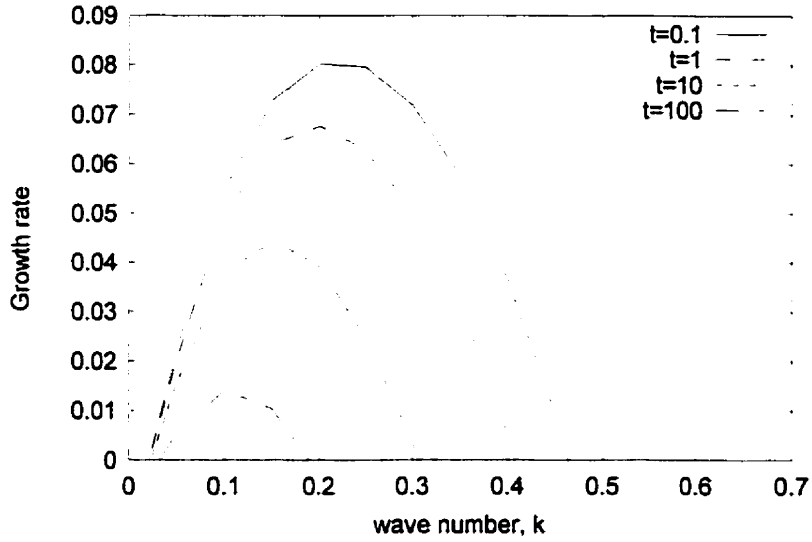

Fig. 4.3 Instability characteristics for R = 2, Newtonian fluid displacing Newtonian fluid.

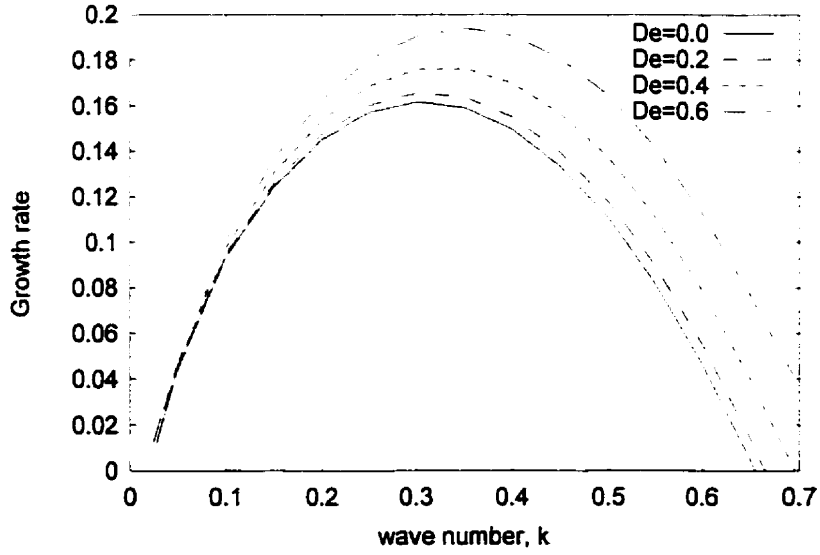

Fig. 4.4 Instability characteristics for R = 3, n = 0.2, t_0 = 0.1, non-Newtonian fluid displacing Newtonian fluid: effect of De.

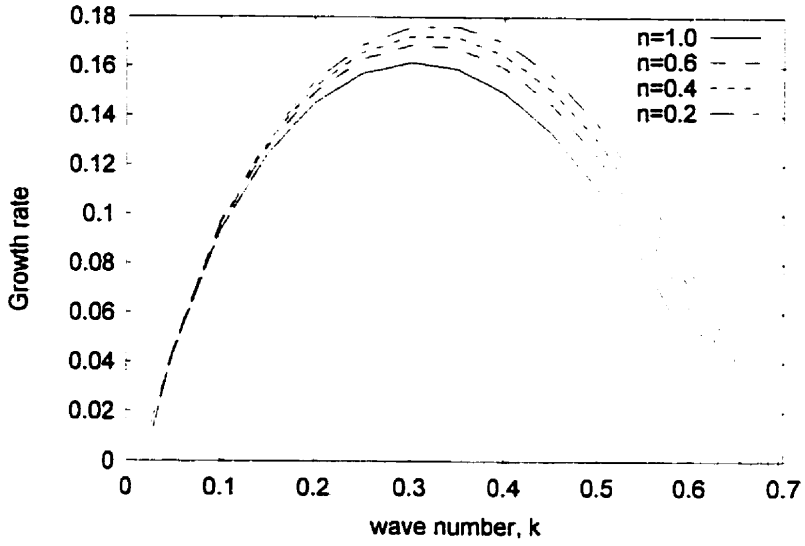

Fig. 4.5 Instability characteristics for R = 3, De = 0.4, t_0 = 0.1, non-Newtonian fluid displacing Newtonian fluid: effect of n.

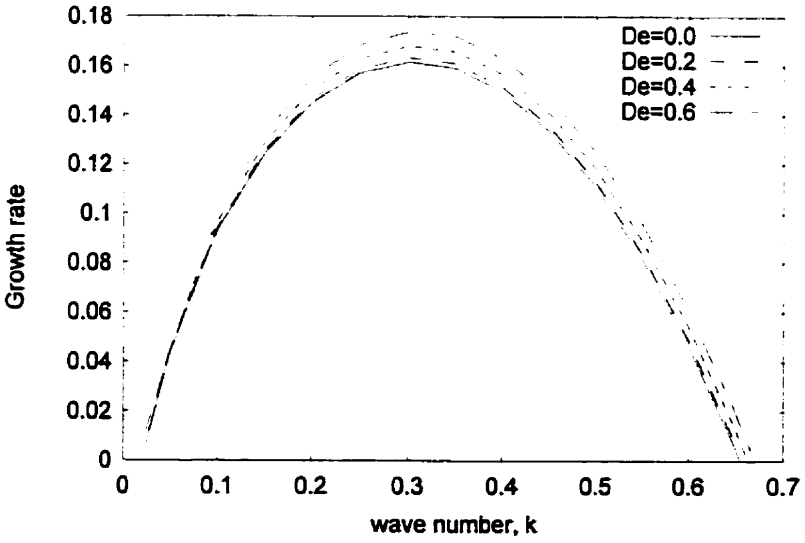

Fig. 4.6 Instability characteristics for R = 3, n = 0.4, t_0 = 0.1, Newtonian fluid displacing non-Newtonian fluid: effect of De.

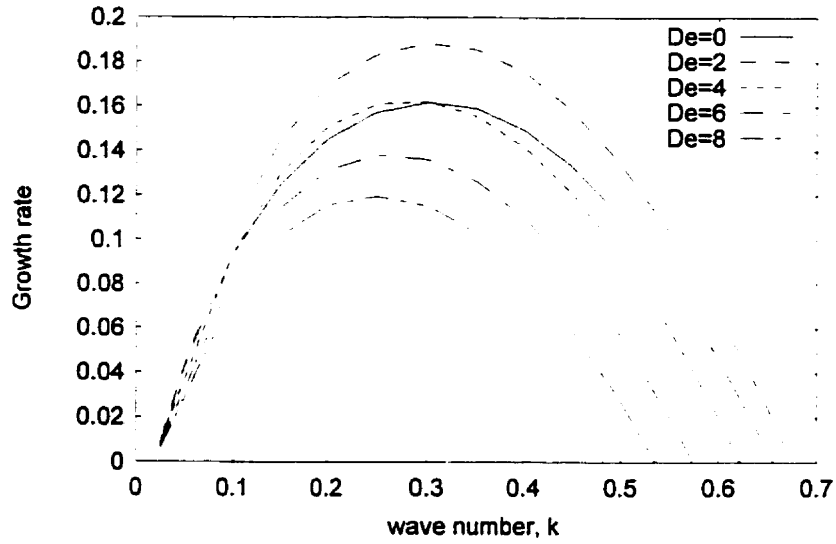

Fig. 4.7 Instability characteristics for R = 3, n = 0.4, t_0 = 0.1, Newtonian fluid displacing non-Newtonian fluid: effect of De.

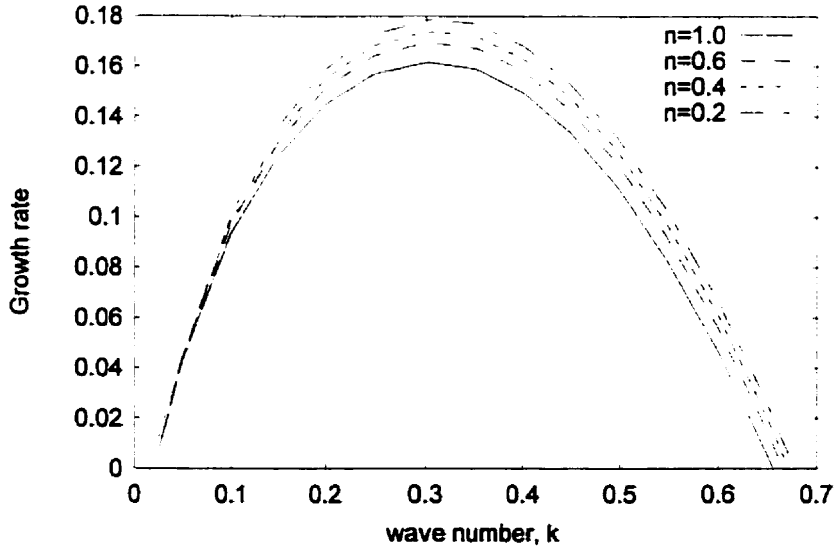

Fig. 4.8 Instability characteristics for R = 3, De = 0.4, t_0 = 0.1, Newtonian fluid displacing non-Newtonian fluid : effect of n.

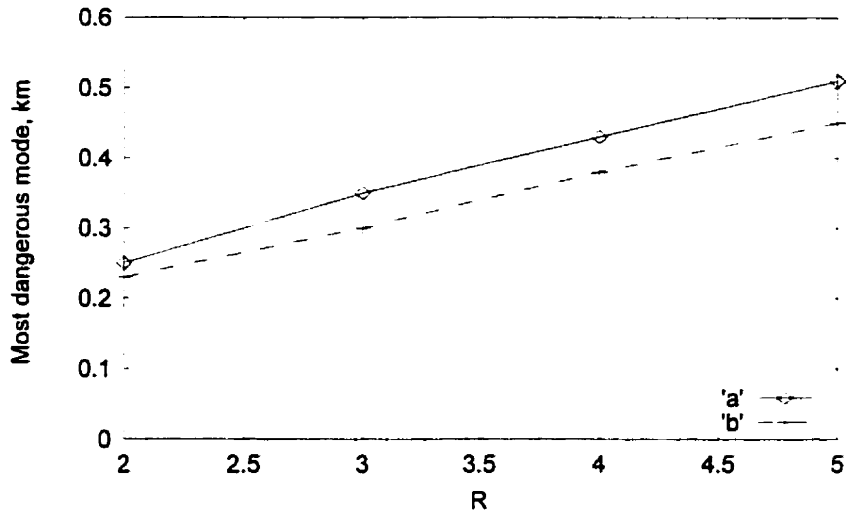

Fig. 4.9 Most dangerous mode, k_m versus R, at $t_0 = 0.1$, De = 0.6, n = 0.2.
(a) Non-Newtonian fluid displacing Newtonian fluid (b) Newtonian fluid displacing non-Newtonian fluid.

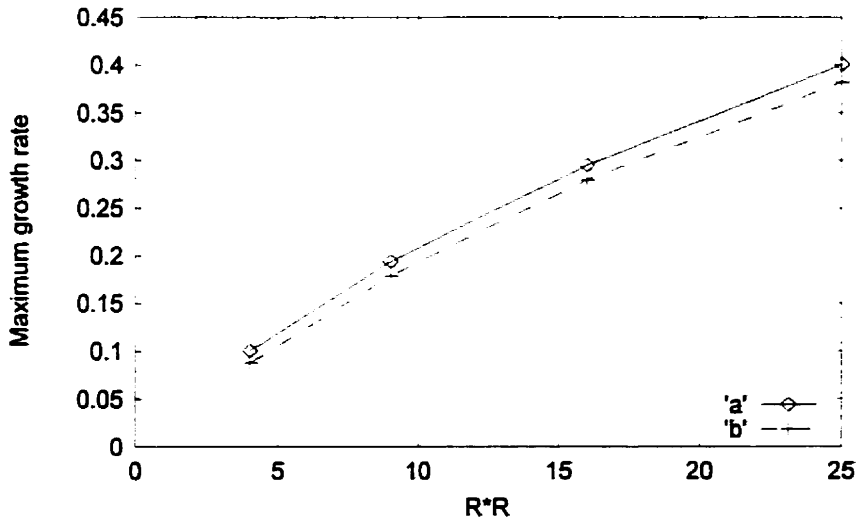

Fig. 4.10 Maximum growth rate, σ_m versus R^2, at $t_0 = 0.1$, De = 0.6, n = 0.2.
(a) Non-Newtonian fluid displacing Newtonian fluid (b) Newtonian fluid displacing non-Newtonian fluid.

CHAPTER 5

NONLINEAR SIMULATIONS

In this chapter the numerical solution technique used to solve the non-linear equations of unstable miscible displacements in a rectilinear Hele-Shaw cell is described. This numerical technique consists of a combination of spectral and finite difference methods. A brief description of the Hartley transform is given. The equations are presented in the transformed space, and the computational algorithm is discussed, together with the appropriate initial conditions. Results of the nonlinear simulations are presented for different values of the parameters of the flow, and compared with existing results for pure Newtonian displacements.

5.1 Introduction

In this work, one of the very powerful tools for numerical calculations, known as the spectral method has been used to simulate the nonlinear viscous fingering. This method has been widely used in fluid mechanics, and the details of the implementation of the method can be found in the work of Hussaini and Zang (1986) as well as in the book of Canuto et al. (1987). In some earlier numerical works dealing with the problem of viscous fingering, the finite difference method was used, but revealed to have some disadvantages that limit the scope of its application. First, the finite difference method often requires very large storage size and computation time, thus limiting the domain and number of grid points. Second, the numerical dispersion introduced into the system might be larger than the physical dispersion which forces the fingers to damp out. Another problem associated with the finite difference method is the treatment of nonlinear terms, and a

fully implicit scheme is required to eliminate that. On the other hand, the advantages of the spectral methods are :

1. The spatial derivatives are computed to a high degree of accuracy.
2. Physical dispersion can be resolved even for large domain size, without the complications of false numerical dispersion.
3. For N modes, this method involves $N \log N$ operations, which is much less than the finite difference method.

5.2 Numerical Method

In this section we present a full description of the numerical technique, including the boundary conditions and the scheme for the time advancement of the solution. The convergence and accuracy of the nonlinear solutions are also discussed in brief.

5.2.1 Hartley Transform

The Fourier transform is one of the most important mathematical tools in science and engineering and is widely used by mathematicians and engineers in the solution of differential, integral, and other equations. The Hartley transform is similar to the Fourier transform, and the difference is explained below.

The continuous time Fourier transform of a function $g(t)$ defined in a domain τ, is :

$$F(s) = \int_{\epsilon\tau} g(t)\left[\cos(2\pi st) + i\sin(2\pi st)\right]dt, \tag{5.1}$$

which in general is a real to complex transform. A similar real to real transform, known as the Hartley transform is defined as :

$$H(s) = \int_{\epsilon\tau} g(t)\left[\cos(2\pi st) + \sin(2\pi st)\right]dt. \tag{5.2}$$

Many of the properties and applications of the Hartley transform are similar to those of the Fourier transform. With this definition, the two-dimensional discrete Hartley transform is given by :

$$H\langle g(x,y)\rangle = \hat{G}(k_x,k_y) = \frac{1}{\sqrt{N_x N_y}}\sum_x\sum_y g(x,y)cas\left(\frac{2\pi x k_x}{N_x}+\frac{2\pi y k_y}{N_y}\right), \qquad (5.3)$$

where N_x and N_y are the number of collocation points, and k_x and k_y are the wave numbers in the x and y directions respectively. The cas is "cosine and sine" function, which is the sum of the cosine and sine of its argument x :

$$\text{cas}(x) = \cos(x) + \sin(x). \qquad (5.4)$$

Throughout this study, the transform of a function will be written in cap letters. The Hartley transform is easy to invert, and has been successfully used by Zimmerman and Homsy, (1991) in their simulations.

The transform of the derivatives of a function can be easily computed by using the Hartley transform derivative theorem :

$$H\left\langle\frac{\partial}{\partial x}g(x,y)\right\rangle = -2\pi k_x\hat{G}(-k_x,-k_y), \qquad (5.5)$$

$$H\left\langle\frac{\partial}{\partial y}g(x,y)\right\rangle = -2\pi k_y\hat{G}(-k_x,-k_y), \qquad (5.6)$$

$$H\left\langle\frac{\partial^2}{\partial x^2}g(x,y)\right\rangle = -4\pi^2 k_x{}^2\hat{G}(k_x,k_y), \qquad (5.7)$$

$$H\left\langle\frac{\partial^2}{\partial y^2}g(x,y)\right\rangle = -4\pi^2 k_y{}^2\hat{G}(k_x,k_y), \qquad (5.8)$$

$$H\left\langle\frac{\partial^2}{\partial x\partial y}g(x,y)\right\rangle = -4\pi^2 k_x k_y\hat{G}(k_x,k_y). \qquad (5.9)$$

5.2.2 Initial and boundary conditions

The Hartley transform method requires periodic boundary conditions in the variables of the problem. As seen in chapter 3, the boundary conditions are periodic in the transverse direction y, but in the x direction periodicity of the concentration poses a problem. One method to apply periodic conditions for the concentration in the x direction consists of doubling the domain size through a reflection at the right boundary x = L. Tan and Homsy (1988) and Zimmerman and Homsy (1991) used this approach in their simulations. This method of doubling the domain makes the problem computationally more expensive.

In this work another approach has been used to handle the concentration periodicity in the x direction, and was first suggested by Manickam and Homsy (1993) in their formulation. The total concentration at any time in the space is expressed as :

$$c(x,y,t) = \bar{c}(x,t_0) + c'(x,y,t)\,, \tag{5.10}$$

where $\bar{c}(x,t_0)$ is the solution of the one-dimensional convective-diffusion equation, given as :

$$\bar{c}(x,t_0) = \frac{1}{2}\left[1 - erf\left(x/\sqrt{4t_0}\right)\right]. \tag{5.11}$$

Therefore, instead of solving for the total concentration, we solve only for the disturbance concentration c' and then the total concentration can be obtained from equation (5.10). The disturbance concentration c' is zero at both boundaries $x = 0$, and $x = P_e$, which makes the concentration periodic in the x direction. By solving for the disturbance concentration c' instead of the total concentration, the need for doubling the domain is avoided, which makes the method computationally more efficient. The simulations are stopped well before the fingers reach the other streamwise boundary. The new periodic boundary conditions in the x direction are :

$$(\mathbf{u},c')(0,y,t) = (\mathbf{u},c')(P_e,y,t)\,. \tag{5.12}$$

With the total concentration expressed as the disturbance plus the base state, the convective-diffusion equation developed in chapter 3 is reformulated as shown below :

$$\frac{\partial \bar{c}}{\partial t}+\frac{\partial c'}{\partial t}+\frac{\partial \psi}{\partial y}\left(\frac{\partial \bar{c}}{\partial x}+\frac{\partial c'}{\partial x}\right)-\frac{\partial \psi}{\partial x}\frac{\partial c'}{\partial y}=\frac{\partial^2 \bar{c}}{\partial x^2}+\frac{\partial^2 c'}{\partial x^2}+\frac{\partial^2 c'}{\partial y^2}. \quad (5.13)$$

Since the base state concentration $\bar{c}$ satisfies :

$$\frac{\partial \bar{c}}{\partial t}=\frac{\partial^2 \bar{c}}{\partial x^2}, \quad (5.14)$$

equation (5.13) can be written as :

$$\frac{\partial c'}{\partial t}=-J+\frac{\partial^2 c'}{\partial x^2}+\frac{\partial^2 c'}{\partial y^2}, \quad (5.15)$$

where

$$J=\frac{\partial \psi}{\partial y}\left(\frac{\partial \bar{c}}{\partial x}+\frac{\partial c'}{\partial x}\right)-\frac{\partial \psi}{\partial x}\frac{\partial c'}{\partial y}. \quad (5.16)$$

The nonlinear term N in the vorticity formation equation becomes :

$$N=\frac{\partial \psi}{\partial x}\left(\frac{\partial \bar{c}}{\partial x}+\frac{\partial c'}{\partial x}\right)+\frac{\partial \psi}{\partial y}\frac{\partial c'}{\partial y}+\frac{\partial c}{\partial y}. \quad (5.17)$$

In the above equation, ψ is the stream function which is related to the vorticity through the equation (3.28) given in chapter 3.

The initial condition used for the concentration profile needs to be discussed in detail. We introduce random disturbance of very small magnitude in the base state concentration, at the interface in the y direction . A mathematical description of the initial condition is :

$$c(x,y,t=t_0)=\bar{c}(x,t_0)+\delta*rand(y)*\exp(-x^2/\sigma^2), \quad (5.18)$$

where δ is the magnitude of the disturbance, *rand* is a random number between -1 and 1, σ is a parameter that determines the penetration of the disturbance from the front, t_0 is the initial time at which the base state is considered and determines the diffusive character of the front. The parameters δ, σ, and t_0 all are small relative to unity, and the choice of

these variables determines the qualitative nature of the front. The use of random numbers as small perturbation allows to include the whole spectrum of wavenumbers. In all what follows, for convenience the primes will be dropped from the disturbance terms.

5.2.3 Simulation advancement in time

Once the problem has been formulated in terms of the streamfunction and vorticity, we are left with three variables c, ψ, and ω to be determined at each step. First, all equations are recast into the transform space using the discrete Hartley transform. Let us denote by $\hat{c}_{m,n}$, $\hat{\psi}_{m,n}$ and $\hat{\omega}_{m,n}$ the discrete fast Hartley transform of the real values of the concentration disturbance c, the streamfunction ψ and the vorticity ω, at the collocation points x_m and y_n defined as :

$$\begin{aligned} x_m &= (m/N_x)P_e; \quad m = 0,1,2,.....N_x - 1, \\ y_n &= (n/N_y)P_e/A; \quad n = 0,1,2,.....N_y - 1. \end{aligned} \tag{5.19}$$

After applying the discrete Hartley transform, the equations for the concentration and the vorticity-streamfunction relationship are written as :

$$\frac{d\hat{c}_{m,n}}{dt} = -\hat{J}_{m,n} - (k_m^{\,2} + k_n^{\,2})\hat{c}_{m,n}, \tag{5.20}$$

$$(k_m^{\,2} + k_n^{\,2})\hat{\psi}_{m,n} = \hat{\omega}_{m,n}, \tag{5.21}$$

where $$k_m = 2\pi m/P_e, \text{ and } k_n = 2\pi n/(P_e/A). \tag{5.22}$$

In the above equations, we have used the derivative theorem discussed earlier (Eqs. 5.5 - 5.9). The treatment of the convective term J will be discussed later.

The vorticity relations for the three different cases under consideration in the real space are :

(i) Newtonian fluid displacing Newtonian fluid :

$$\hat{\omega}_{m,n} = -R\hat{N}_{m,n}, \tag{5.23)a}$$

(ii) Non-Newtonian fluid displacing Newtonian fluid :

$$\hat{\omega}_{m,n} = \hat{O}_{m,n} + \hat{M}_{m,n} - R\hat{N}_{m,n}, \tag{5.23)b}$$

(iii) Newtonian fluid displacing non-Newtonian fluid

$$\hat{\omega}_{m,n} = \hat{L}_{m,n} - \hat{O}_{m,n} - \hat{M}_{m,n} - R\hat{N}_{m,n}. \tag{5.23)c}$$

The nonlinear terms are expressed in real space as :

$$J = \frac{\partial \psi}{\partial y}\left(\frac{\partial \bar{c}}{\partial x} + \frac{\partial c}{\partial x}\right) - \frac{\partial \psi}{\partial x}\frac{\partial c}{\partial y}, \tag{5.24}$$

$$N = \frac{\partial \psi}{\partial x}\left(\frac{\partial \bar{c}}{\partial x} + \frac{\partial c}{\partial x}\right) + \frac{\partial \psi}{\partial y}\frac{\partial c}{\partial y} + \frac{\partial c}{\partial y}, \tag{5.25}$$

$$P = \left(\frac{n-1}{2}\right)\ln\left(1 + D_e{}^2 V^2\right), \tag{5.26}$$

$$L = \frac{(n-1)D_e{}^2}{1 + D_e{}^2 V^2}\left[\left(\frac{\partial \psi}{\partial x}\right)^2 \frac{\partial^2 \psi}{\partial x^2} + \left(\frac{\partial \psi}{\partial y} + 1\right)^2 \frac{\partial^2 \psi}{\partial y^2} + 2\frac{\partial \psi}{\partial x}\left(\frac{\partial \psi}{\partial y} + 1\right)\frac{\partial^2 \psi}{\partial x \partial y}\right], \tag{5.27}$$

$$M = PN, \tag{5.28}$$

$$O = c_T L, \tag{5.29}$$

where $$V^2 = \left(\frac{\partial \psi}{\partial x}\right)^2 + \left(\frac{\partial \psi}{\partial y}\right)^2 + 2\frac{\partial \psi}{\partial y} + 1, \tag{5.30}$$

and c_T is the total concentration, calculated by adding up the base state and disturbance concentration at a given time.

Since the Hartley transform of the product of two functions is not the product of the Hartley transform of these two functions, one has to be careful in determining the Hartley transform of the above nonlinear terms. The strategy we followed consists of determining the nonlinear term in the real space and then taking the Hartley transform. This approach is used to determine the values of the above nonlinear terms given by equations (5.24) - (5.30), in the transform space.

It is clear that equations (5.21) and (5.23) are algebraic equations, while equation (5.20) is a first-order differential equation in time. In order to solve this ordinary differential equation and advance the concentration in time, a second-order Adams-Bashforth predictor-corrector technique is used. An operating splitting algorithm is used to solve equation (5.20). First the nonlinear terms are integrated to get the provisional values of the concentration. The linear (dispersion) operator is then applied to these provisional values to predict the concentration at the next time. A semi-implicit correction scheme is used to correct for the concentration. Then, equations (5.23) and (5.21) are used to update the vorticity and streamfunction.

Applying Adams-Bashforth method to the convective terms only in Eq. (5.20) :

$$\frac{\tilde{c}_{m,n}(t+\Delta t)}{\Delta t} = -\left(\frac{3}{2}\hat{J}_{m,n}(t) - \frac{1}{2}\hat{J}_{m,n}(t-\Delta t)\right), \tag{5.31}$$

then the concentration is predicted as :

$$\bar{c}_{m,n}(t+\Delta t) = \tilde{c}_{m,n}(t+\Delta t)e^{-\left(k_m^2+k_n^2\right)\Delta t}, \tag{5.32}$$

where Δt is the time step. From the above predicted value of the concentration, the updated vorticity $\bar{\omega}_{m,n}(t+\Delta t)$ is calculated using equation (5.23). The updated streamfunction $\bar{\psi}_{m,n}(t+\Delta t)$ is then easily determined using equation (5.21), and the nonlinear term J is determined in real space using equation (5.24) and transformed to obtain $\bar{J}_{m,n}(t+\Delta t)$. The solution is corrected by the trapezoidal rule to get the correct value of the concentration at the next time interval :

$$\begin{aligned}\frac{\hat{c}_{m,n}(t+\Delta t)-\hat{c}_{m,n}(t)}{\Delta t} = &-\left(\frac{\bar{J}_{m,n}(t+\Delta t)+\hat{J}_{m,n}(t)}{2}\right) \\ &-(k_m^2+k_n^2)\left(\frac{\bar{c}_{m,n}(t+\Delta t)-\hat{c}_{m,n}(t)}{2}\right).\end{aligned} \tag{5.33}$$

The above correction-evaluation scheme is iterated many times to make this method as semi-implicit as desired, which ensures a more accurate time stepping. A detailed computational algorithm of the above solution technique is given below :

1. Start with the initial values of $\hat{c}_{m,n}(t)$, and $\hat{\psi}_{m,n}(t)$.
2. Compute $\hat{N}_{m,n}(t)$, $\hat{P}_{m,n}(t)$, $\hat{L}_{m,n}(t)$, $\hat{M}_{m,n}(t)$, $\hat{O}_{m,n}(t)$ using Eqs. (5.25) - (5.29).
3. Compute $\hat{\omega}_{m,n}(t)$ using Eq. (5.23).
4. Compute $\hat{J}_{m,n}(t)$ using Eq. (5.24).
5. Predict $\bar{c}_{m,n}(t+\Delta t)$ using second order Adams-Bashforth, Eq. (5.32).
6. Compute $\bar{\omega}_{m,n}(t+\Delta t)$, $\bar{\psi}_{m,n}(t+\Delta t)$, and $\bar{J}_{m,n}(t+\Delta t)$.
7. Apply correction scheme to get $\hat{c}_{m,n}(t+\Delta t)$ using Eq. (5.33).
8. Take inverse transform to get the real $c_{m,n}(t+\Delta t)$.
9. Go to 6 and iterate for desired number of times.
10. Exit iteration loop, go to 4 compute the values at next time step, and march forward in time.

5.2.4 Convergence and accuracy

The numerical scheme is semi-implicit and second order in time. The most time consuming step is the transformation of variables between the real space and the Hartley space. The simulations are to be halted before the fingers reach the other boundary, which is a constraint in this numerical scheme. Typically, 256×256 modes were used in the simulations for high values of the Peclet number Pe and the parameter R. Since the scheme is not fully implicit in time, simulations occasionally show numerical instability at high values of R and P_e, for a given spatial resolution and time step. The correction-evaluation scheme was iterated 2 to 5 times depending on the values of the Peclet number. The simulations were repeated for the same parameter values, but with different grid size and time step, to study the convergence properties of the solution. The

simulation time for a typical run with 256×256 modes, and a time step of 5×10^{-2} is approximately 600 minutes on a DIGITAL DEC Alpha (600au) workstation.

5.3 Results and discussion

In all the simulations, we start with random disturbances of small magnitude δ in the transverse direction at the interface, with typical values of δ of the order of 0.01. As it will be shown later in the figures, all disturbances quickly develop into fingers which grow with different mechanisms in time. The simulations are stopped before fingers reach the other boundary of the system.

First the nonlinear simulation results are compared with our linear stability analysis. In the next subsections, various mechanisms for the evolution of fingers are given, and new observed mechanisms are discussed in detail. One of the most important parameters in these simulations is R which is related to the mobility ratio. We remind the reader of the expressions of the parameter R in the three cases under consideration :

- Newtonian fluid displacing Newtonian fluid, $R = \ln \frac{\mu_2}{\mu_1}$; where μ_2 and μ_1 are the viscosities of the displaced and the displacing fluid respectively.
- Non-Newtonian fluid displacing Newtonian fluid, $R = \ln \frac{\mu_2}{\mu_0}$; where μ_2 is the viscosity of the displaced fluid, and μ_0 is the zero-shear viscosity of the displacing fluid.
- Newtonian fluid displacing non-Newtonian fluid, $R = \ln \frac{\mu_0}{\mu_1}$; where μ_1 is the viscosity of the displacing fluid, and μ_0 is the zero-shear viscosity of the displaced fluid.

5.3.1 Comparison with the linear theory

Results of different non-linear simulations are presented here for the three different combinations of Newtonian and non-Newtonian fluids. In Fig. 5.1 the variation of the base-state is shown with time, which is also a solution of the one-dimensional

convective-diffusion equation. Clearly the flow is stable for this case when R = 0 (MR = 1). Initially, the base state is a step profile and it diffuses with time due to the dispersion. Comparison of the initial growth rate between the full simulations and quasi-steady-state theory is done and results are presented in this section. First we do a quantitative comparison and next a qualitative comparison is made. A nonlinear simulation was conducted for the case of a non-Newtonian fluid displacing a Newtonian fluid with R = 3, De = 0.2, and n = 0.2. In order to compare the nonlinear simulation results with linear stability theory, we introduce the concentration perturbations of a single mode in the transverse direction at a given base state time t_0. The average growth rate of discrete modes is computed at early time using the energy method and compared with the linear stability results. Fig. 5.2 shows the comparison of the growth rate between the nonlinear simulation and linear stability theory for a discrete set of wavenumbers at time $t_0 = 20$. It is seen from the figure that the nonlinear simulation results follow the same trend, with lower growth rate values than the corresponding linear stability results. This difference is due to the fact that in linear stability analysis, quasi-steady-state approximation is applied which assumes a steady base state concentration profile at time t_0. While in nonlinear simulations the base state concentration profile changes with time and dispersion acts to stabilize the displacement.

In all the nonlinear simulation results, concentration contours are plotted between the values of 0.1 and 0.6 with increments of 0.1. Two simulations were carried out to study and analyze the effects of shear-thinning behavior on the flow instability, and the concentration contours are shown in Fig. 5.3. Both simulations were conducted for the same geometric parameter values of Pe = 500, A = 4, and with a mobility ratio MR = 1. It is clear from the concentration contours shown at t = 800, that in the first case of a Newtonian fluid displacing another Newtonian fluid the flow is stable. In the second case of a non-Newtonian fluid displacing a Newtonian fluid the flow is unstable and fingering starts to develop even though the mobility ratio is 1. This observation can be explained by the fact that for a displacement involving Newtonian fluids the mobility ratio remains the

same as viscosity does not change with flow. On the other hand, the viscosity of the non-Newtonian displacing fluid decreases with shear rate which in turn increases the mobility ratio leading to an unstable flow. Thus the shear-thinning nature of non-Newtonian fluids plays an important role in the flow processes.

Fig. 5.4 and 5.5 describe the effect of varying the parameter De on the flow stability for two different cases of a non-Newtonian fluid displacing a Newtonian fluid and a Newtonian fluid displacing a non-Newtonian fluid respectively. By increasing the value of De, the instability decreases in the case of a Newtonian fluid displacing non-Newtonian fluid as seen in Fig. 5.4 (a) - (c). Results of a different simulation with non-Newtonian fluid displacing Newtonian fluid show increased instability with De, as illustrated in Fig. 5.5 (a) - (c). These nonlinear simulation results are in agreement with the linear stability theory [Figs. 4.4, 4.7].

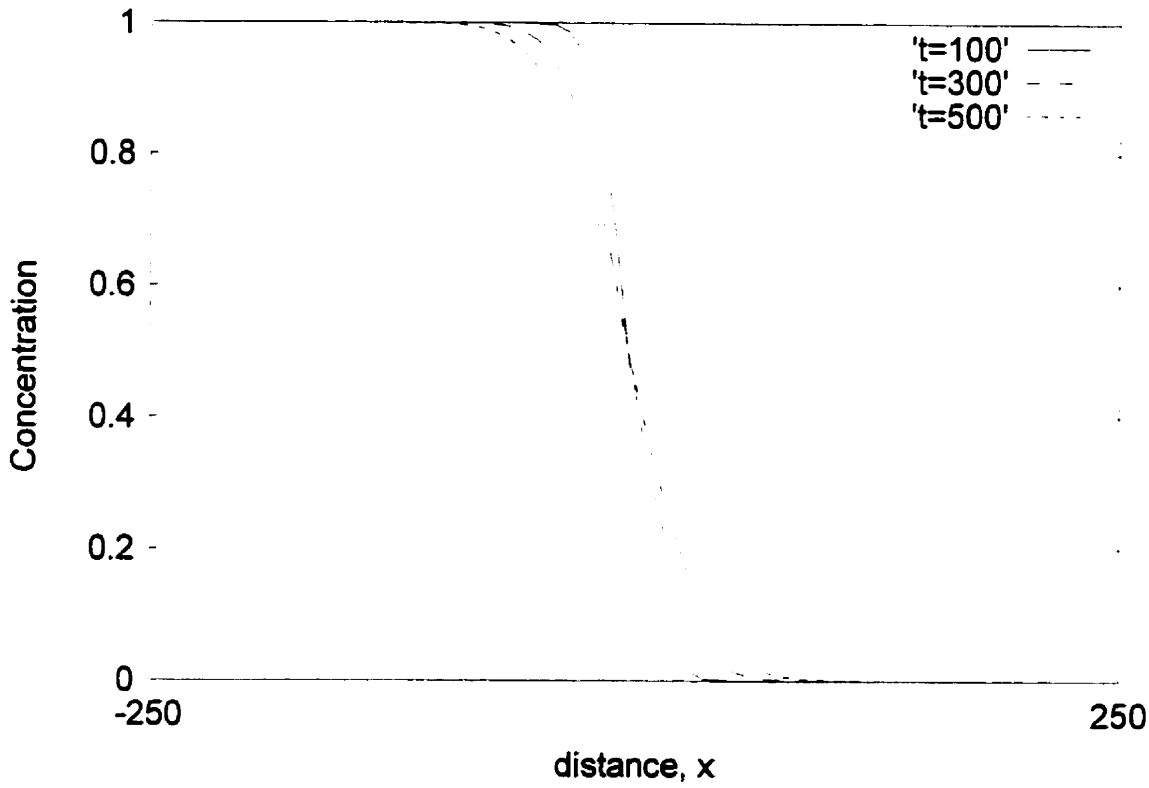

Fig. 5.1 Base state concentration profile : one-dimensional convection-diffusion equation.

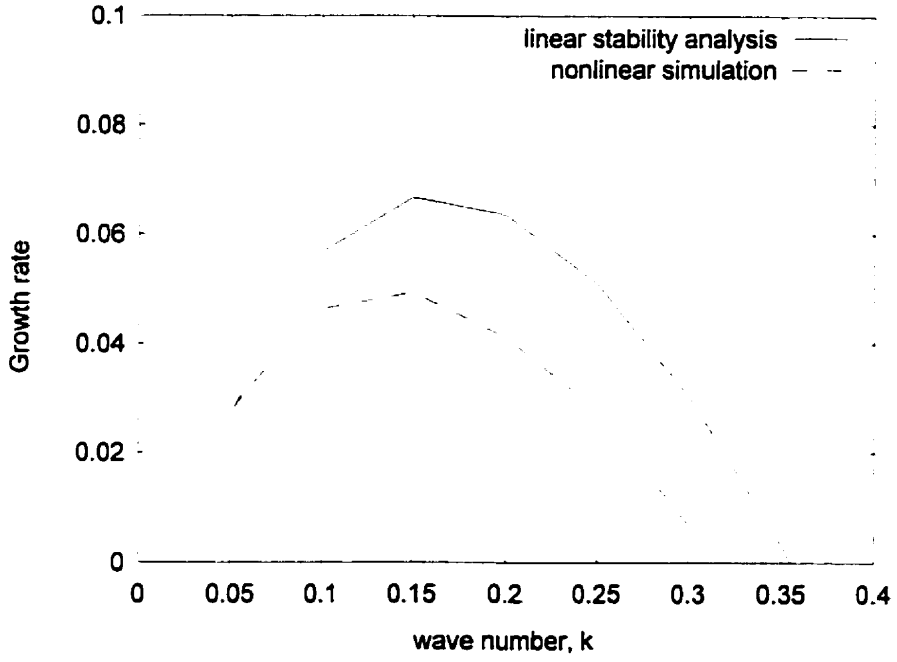

Fig. 5.2 Comparison of the initial growth rate between the nonlinear simulation and the linear stability theory at $t_0 = 20$.

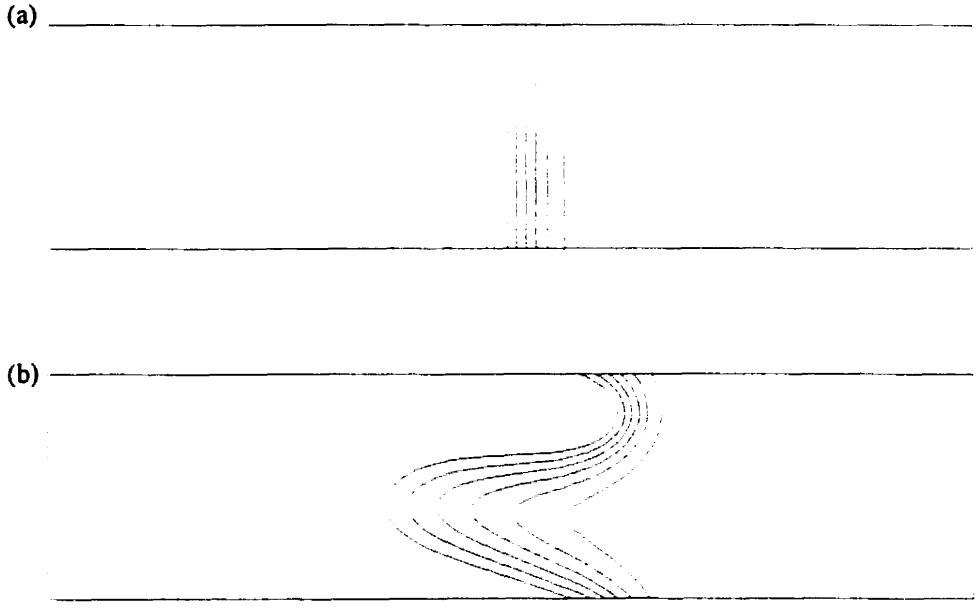

Fig. 5.3 Concentration contours (between 0.1-0.6, with increments of 0.1) of a simulation at time t = 800, for Pe = 500, A = 4, R = 0 : effects of shear-thinning on stability. (a) Newtonian fluid displacing Newtonian fluid, (b) Non-Newtonian fluid displacing Newtonian fluid De = 3, n = 0.5

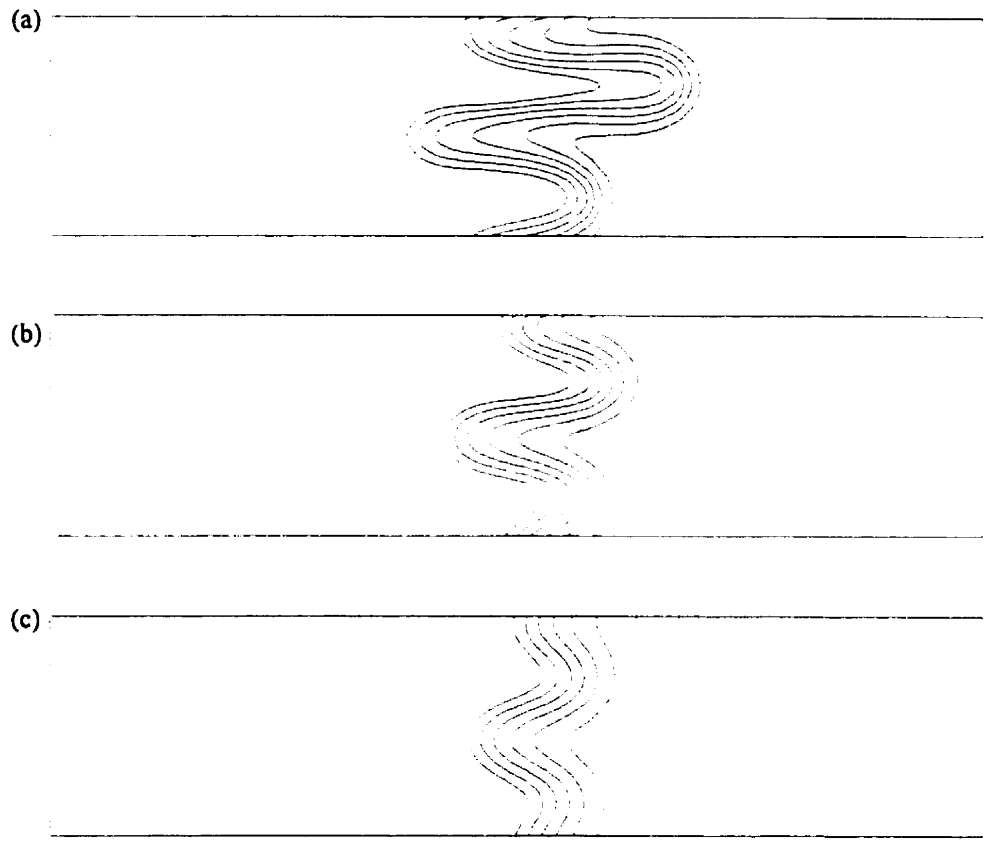

Fig. 5.4 Concentration contours (between 0.1-0.6, with increments of 0.1) of a simulation for R = 2, Pe = 500, A = 4, n = 0.5 and t = 400. Newtonian fluid displacing non-Newtonian fluid : effect of De on stability. (a) De = 1, (b) De = 3, (c) De = 4

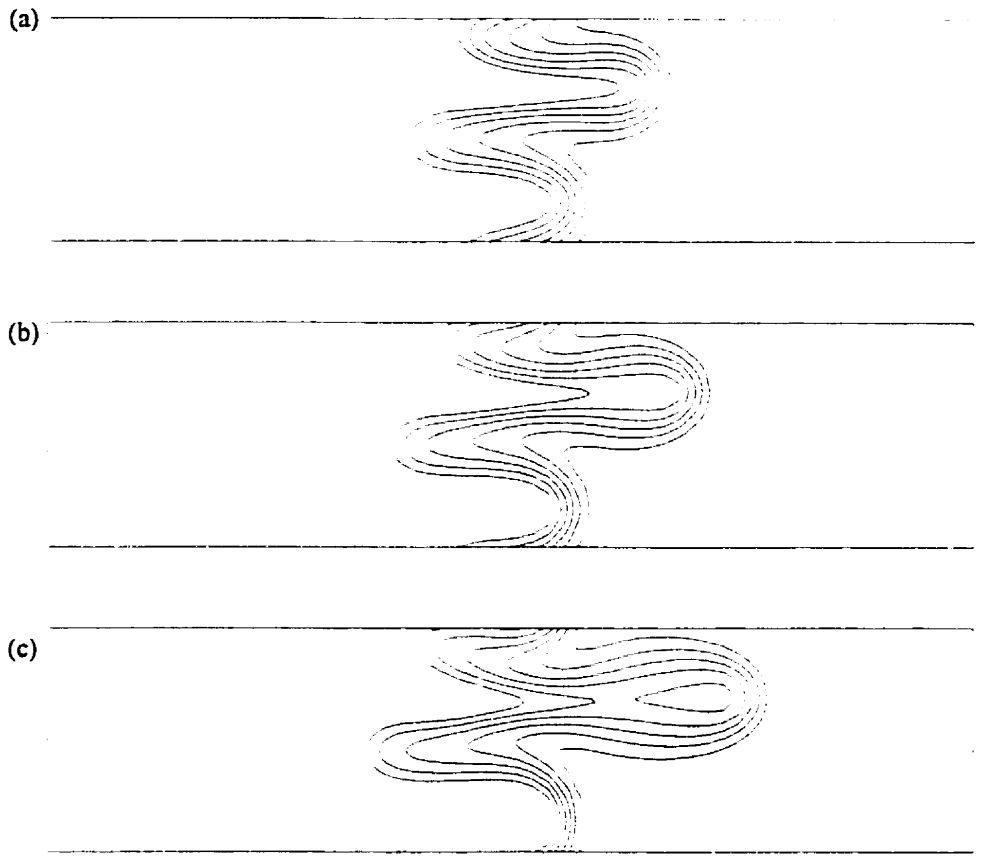

Fig. 5.5 Concentration contours (between 0.1-0.6, with increments of 0.1) of a simulation, for R = 2, Pe = 500, A = 4, n = 0.5 and t = 400. Non-Newtonian fluid displacing Newtonian fluid : effect of De on stability. (a) De = 0.2, (b) De = 0.5, (c) De = 0.8

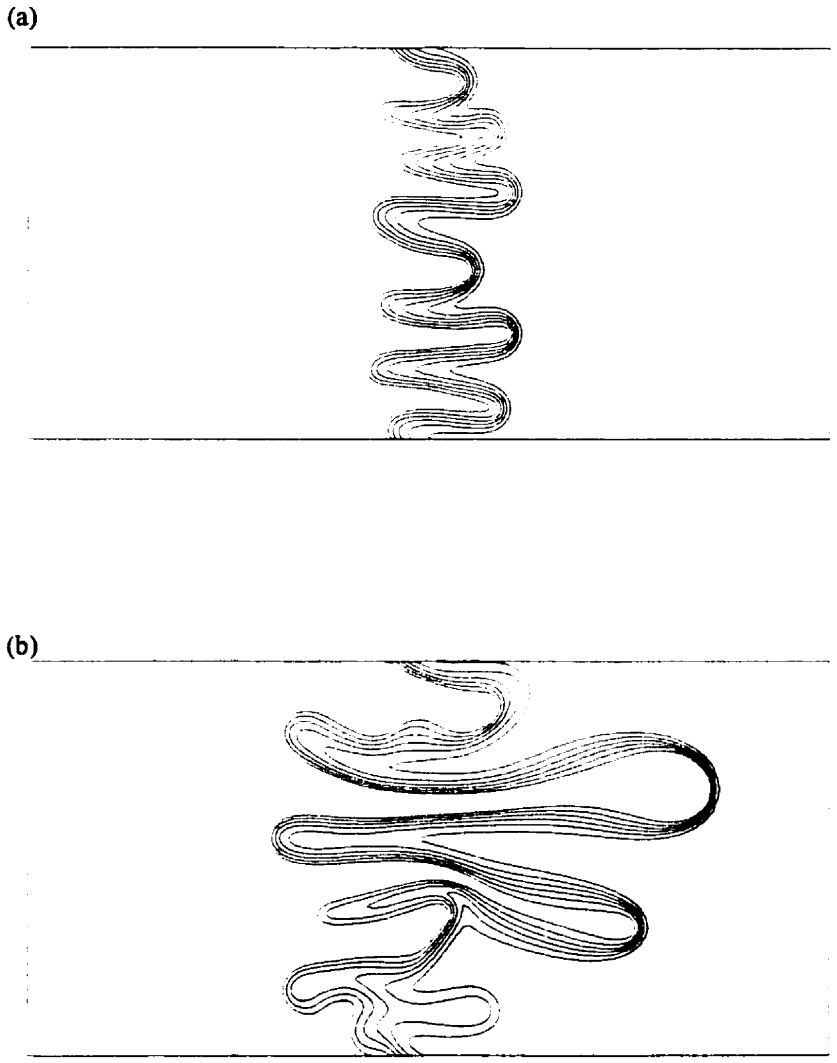

Fig. 5.6 Concentration contours (between 0.1-0.6, with increments of 0.1) of a simulation for Pe = 1000, A = 2, at time t= 500. Newtonian fluid displacing Newtonian fluid : effect of mobility ratio. (a) R = 2, (b) R = 3.

5.3.2 General features of nonlinear fingering

In this section, our objective is to study the nonlinear fingering mechanisms in a rectilinear Hele-Shaw cell. First, we will present the results for pure Newtonian displacements. Comparison with results of earlier studies is used as a first check to validate the numerical code we have developed for this study. Next we focus on the displacement of a Newtonian fluid by a non-Newtonian fluid, and analyze the fingering mechanisms and patterns observed from the different simulation results. These results will be contrasted with what is usually observed in the case of pure Newtonian fluids.

5.3.2.1 Newtonian displacements

The effect of the mobility ratio on stability is presented in Fig. 5.6. Two simulations were carried out with different mobility ratios R = 2 (MR = 7.39) and R = 3 (MR = 20.09) and results are shown in Fig. 5.6 (a) and (b) respectively. As expected the instability increases with an increase in the mobility ratio, which was also seen from linear stability analysis [Figs. 4.1, 4.3].

A time evolution of the fingers is presented in Fig. 5.7 for the case of a Newtonian fluid displacing another Newtonian fluid. This simulation was conducted for Pe = 1000, A = 1, and R = 3. A careful examination of the patterns reveals that initially (t = 200) there is a large number of small fingers. At later times the fingers become wider and their number decreases. Although the development of these fingers is a complex phenomena, there are certain fingering mechanisms which explain the evolution and growth of these fingers. Some of these mechanisms observed in Fig. 5.7 have already been reported in the isotropic simulations of Tan and Homy (1988) and the anisotropic simulations of Zimmerman and Homsy (1991).

Spreading : It is seen from the simulation result of Fig. 5.8 that fingers change their horizontal scale and become wider. This mechanism is referred to as spreading.

Shielding : In the process of shielding [frame t = 200, Fig. 5.7], one finger noses ahead of the neighboring finger by shielding its growth. As the shielding finger grows, the concentration gradient steepens between the finger and the surrounding viscous fluid, resulting in a wider and longer finger.

Fading : This phenomena was first reported by Zimmerman and Homsy (1991) in their anisotropic simulations, and was not seen in the isotropic simulations of Tan and Homsy (1988). However, it has been observed in our isotropic simulations as well [frame t = 400, Fig. 5.7]. Sometimes, a moving finger prefers to flow through the adjacent finger, which is less viscous than the phase II fluid. This finger fades in the concentration of the neighboring finger, which moves ahead.

Coalescence : This mechanism was first reported by Zimmerman and Homsy (1991) in their anisotropic simulations, and later they observed it in the isotropic simulations as well [Zimmerman and Homsy, 1992]. Fig. 5.7 shows two good examples of coalescence in the frame t = 300 and 400 respectively. In this process, the tip of a finger merges into the body of the adjacent finger. The concentration gradients smooth out as it mixes within the adjacent finger, finally forming a long and wider finger. By this mechanism, much of the more viscous fluid is quickly and easily bypassed by the less viscous displacing fluid. In their experiments, Slobod and Thomas (1963) observed this mechanism using x-ray technique.

To study the effects of the parameter A on the fingering pattern, another simulation was conducted with the same values of the parameter Pe and R, and a different aspect ratio A = 4. The resulting concentration contours are shown in Fig. 5.8. Finger evolution takes place through the same mechanisms discussed earlier, however the number of fingers has decreased in comparison with the previous result for A = 1 (Fig. 5.7). Thus the aspect ratio has a direct effect on the number of fingers developing at the interface. Again the

shielding, coalescence, and fading is observed and the number of fingers decreases with time.

5.3.2.2 Non-Newtonian fluid displacing Newtonian fluid

We conducted a simulation for a non-Newtonian fluid displacing a Newtonian fluid with parameter values of Pe = 1000, A = 4, R = 3, De = 0.4, and n = 0.5. The resulting time evolution of fingers is shown in Fig. 5.9. The initial time evolution of the fingers is similar to what has been described earlier. Initially there is a large number of small fingers and this number decreases as the fingers merge and coalesce together. Aside from the various mechanisms observed in the previously described Newtonian displacements, a spectacular tip-splitting of the finger is observed. This tip-splitting was first reported by Tan and Homsy (1988) in their isotropic simulations involving Newtonian fluids, and was later observed by Zimmerman and Homsy (1991) in their anisotropic simulations as well. Among the experimental studies involving Newtonian fluids, this mechanism was observed in miscible displacements by Wooding (1969), and in immiscible displacements by Park and Homsy (1985), Kopf-Sill and Homsy (1988), and recently by Kawaguchi et al. (1997). From our simulation results in the case of Newtonian displacements, this tip splitting phenomena seems to be grid sensitive, and disappears with very fine grid spacing. A physical explanation of the mechanism of tip-splitting is given below :

Tip-splitting : The front of the finger spreads wide enough to allow more than two waves to grow. At the same time because of the cross-flow, the concentration gradients at the tip becomes very steep, which enhances the growth rate of the disturbances and the tip splits. In tip-splitting, the flow field near the front stretches and becomes steep.

A coalescence of different nature is observed in the frame t = 500 of Fig. 5.9. Here, initially the tip of the merging finger bends into the body of the adjacent finger but it does not dissolve and forms a smooth long finger as we have seen in the Newtonian simulation. As observed, the tip of the finger bends into the adjacent finger, however the

remaining of the body flattens and as a result it does not accelerate the growth of the adjacent finger. It can be concluded from the above two sets of simulations that not only the patterns of the fingers are different, but also the evolution takes place through different mechanisms.

In the simulation results to follow, in addition to the fingering mechanisms that have been observed in Newtonian displacements, new mechanisms and finger shapes are observed. A simulation was conducted for Pe = 1200, A = 4, and R = 3 with rheological parameters values of De = 0.5, n = 0.3 and the contours are shown in Fig. 5.10. The instability starts to develop at t = 200 in the form of small fingers. As seen from the figure, finger evolution takes place through different mechanisms observed in the previous simulations. Eventually [frame t = 500] a long uniform horizontal finger is formed. When value of the parameter De was increased from 0.5 to 0.7 in the previous simulation the resulting contours are shown in Fig. 5.11. By the time t = 300, the front of one finger spreads wider and concentration gradients become steep at the tip resulting in a tip-splitting instability. Now, it is to be noted from the figure that the finger which has undergone tip-splitting is not symmetrical and horizontal but is slightly tilted downwards. As a result, the concentration gradient becomes steeper on the upper side of the finger. Thus the upper side of the finger stretches with cross-flow and becomes unstable, allowing the disturbances to grow more quickly. This allows more disturbance waves to grow on the upper side leading to a branching pattern formation, and as seen from the time frames the diagonal movement of the finger continues. We refer to this mechanism as *side-branching*. In frame t = 400, a trailing lobe forms at the root of the branched finger. Now, because of the shear-thinning nature of the displacing fluid, the viscosity of the fluid drops down which enhances the front movement leaving the more viscous trailing lobe behind, in the surrounding fluid. Later the lobe quickly diffuses in the surrounding fluid [frame t = 500]. This mechanism which will be referred to as *trailing-lobe-detachment*, was also observed in the simulations of Rogerson and Meiburg (1993) for Newtonian displacements with tangential shearing.

Concentration contours of another simulation are shown in Fig. 5.12. This simulation, again corresponds to a non-Newtonian fluid displacing a Newtonian fluid for Pe = 1400, A = 5, De = 0.7, n = 0.3. The development of the fingering patterns is similar to what has been described in the previous simulation. However, if we compare with Fig. 5.11, it is observed that the instability starts to develop earlier. This is due to the increase in the value of De from 0.6 to 0.7, Since by increasing the value of De, the shear-thinning is observed earlier. The mechanism of the time evolution of fingers is same as explained in the previous paragraph. Side-branching along with diagonal fingering is observed. The corresponding shear-rate contours are presented in Fig. 5.13. From this figure, it is seen that the main shear occurs along the body of the finger, directed diagonally downward. Initially [frame t = 300], there is substantial amount of shear along the branches of the unstable finger. Later, due to the mixing within the body of the finger, the concentration gradient flattens and as a result most of the shear is directed along the main body of the finger [frame t = 500]. This is one of the reasons of the fading of some of the side branches as seen in the figure 5.12. It is observed from the different set of results, that this fading of the side branches is decided by the degree of the inclination. In Fig. 5.12 the unstable finger is diagonally more inclined than the previous result (Fig. 5.11). As a result, the concentration gradient at the front of the finger becomes very steep allowing the disturbances to grow much faster. This fast growth at the tip, draws some of the less viscous fluid from the root of the finger and fading of the branches takes place.

As presented earlier, the growth and shape of the developing fingers is affected by the presence of the shear-thinning fluid. The shear-thinning fluid is characterized by two rheological parameters of the model, De and n. Now we would like to illustrate the effect of these parameters on the fingering mechanisms. Two simulations were carried out for this purpose with parameter values of De = 0.6, n = 0.5 and De = 0.6, n = 0.2. The corresponding simulation results are presented in Figs. 5.14 and 5.15 respectively. In the first case, horizontal smooth fingers are formed as seen from Fig. 5.14. In frame t = 550, a tip-splitting of the finger has taken place, and no side instability is observed. The two

splitted tips of the finger grow in a very uniform manner forming smooth long fingers. Frame t = 650, presents a very good example of the mechanism of coalescence. However, in the second case, presented in Fig. 5.15 the fingering patterns are entirely different. The dynamics of the interface changes when the rate of shear-thinning is increased from n = 0.5 to n = 0.2 while keeping De constant. In frame t = 250 we see that one finger has spread wide enough to allow tip-splitting and at the same time it is inclined downward. Again this diagonal movement of the finger induces a shear at a certain angle making the concentration gradient steeper on the upper side. The upper side of the finger becomes unstable, and the finger grows diagonally downward. This results in a side-branched, diagonal finger. Beside the mechanism of side-branching one also observes the fading of the smaller fingers. In frame t = 250, there are smaller fingers below the wider finger which have almost faded by the time t = 550. A lob detachment is observed in frame t = 450, which later disappears by diffusing in the phase I. From a close comparison of the above two simulation results, it is concluded that the power-law index n of the shear-thinning curve, is one the parameters that are responsible for the transition from horizontal symmetric, to diagonal, side-branching pattern formation.

5.3.3 Single wavelength simulations

In this section we focus on studying the growth rate of disturbances of a single mode. In all the simulation results in this section, two periods are shown in the y direction for a complete display of the unstable finger. To study this we conducted a simulation with parameter values Pe = 1200, A = 4, and R = 3 by introducing the concentration perturbations of a single mode ($k_m = 0.36$) in the transverse direction at the interface. This wavenumber corresponds to the maximum growth rate as predicted by the linear stability characteristic curve in Fig. 5.16. This simulation is characterized by a very interesting instability development at the interface, as shown in Fig. 5.17. This figure presents an example where the growth rate of the disturbance is very fast which results into a tip-splitting at a much earlier time [frame t = 250]. Fingers have developed both in

diagonally upward and downward directions, where the upper diagonal finger becomes more unstable, and side-branching is observed. The tip of the upper diagonal finger further splits into two, with upper side-branching is observed on the lower branch. We will refer to this phenomena as *multiple side-branching*.

Next, we studied the shear-thinning effects of the non-Newtonian fluid in terms of the rheological parameters De and n. This was achieved by conducting simulations for different values of De and n at a given wavenumber k = 0.18. First we present the simulation results (Figs. 5.18 - 5.20) showing the effects of parameter n on the development of instability, while keeping parameter De constant. In these simulations we fixed the parameters Pe = 1200, A = 4, R = 3, De = 0.7 and varied the n between 0.3 to 0.6. For small values of the power-law index (n = 0.3), in which case the effects of shear-thinning are more pronounced, the flow is more unstable as shown in Fig. 5.18. This figure shows a very good example of both lower and upper side-branching. This observation can also be explained similarly to the one side-branching mechanism. From frame t = 300, we have a symmetric long finger which has spread wide enough to allow the tip-splitting. The peculiarity of this tip-slitting is that the tips are not smooth and horizontal, they are slightly directed upward and downward. This movement of the tips generates the shear in two different directions, making the concentration gradients steeper on the lower side of the upper finger and on the upper side of the lower finger. As the disturbances on the sides of the fingers grow, the fingers continue to grow and split resulting in a side-branching phenomena. Eventually [frame t = 450] we have two side-branched opposite diagonal fingers. Next in Fig. 5.19 simulation results are presented for a higher value of n = 0.4. As it is clear from the concentration contours, the flow is less unstable in comparison with the previous simulation for n = 0.3. One diagonal finger is formed with upper side-branching. In Fig. 5.20 the results are shown for n = 0.6. As expected the flow becomes less and less unstable with increasing values of n (weak shear-thinning). A horizontal smooth finger is formed which exhibits a tip-splitting at later times t = 450.

To further investigate the effects of shear-thinning, we carried out two different simulations with such combinations of De and n which represent a close shear-thinning behavior. One such combination is shown in Fig. 5.21 for De = 0.7, n = 0.6 and De = 0.5, n = 0.5. From the shear-thinning curve, both sets of parameters have almost the same viscosity variation with shear rate. The corresponding simulation results are as shown in figures 5.20 and 5.22 respectively. A close comparison of the two results reveals that in both cases the fingering patterns match very well throughout the simulation. From these results it can be concluded that it is the nature of the shear-thinning which decides the instability development at the interface between the two fluids. Any combination of the two rheological parameters De and n which gives the same shear-thinning behavior will lead to a similar evolution of the fingers.

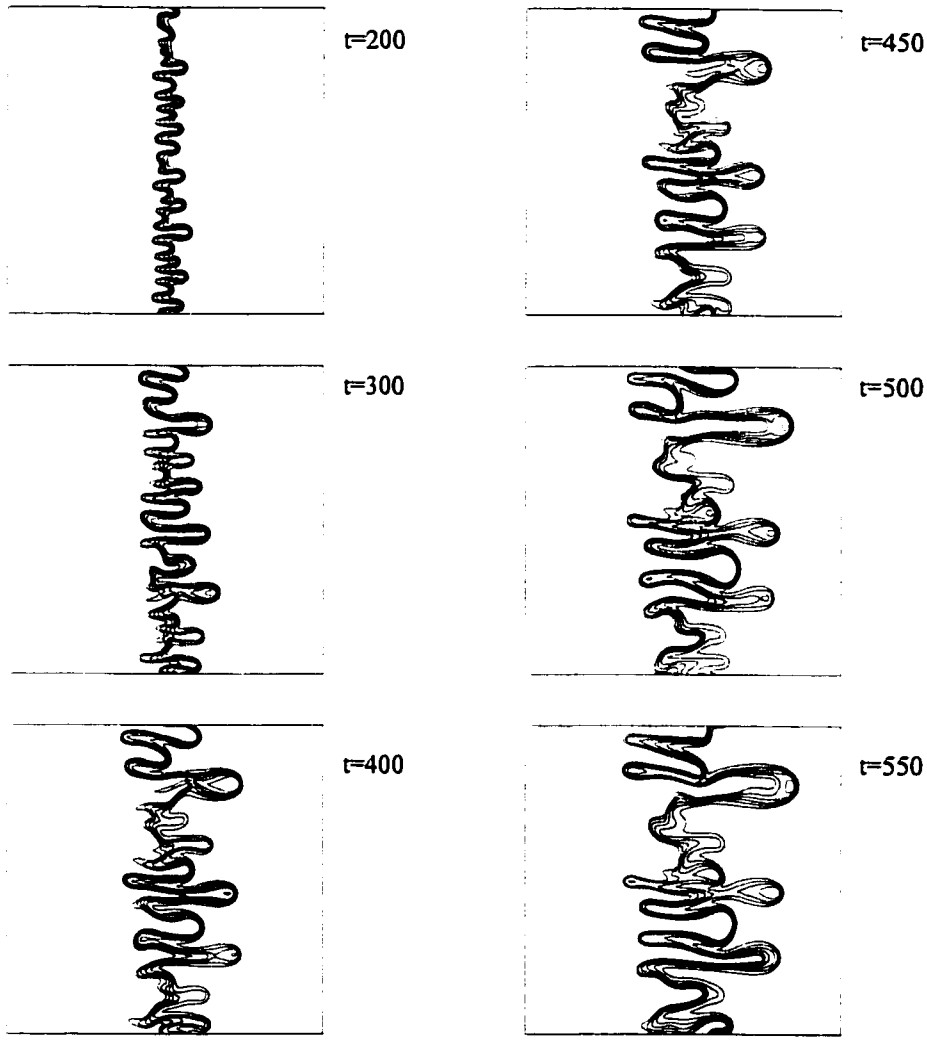

Fig. 5.7 Concentration contours (between 0.1-0.6, with increments of 0.1) of a simulation for Pe = 1000, A = 1, R = 3. Newtonian fluid displacing Newtonian fluid.

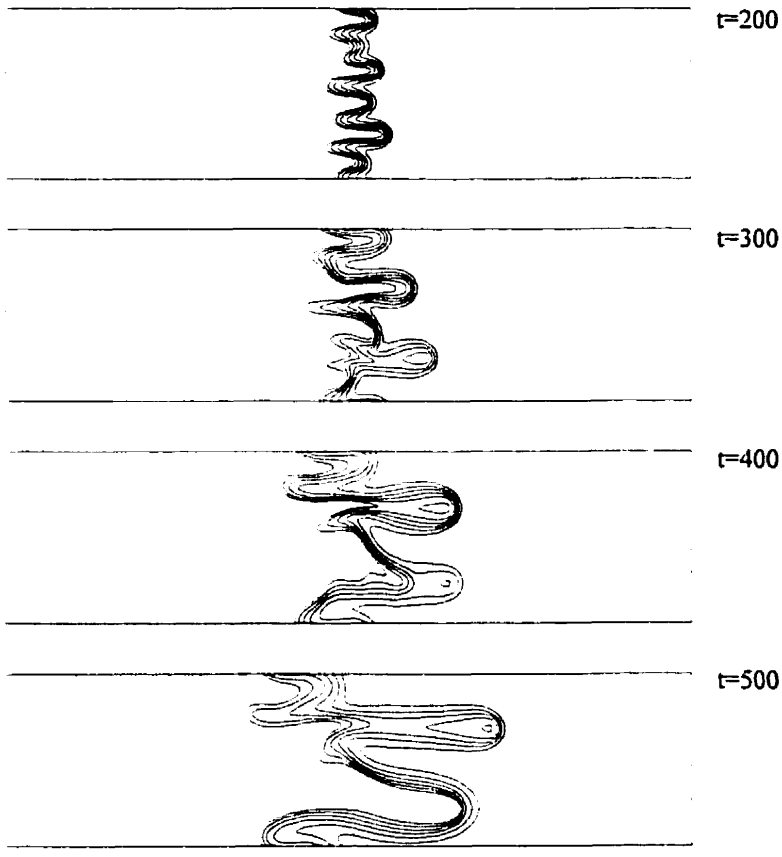

Fig. 5.8 Concentration contours (between 0.1-0.6, with increments of 0.1) of a simulation for Pe = 1000, A = 4, R = 3. Newtonian fluid displacing Newtonian fluid.

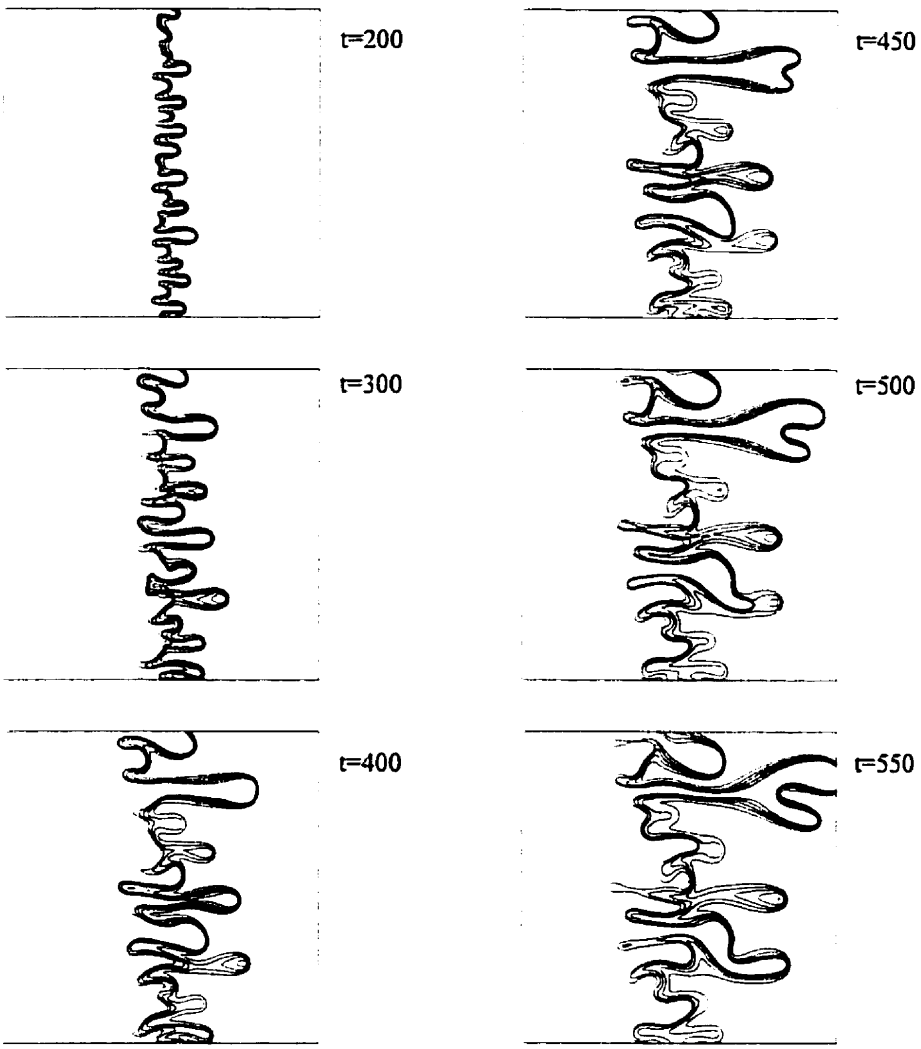

Fig. 5.9 Concentration contours (between 0.1-0.6, with increments of 0.1) of a simulation for Pe = 1000, A = 1, R = 3, De = 0.4, n = 0.5. Non-Newtonian fluid displacing Newtonian fluid.

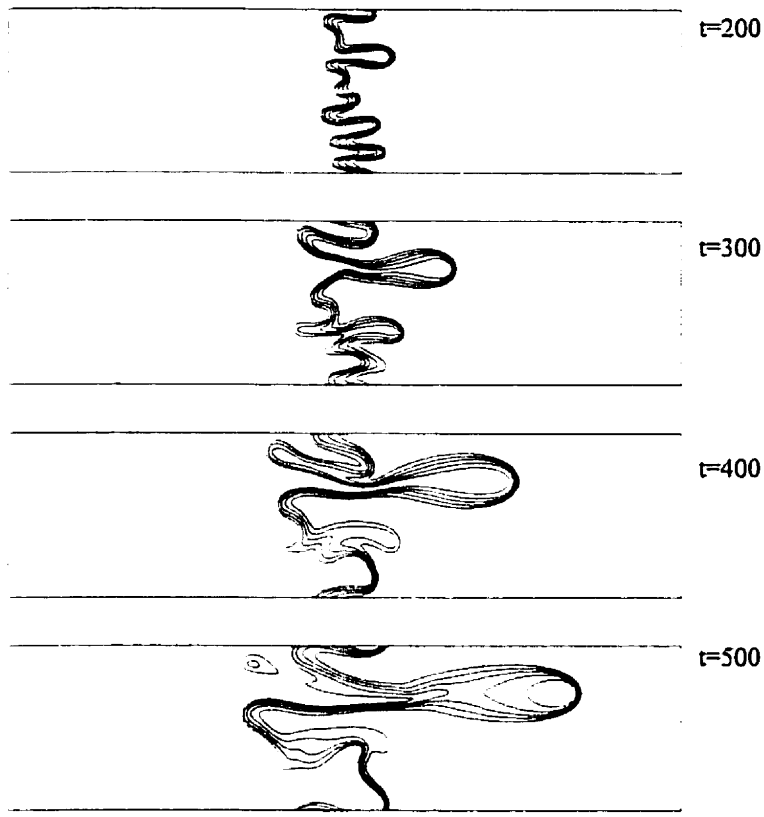

Fig. 5.10 Concentration contours (between 0.1-0.6, with increments of 0.1) of a simulation for Pe = 1200, A = 4, R = 3, De = 0.5, n = 0.3. Non-Newtonian fluid displacing Newtonian fluid.

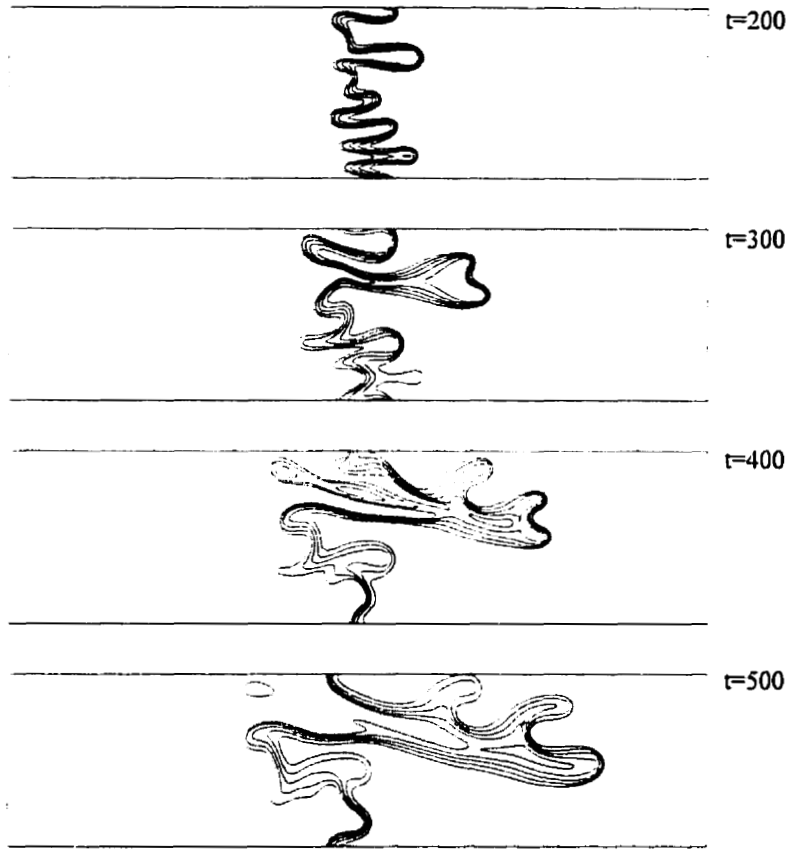

Fig. 5.11 Concentration contours (between 0.1-0.6, with increments of 0.1) of a simulation for Pe = 1200, A = 4, R = 3, De = 0.7, n = 0.3. Non-Newtonian fluid displacing Newtonian fluid.

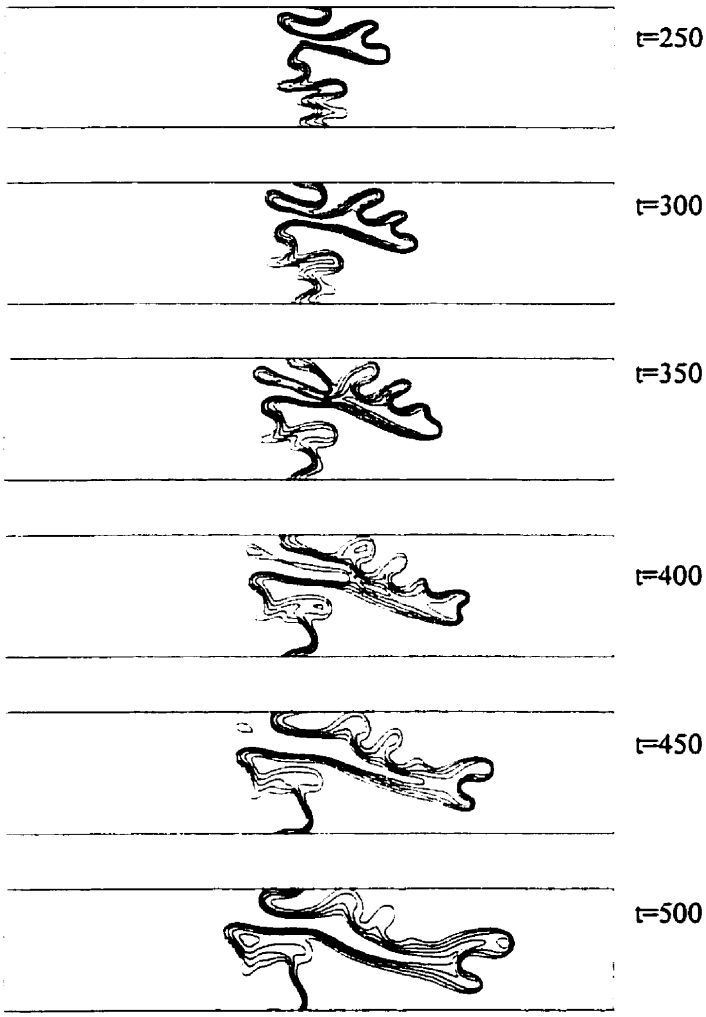

Fig. 5.12 Concentration contours (between 0.1-0.6, with increments of 0.1) of a simulation for Pe = 1400, A = 5, R = 3, De = 0.7, n = 0.3. Non-Newtonian fluid displacing Newtonian fluid.

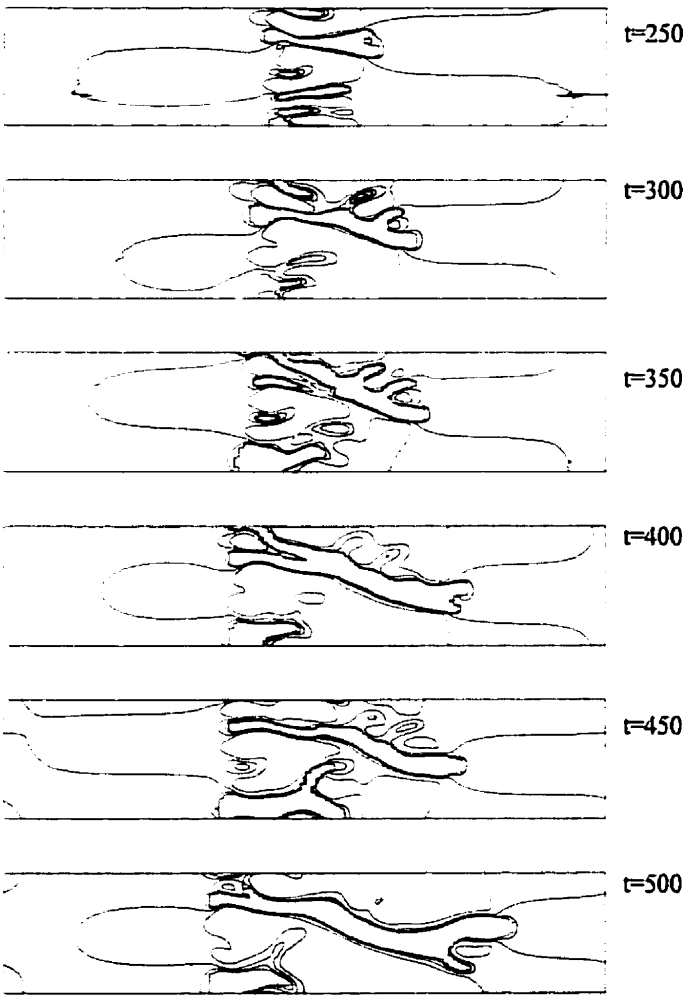

Fig. 5.13 Shear rate contours (between 0.1-0.6, with increments of 0.1) of a simulation for Pe = 1400, A = 5, R = 3, De = 0.7, n = 0.3. Non-Newtonian fluid displacing Newtonian fluid.

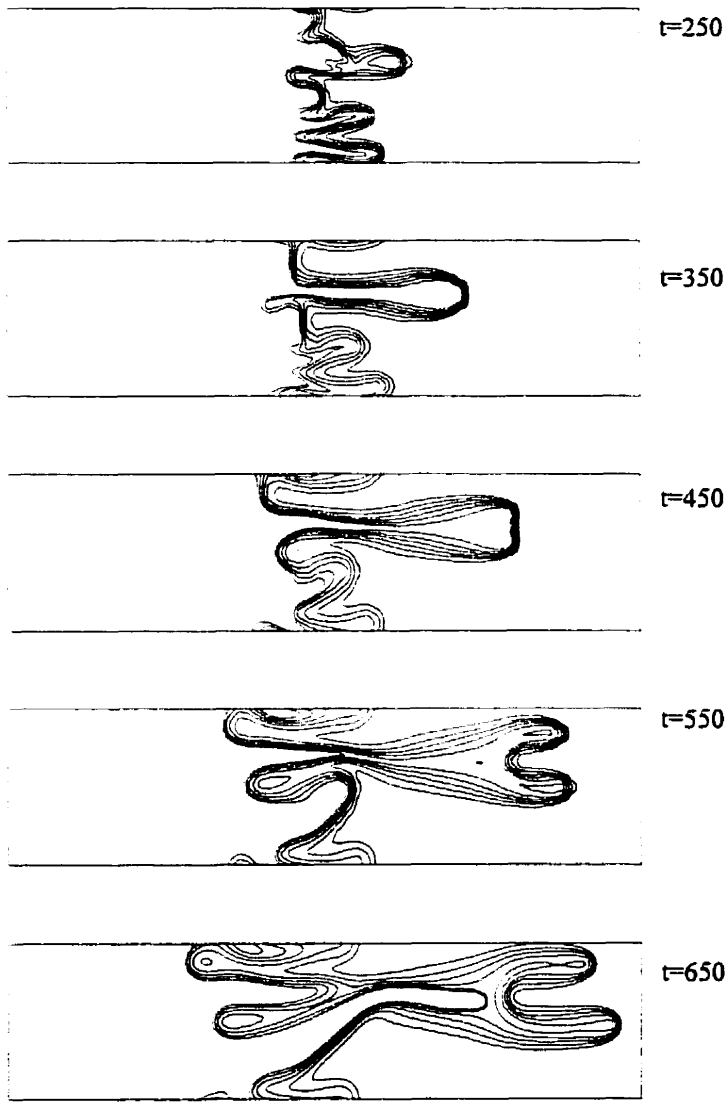

Fig. 5.14 Concentration contours (between 0.1-0.6, with increments of 0.1) of a simulation for Pe = 1200, A = 4, R = 3, De = 0.6, n = 0.5. Non-Newtonian fluid displacing Newtonian fluid.

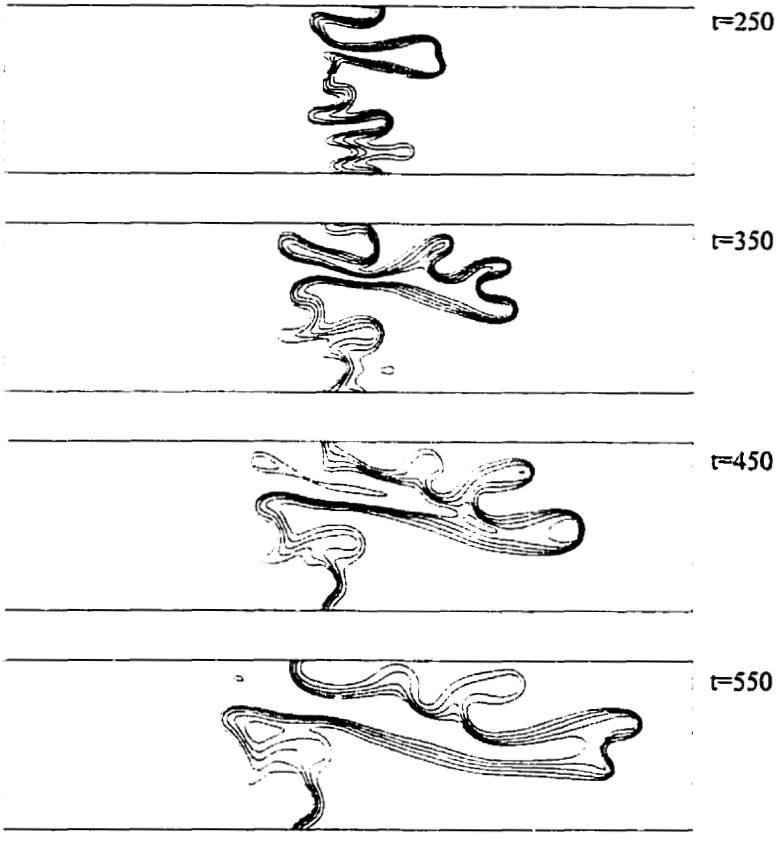

Fig. 5.15 Concentration contours (between 0.1-0.6, with increments of 0.1) of a simulation for Pe = 1200, A = 4, R = 3, De = 0.6, n = 0.2. Non-Newtonian fluid displacing Newtonian fluid.

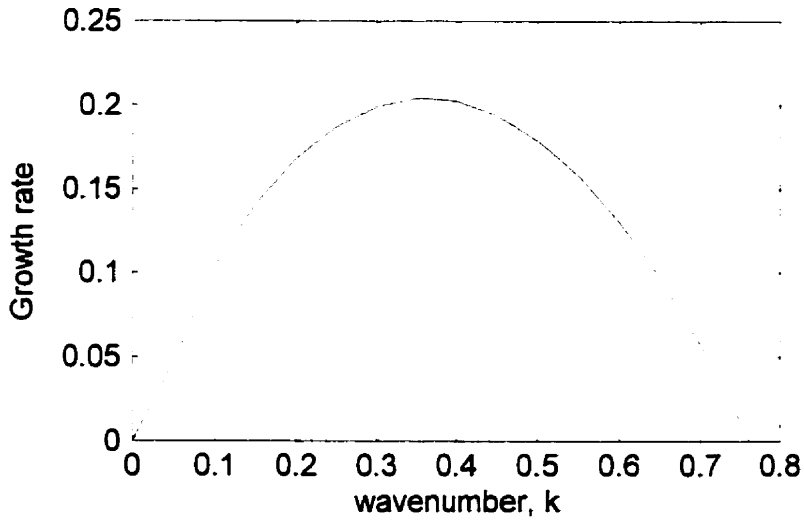

Fig. 5.16 The QSSA growth rate versus wavenumber at $t_0 = 0.05$. Non-Newtonian fluid displacing Newtonian fluid, R = 3, De = 0.7, n = 0.3.

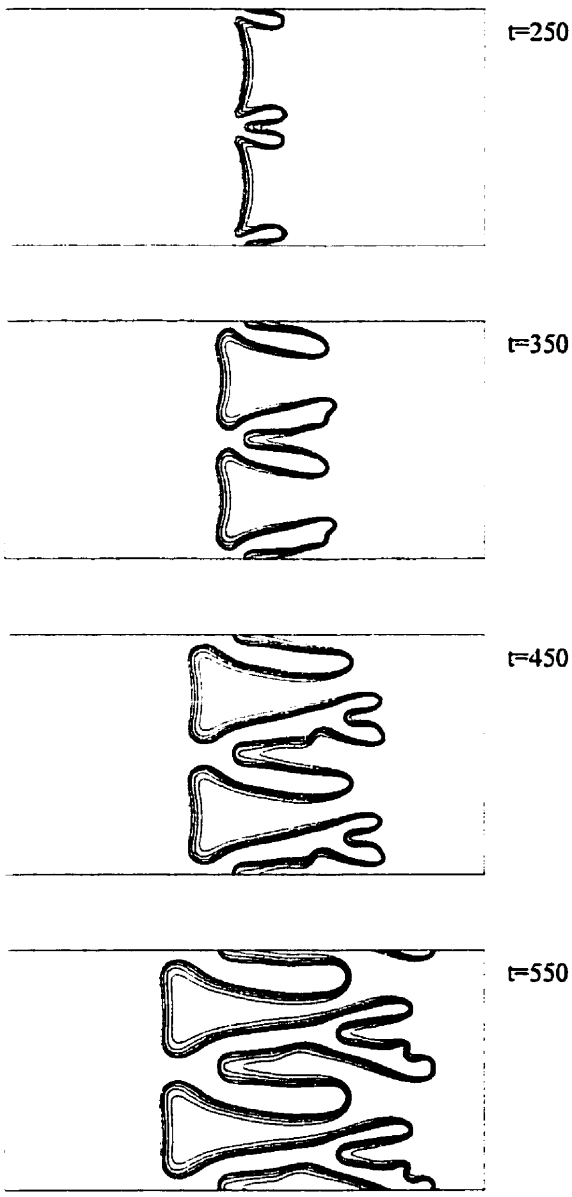

Fig. 5.17 Concentration contours (between 0.1-0.6, with increments of 0.1) of a simulation for Pe = 1200, A = 4, R = 3, De = 0.7, n = 0.3 with disturbance of a single mode, k_m = 0.36. Non-Newtonian fluid displacing Newtonian fluid, two periods are shown in y direction.

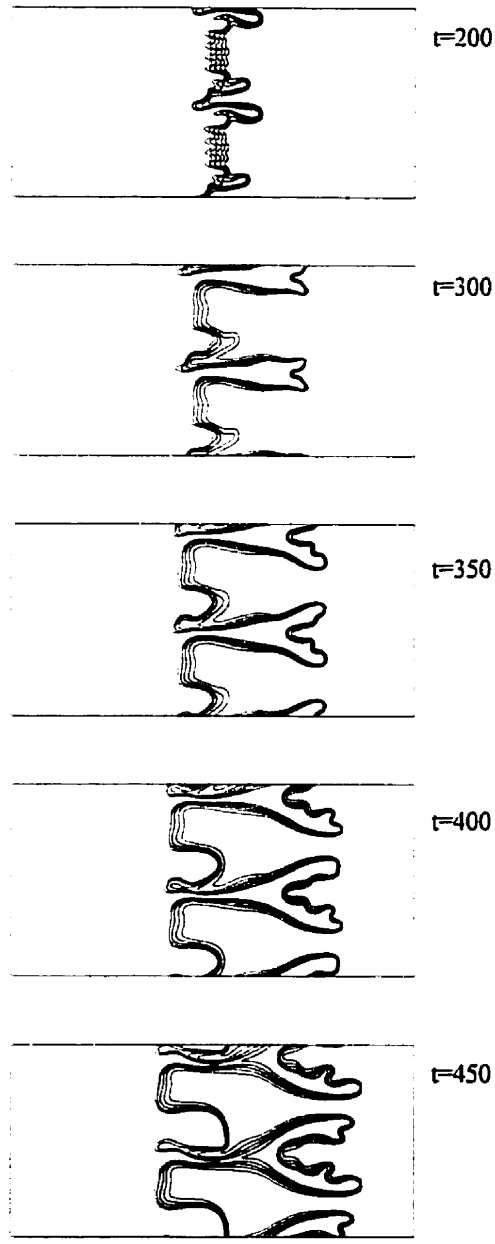

Fig. 5.18 Concentration contours (between 0.1-0.6, with increments of 0.1) of a simulation for Pe = 1200, A = 4, R = 3, De = 0.7, n = 0.3 with disturbance of a single mode, k = 0.18. Non-Newtonian fluid displacing Newtonian fluid.

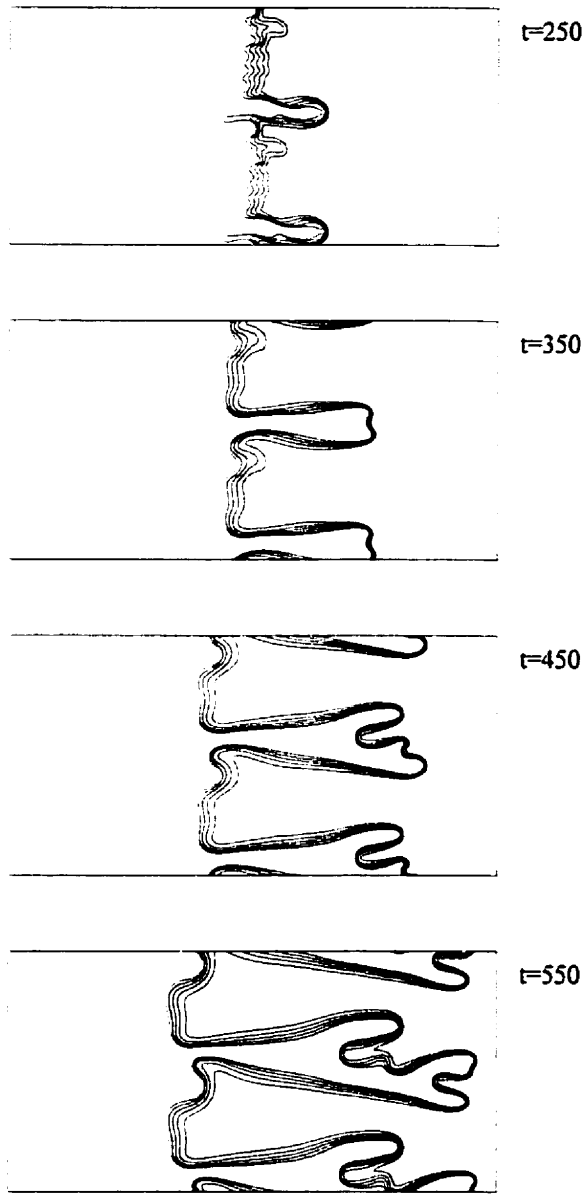

Fig. 5.19 Concentration contours (between 0.1-0.6, with increments of 0.1) of a simulation for Pe = 1200, A = 4, R = 3, De = 0.7, n = 0.4 with disturbance of a single mode, k = 0.18. Non-Newtonian fluid displacing Newtonian fluid.

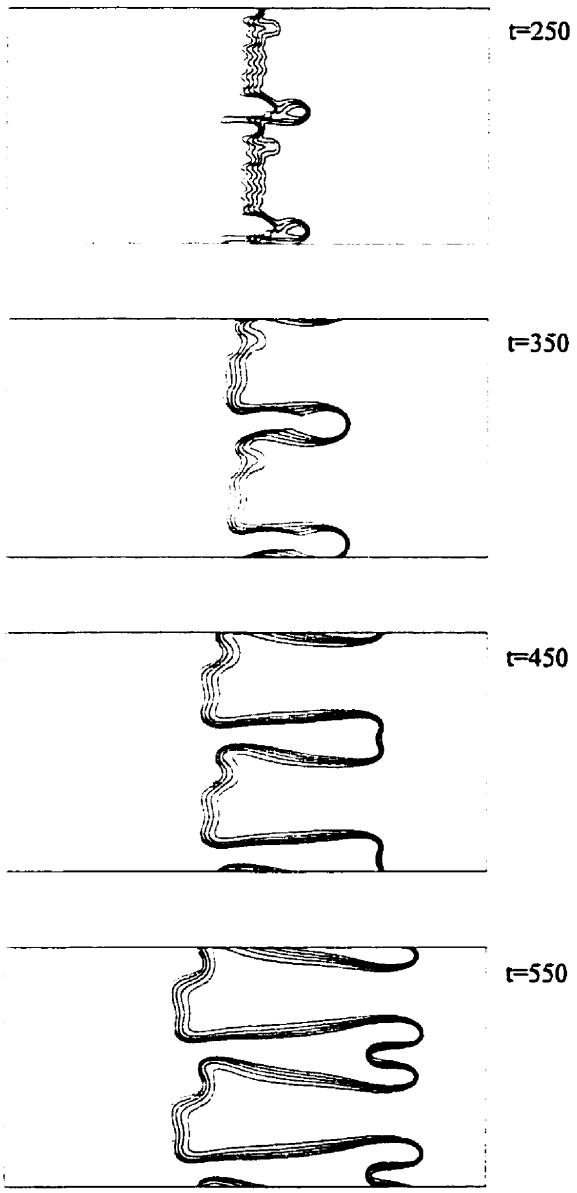

Fig. 5.20 Concentration contours of a simulation (between 0.1-0.6, with increments of 0.1) for Pe = 1200, A = 4, R = 3, De = 0.7, n = 0.6 with disturbance of a single mode, k = 0.18. Non-Newtonian fluid displacing Newtonian fluid.

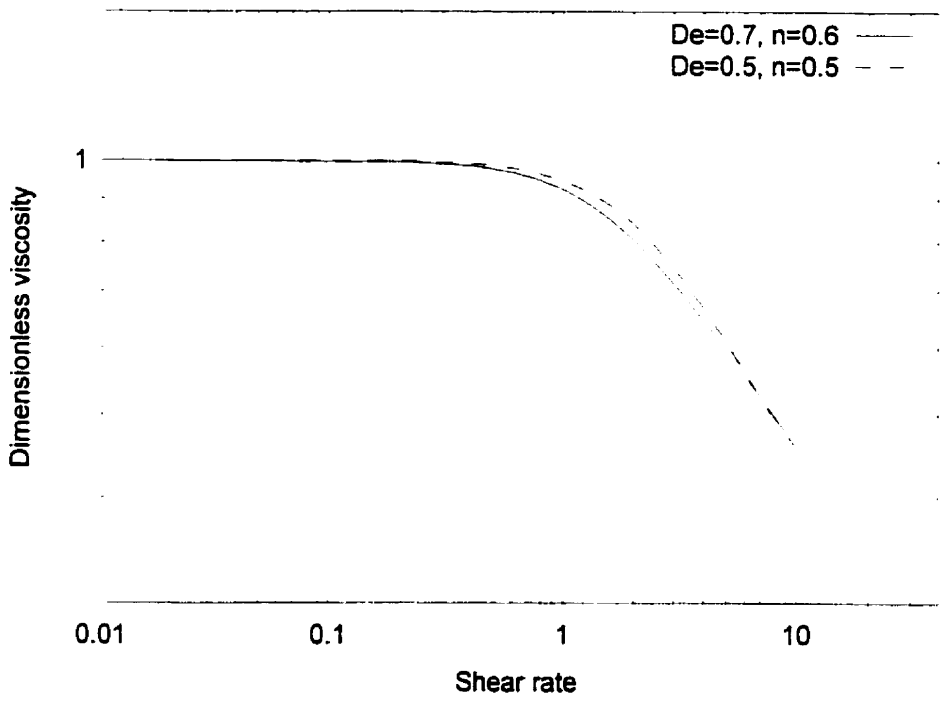

Fig. 5.21 Dimensionless viscosity (μ/μ_0) variation with dimensionless shear-rate for two simulations with parameter values of Pe = 1200, A = 4, R = 3. Non-Newtonian fluid displacing Newtonian fluid.

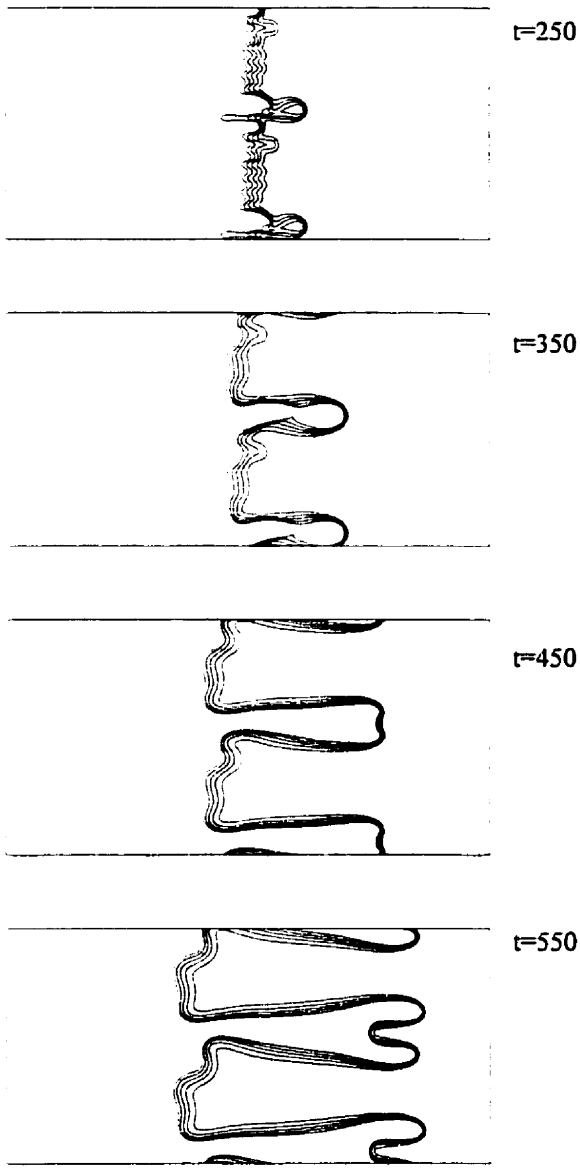

Fig. 5.22 Concentration contours (between 0.1-0.6, with increments of 0.1) of a simulation for Pe = 1200, A = 4, R = 3, De = 0.5, n = 0.5 with disturbance of a single mode, k = 0.18. Non-Newtonian fluid displacing Newtonian fluid.

5.3.4 Mixing Length

An important quantity of interest is the measure of the region where the two fluids mix. Mixing length is a measure of the severity of viscous fingering. Although there are several ways to define the mixing zone, we define it as the distance between $\bar{c} = 1 - \delta$ and $\bar{c} = \delta$ in the transversely averaged concentration profile :

$$L_\delta = x\big|_{\bar{c}=\delta} - x\big|_{\bar{c}=1-\delta} . \tag{5.34}$$

where δ is a small positive number and $\bar{c}$ is the transversely averaged concentration. The definition (5.34) depends on the values of δ. In our simulations, the value of δ was chosen as 0.01. The mixing length gives a good idea of the front advancement and broadening of the mixing zone. For a stable displacement, the mixing length is proportional to $t^{1/2}$. Mixing length for an unstable front also varies initially as $t^{1/2}$, provided the initial perturbation is small. As the nonlinear fingering develops, the mixing length becomes a complicated function of time. Some one-dimensional models [Todd et al. 1972, Koval 1963] assume that it is a linear function in time, and Perkins et al. (1965), observed a similar behavior from their experimental results.

Tan and Homsy (1988) plotted the mixing length in the case of Newtonian displacements for different cases and concluded that at high values of the Peclet number, it is independent of Pe. They also observed that if the initial disturbances are small (< 1%), the mixing length first varies as $t^{1/2}$, then shifts to a linear dependence in t. This was later supported by Zimmerman and Homsy (1991) from their simulation results. They found that the asymptotic mixing rate is approximately 1.5 for displacements with R = 3. Lately, Rogerson and Meiburg (1993), found that despite the variation in tangential shear and new fingering dynamics, the mixing rate remains the same. This asymptotic mixing rate was found to be approximately 1.5, the same as the one reported by Zimmerman and Homsy (1991).

Fig. 5.23 shows the variation of the mixing length with time as defined by Eq. (5.34), for different simulations. The plots indicate that the dependence of the mixing length on time is determined by two mechanisms: dispersion causes the mixing length to grow like $t^{1/2}$, and nonlinear fingering causes it to grow linearly in t. As a result, two zones with different mixing rates are observed as seen from Fig. 5.23. Initially (t < 150), when the dispersion dominates, the mixing rate is small and later when nonlinear fingering occurs, it increases and is approximately 1.5 as found in the previous studies [Tan and Homsy 1988, Zimmerman and Homsy 1991]. The two distinct zones are observed in both cases of a Newtonian fluid displacing a Newtonian fluid, and a non-Newtonian fluid displacing a Newtonian fluid. However, a higher mixing length and a higher mixing rate is observed in the case of a non-Newtonian fluid displacing a Newtonian fluid in comparison with the Newtonian fluid displacing another Newtonian fluid. This observation can be explained as follows : In the case of a non-Newtonian fluid displacing a Newtonian fluid, the viscosity of the shear-thinning displacing fluid decreases with time giving rise to an increase in the mobility ratio. This increase in the mobility ratio enhances the growth of the nonlinear viscous fingering resulting in a higher mixing rate. This increase in mixing rate was not observed in the simulations of Rogerson and Meiburg (1993), although their fingering patterns are similar to those of ours. Which is because of the fact that in their simulations both the fluids are Newtonian, and hence the mobility ratio remains constant during the entire simulation. The insensitivity of the asymptotic mixing rate to the Peclet number is observed again in the case of a non-Newtonian fluid displacing a Newtonian, and is found to be approximately 1.7.

5.4 Summary

In these simulations involving the displacement of a Newtonian fluid by a non-Newtonian fluid, the effect of the shear-thinning nature has lead to new interfacial dynamics, and ramified pattern formation. In addition to the mechanisms of shielding, spreading, fading, coalescence, and tip-splitting which were observed in the case of Newtonian fluid

displacing Newtonian, new mechanisms such as : side-branching, multiple side-branching, diagonal fingering, and trailing-lobe detachment are present. Also, due to the shear-thinning nature of the non-Newtonian fluid, the instability sets earlier and grows faster depending on the values of the rheological parameters of the model. The interfacial instability increases with an increase in the value of the parameter De and a decrease in the power-law index n. However, any such combination of the two rheological parameters De and n which gives rise to the same shear-thinning behavior leads to a similar fingering pattern.

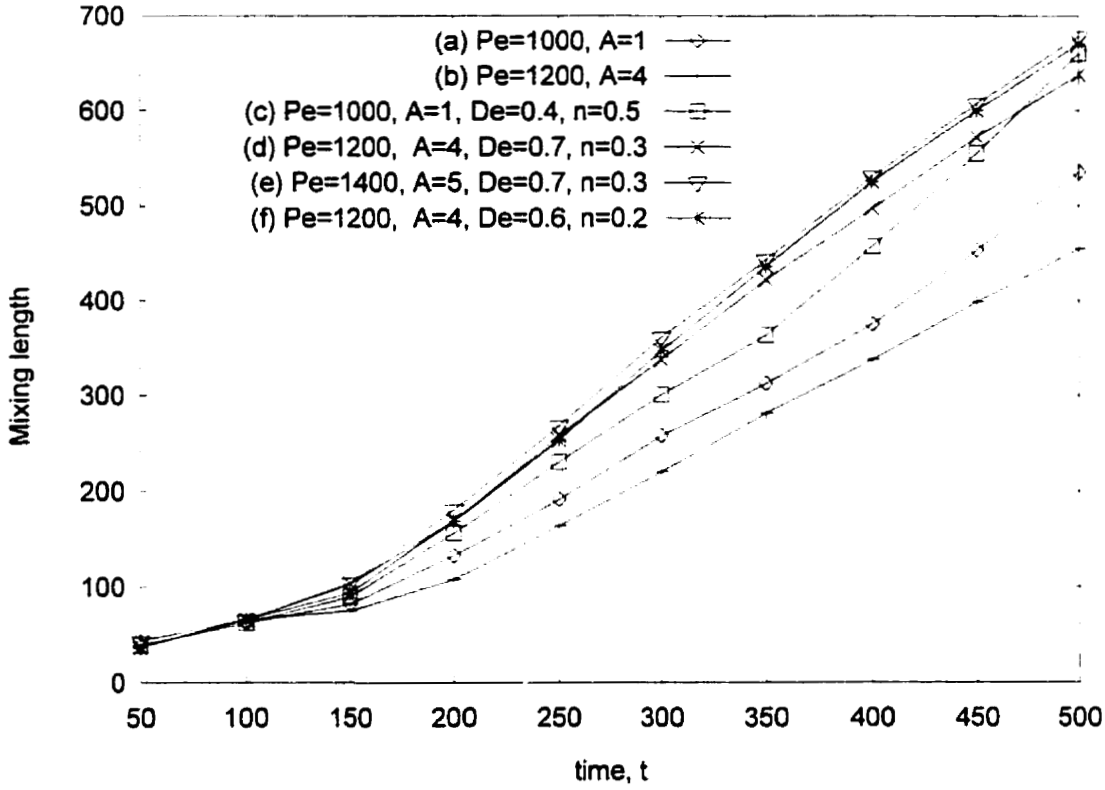

Fig. 5.23 Comparison of the mixing length of different simulations for R = 3.

(a) - (b) Newtonian fluid displacing Newtonian fluid,

(c) - (f) Non-Newtonian fluid displacing Newtonian fluid.

CHAPTER 6

CONCLUSIONS AND RECOMMENDATIONS

In this chapter, the conclusions from this study and the recommendations for future work are given. The interesting results obtained with the use of a shear-thinning fluid in the displacement processes are summarized below.

6.1 Conclusions

We have studied the miscible displacement processes involving both Newtonian and non-Newtonian fluids in a rectilinear Hele-Shaw model. Three different combinations of a Newtonian fluid displacing another Newtonian fluid, a non-Newtonian fluid displacing a Newtonian fluid, and a Newtonian fluid displacing a non-Newtonian fluid were considered. A well known Carreau model was used to study the effects of shear-thinning on the instability of these processes. This model involves two dimensionless parameters De and n. We examined both linear and nonlinear aspects of instabilities in miscible displacements.

6.1.1 Linear stability analysis

First, we have carried out a linear stability analysis of the problem to determine the growth rate of the disturbances. The quasi-steady-state-approximation (QSSA) has been used to study the linear stability of the displacement processes under consideration.

1. In the case of a Newtonian fluid displacing another Newtonian fluid, our results show a very good agreement with the linear stability results of Tan and Homsy (1986).

2. The linear stability results show that any displacement with an unfavorable mobility ratio is unstable. An increase in the growth rate of the disturbances is observed with an increase in the mobility ratio. For a given mobility ratio, the growth rate is maximum at t = 0, then it decays with time.
3. In the case of a non-Newtonian fluid displacing a Newtonian fluid, the growth rate of the disturbances increases with increase in the parameter De. The growth rate also increases with decreasing values of the power-law index, n. An increase in De and decrease in n has the effect of shifting the most dangerous mode k_m and maximum growth rate σ_m towards smaller wavelengths.
4. The parameter De has two different effects on the displacements of a non-Newtonian fluid by a Newtonian fluid. First, with small increase in the values of De, an increase in the growth rate is observed. Second, with large increase in the values of the De (order of 1), a decrease in the growth rate is observed.
5. In the case of Newtonian displacements, it is found that the most dangerous mode k_m is proportional to R and the maximum growth rate σ_m to R^2 respectively. This variation was also observed by Tan and Homsy (1986).

6.1.2 Nonlinear simulations

A numerical scheme, based on a combination of the finite-difference and spectral methods has been successfully implemented to simulate the nonlinear mechanisms of viscous fingering. This numerical technique is capable of simulating the nonlinear viscous fingering with high accuracy, for a sufficiently high mobility ratio. Simulation results can be useful to learn about the flow and the mechanisms involved in the formation of viscous-fingering patterns for different combinations of displacing and displaced fluids.

Our results show that shear-thinning has the effect of accelerating growth rates of fingering patterns in comparison to Newtonian fluids, thus leading to a rapid development

of viscous-fingering patterns. The physical implications of these results are significant in the formation of fractal viscous-fingering patterns.

For the mobility ratio (MR $\leq$ 20.9) under consideration, the displacement of a non-Newtonian fluid of shear-thinning nature by a Newtonian fluid is unstable and shows a decrease in instability with time. On the other hand, for the same mobility ratio, the displacement of a Newtonian fluid by a non-Newtonian fluid shows an increased instability with formation of new fingering patterns.

We performed simulations with different values of the parameters to investigate the effects of different geometric and rheological parameters. The finger interaction mechanisms reported by previous researchers in the case of Newtonian displacements, are also present in our simulation results. In the case of a non-Newtonian fluid displacing a Newtonian fluid, new interesting mechanisms of side-branching, multiple side-branching, diagonal fingering, and trailing-lobe detachment have been observed. Some of the features of these modified patterns are similar to those observed by Rogerson and Meiburg (1993) in Newtonian displacements with tangential shearing. We have also found that it is the nature of the shear-thinning which decides the instability development at the interface between the two fluids. Any combination of the two rheological parameters De and n which gives the same shear-thinning behavior will lead to a similar evolution of the fingers.

We also studied the mixing length and compared for different simulations. Two mixing zones with different mixing rates were observed in all the simulations. In case of a non-Newtonian fluid displacing a Newtonian fluid, we found that the shear-thinning enhances the growth of the fingers, leading to a higher asymptotic mixing rate in comparison with the Newtonian displacements. The asymptotic mixing rate is again found to be insensitive to the Peclet number, for higher values of Pe.

From this study, we conclude that if the zero shear viscosity μ_0 of the non-Newtonian displacing fluid is much smaller than the viscosity of the displaced fluid, the displacement is unstable and the dynamics of the interface are more complicated. However, in practical applications, the instability can be minimized by improving the mobility with the use of high zero shear viscosity polymers.

6.2 Recommendations

In this work, we have considered an exponential viscosity-concentration relationship. However, any other relation can be used to further investigate its influence on the dynamics of the flow. The effect of the gravity on the stability of the displacements can also be studied by considering the interface aligned at some angle.

Studying effects of the anisotropy and velocity dependence of dispersion on the nonlinear evolution of viscous fingering could be an interesting problem.

There is a scope to incorporate a quasi-Newtonian fluid model in the simulations, which includes both shear-thinning and extension thickening of the viscosity. Many polymers solutions exhibit this kind of behavior, where viscosity decreases with the shear rate and increases with the extension rate.

Our model can be extended to study the instability in a three-dimensional flow system.

Viscous fingering experiments should be performed to visualize the pattern formation in a rectilinear Hele-Shaw cell, and the results can be compared with our numerical simulations.

Effects of elasticity can be studied by including more comprehensive models that account for normal stresses.

BIBLIOGRAPHY

1. Abou-Kassem, J. H., and Farouq Ali, S. M., JCPT 34, 30 (1995).
2. Allen, E., and Boger, D. V., SPE 18097, 449 (1988).
3. Araktingi, U. G., and Orr, F. M., J. SPE 20176, presented at the SPE 7th symposium, Tulsa, Okhlahoma, April 1990.
4. Bacri, J. C., Rakotomalala, N., Salin, D., and Woumeni, R., Phys. Fluids A 4, 1611 (1992).
5. Beham, A. L., and Olson, R. W., Soc. Pet. Eng. J. 3, 138 (1963).
6. Bensoussan, A., Lions, J. L., and Papanicolaou, G., Asymptotic Analysis for Periodic Structures, North-Holland, Amsterdam (1978).
7. Bird, R. B., Armstrong, R. C., and Hassager, O., Vol. 1, Wiley, New York (1987).
8. Blackwell, R. J., Rayne, J. R., and Terry, W. M., Trans. Soc. AIME 216, 1 (1959).
9. Bonn, D., Kellay, H., Braunlich, M., Amar, M. B., and Meunier, J., Physica A 220, 60 (1995).
10. Canuto, C., Hussaini, M. Y., Quarteroni, A., and Zang, T. A., Spectral Methods in Fluid Dynamics Springer-Verlag (1987).
11. Chouke, R. L., von Meurs, P., and van der Poel, C., SPE AIME Trans. 216, 188 (1959).
12. Christie, M. A., SPE Res. Eng. 8, 297 (1989).
13. Christie, M. A., and Bond, D. J., Soc. Pet. Eng. Res. Eng. 2, 514 (1987).
14. Daccord, G., and Nittmann, J., Phys. Rev. Lett. 56, 336 (1986).
15. Dauben, D. L., and Menzie, D. E., Trans. Soc. Pet. Eng. J., 1065 (1967).
16. De Wiest, R. J. M., Flow through porous media, Academic press, New York, (1969).
17. Drazin, P. G., and Reid, W. H., Hydrodynamic stability, (1989).
18. Farmer, C. L., presented at the NATO Advanced Study Inst. July, (1985).
19. Fayers, F. J., SPE Res. Eng. Trans. AIME 285, 551 (1988).
20. Glimm, T., The Math. Res. Simulation, SIAM (1983).

21. Habermann, B., Trans. AIME 219, 264 (1960).

22. Heller, J. P., J. Appl. Phys. 37, 1566 (1966).

23. Hickernell, F. J., and Yortsos, Y. C., Stud. Appl. Math. 74, 93 (1986).

24. Hill, S., Chem. Eng. Sci. 1, 247 (1952).

25. Homsy, G. M., Annu. Rev. Fluid Mech. 19, 271 (1987).

26. Hussaini. M. Y.. and Zang, T. A., Annu. Rev. Fluid Mech. 19, 339 (1986).

27. Huzarewicz, S., Gupta, R. K., and Chhabra, R. P., J. Rheol. 35, 221 (1991).

28. Ikoku, C. U., and Ramey, H. J., Soc. Pet. Eng. J. 19, 164 (1979).

29. Jacquard, P., and Seguier, P., J. de Mecanique 1, 367 (1962).

30. Kawaguchi, M., Makino, K., and Kato, T., Physica D 105, 121 (1997).

31. Kopf-Sill, A. R., and Homsy, G. M., Phys. Fluids 31, 242 (1988).

32. Koval, E. J.. Soc. Pet. Eng. J. 3, 145 (1963).

33. Lee, K. S., and Claridge, E. L., Soc. Pet. Eng. J. 8, 52 (1968).

34. Manickam, O., and Homsy, G. M., Phys. Fluids 6, 95 (1994).

35. Manickam, O., and Homsy, G. M., Phys. Fluids A 5, 1356 (1993).

36. Marshall, R. J., and Metzner, A. B., Ind. Eng. Chem. Fund. 6, 393 (1967).

37. McDonald, A. E., SPE-AIME fifth symposium on Res. Simulation, Denver, CO (1979).

38. Muskat, M., Flow through porous media, McGraw-Hill, New York (1946).

39. Nittmann, J., Physica A 140, 124 (1986).

40. Nittmann, J., Daccord, G., and Stanley, H. E., Fractals in Physics, 193 (1986).

41. Nittmann, J., Daccord, G., and Stanley, H. E., Nature 314, 141 (1985).

42. Odeh, A. S., and Yang, H. T., Soc. Pet. Eng. J. 19, 155 (1979).

43. Park, C. W., and Homsy, G. M., Phys. Fluids 28, 1583 (1985).

44. Pascal, H., Int. J. Non-Linear Mechanics 27, 565 (1992).

45. Pascal, H., J. Colloid Interface Sci. 123, 14 (1988).

46. Pascal, H., Int. J. Eng. Sci. 21, 199 (1983).

47. Paterson, L., Phys. Rev. Lett. 52, 1621 (1984).

48. Peaceman, D. W., and Rachford, H. H., Soc. Pet. Eng. J. 2, 327 (1962).

49. Perkins, T. K., and Johnston, O. C., Soc. Pet. Eng. J., 138 (1969).

50. Perkins, T. K., and Johnston, O. C., Soc. Pet. Eng. J. 3, 70 (1963).

51. Perkins, T. K., Johnston, O. C., and Hoffman, R. N., Soc. Pet. Eng. J. 5, 301 (1965).

52. Perrine, R. L., Soc. Pet. Eng. J. 1, 17 (1961).

53. Peters, E. J., and Flock, D. L., Soc. Pet. Eng. J. 21, 249 (1981).

54. Rogerson, A., and Meiburg, E., Phys. Fluids A 5, 1344 (1993).

55. Rogerson, A., and Meiburg, E., Phys. Fluids A 5, 2644 (1993).

56. Robinson, A. L., Science 228, 834 (1985).

57. Sader, J. E., Chan, D. Y. C., and Hughes, B. D., Physical Review E 49, 420 (1994).

58. Saffman, P. G., and Taylor, G. I., Proc. R. Soc. London Ser. A 245, 312 (1958).

59. Sahimi, M., and Yortsos, Y. C., French Pet. Inst. Conf., Arles, France (1990).

60. Sarma, H. K., Powder Technology, 48, 39 (1986).

61. Savins, J. G., Ind. Eng. Chem., 61, 18 (1969).

62. Schowalter, W. R., AIChE J. 11, 99 (1965).

63. Shah, C. B., and Yortsos, Y. C., AIChE J. 41, 1099 (1995).

64. Slobod, R. L., and Caudle, B. H., Trans. AIME 195, 265 (1952).

65. Slobod, R. L., and Thomas, R. A., Soc. Pet. Eng. J. 3, 9 (1963).

66. Smith, D. E., Wu, X. Z., Libchaber, A., Moses, E., and Witten, T., Phys. Rev. A 45, 2165 (1992).

67. Sorbie, K. S., Clifford, P. J., and Jones, E. R. W., J. Colloid Interf. Sci. 130, 508 (1989).

68. Tan, C. T., and Homsy, G. M., Phys. Fluids 31, 1330 (1988).

69. Tan, C. T., and Homsy, G. M., Phys. Fluids 30, 1239 (1987).

70. Tan, C. T., and Homsy, G. M., Phys. Fluids 29, 3549 (1986).

71. Todd, M. R., and Longstaff, W. J., Soc. Pet. Eng. J. 12, 874 (1972).

72. Van Damme, H., Alsac, E., Laroche, C., and Gatineau, L., Europhys. Lett. 5, 25 (1988).

73. Van Damme, H., Laroche, C., Gatineau, L., and Levitz, P., J. Phys. Paris 48, 1121 (1987).

74. van Meurs, Trans. AIME 210, 295 (1957).

75. Vongvuthipornchai, S., and Raghavan, R., SPE Formation Evaluation, 573 (1987a).

76. Wilson, S. D. R., J. Fluid Mech. 220, 413 (1990).

77. Wooding, R. A., J. Fluid Mech. 39, 477 (1969).

78. Wooding, R. A., ZAMP 13, 255 (1962).

79. Wu, Y. S. and Pruess, K., Advances in Water Resources 21, 351 (1997).

80. Wu, Y. S., Pruess, K., and Witherspoon, P. A., SPE Res. Eng. 0, 369 (1992).

81. Wu, Y. S., Pruess, K., and Witherspoon, P. A., Transport in porous media 6, 115 (1991).

82. Yortsos, Y. C., and Zeybek, M., Phys. Fluids 31, 3511 (1988).

83. Zimmerman, W. B., and Homsy, G. M., Phys. Fluids A 4, 2348 (1992).

84. Zimmerman, W. B., and Homsy, G. M., Phys. Fluids A 4, 1901 (1992).

85. Zimmerman, W. B., and Homsy, G. M., Phys. Fluids A 3, 1859 (1991).

APPENDIX A

DERIVATION OF THE LINEAR STABILITY ANALYSIS EQUATIONS

A.1 Non-Newtonian fluid displacing Newtonian fluid

When the displacing fluid is replaced by a non-Newtonian fluid of shear-thinning behavior (see Fig. 3.2), the new viscosity-concentration relation as developed in chapter 3 is :

$$\mu = e^{R(1-c)}\left(1 + D_e{}^2 V^2\right)^{c(n-1)/2}, \tag{A.1}$$

where De is a parameter as defined in Eq. (3.41), and R is given by Eq. (3.47). The governing equations (4.17) - (4.21) remain the same form as in the case of a Newtonian displacement, and therefore, the first differential equation (4.36) is unchanged. Taking the log of equation (A.1) and introducing small perturbations from the base state, we get :

$$\ln(\bar{\mu} + \mu') = R(1 - \bar{c} - c') + \frac{n-1}{2}(\bar{c} + c')\ln\left[1 + D_e{}^2(\bar{V}^2 + V^{2'})\right], \tag{A.2}$$

where $\bar{V}^2 = 1$, and the first order term $V^{2'} = 2u'$. (A.3)

After linearizing and simplifying equation (A.3), we obtain :

$$\frac{\mu'}{\bar{\mu}} = -Rc' + \left(\frac{n-1}{2}\right)\left(\frac{2D_e{}^2}{1 + D_e{}^2}\right)\bar{c}u' + \left(\frac{n-1}{2}\right)c'\ln(1 + D_e{}^2). \tag{A.4}$$

From equation (A.1), at the base state we have :

$$\bar{\mu} = e^{R(1-\bar{c})}\left(1 + D_e{}^2\right)^{\bar{c}(n-1)/2}, \tag{A.5}$$

which leads to :

$$\frac{1}{\bar{\mu}}\frac{d\bar{\mu}}{d\bar{c}} = -R + \frac{n-1}{2}\ln(1+D_e^{\,2}). \tag{A.6}$$

Differentiating equation (A.4) twice with respect to y and z respectively, we get :

$$\frac{1}{\bar{\mu}}\frac{\partial^2\mu'}{\partial y^2} = A\frac{\partial^2 c'}{\partial y^2} + B\bar{c}\frac{\partial^2 u'}{\partial y^2}, \tag{A.7}$$

and $$\frac{1}{\bar{\mu}}\frac{\partial^2\mu'}{\partial z^2} = A\frac{\partial^2 c'}{\partial z^2} + B\bar{c}\frac{\partial^2 u'}{\partial z^2}, \tag{A.8}$$

where, $$A = \left[-R + \frac{n-1}{2}\ln(1+D_e^{\,2})\right], \tag{A.9}$$

and $$B = \left(\frac{n-1}{2}\right)\left(\frac{2D_e^{\,2}}{1+D_e^{\,2}}\right). \tag{A.10}$$

Substituting equations (A.7) and (A.8) into equation (4.29), and expanding the velocity perturbation into Fourier modes leads to :

$$\frac{\partial^2\phi}{\partial x^2} + A\frac{\partial\bar{c}}{\partial x}(x,t)\frac{\partial\phi}{\partial x} - k^2\phi(1+B.\bar{c}) = Ak^2\psi\,. \tag{A.11}$$

Applying QSSA, and substituting equation (4.35) for the coefficients into the above equation, we get :

$$\left(\frac{d^2}{dx^2} + A\frac{d\bar{c}}{dx}(x,t_0)\frac{d}{dx} - k^2(1+B\bar{c})\right)\phi = Ak^2\psi\,, \tag{A.12}$$

which is a modified second order differential equation. Eq. (A.12) along with (4.36) will be used to study the linear stability analysis of system where a non-Newtonian fluid is displacing Newtonian fluid. For n = 1 or De = 0, the Eq. (A.12) reduces to Eq. (4.38) for the case of a Newtonian fluid displacing another Newtonian fluid.

A.2 Newtonian fluid displacing non-Newtonian fluid

Again in this case the first linearized differential equation (4.36), derived from the convection-diffusion equation remains the same. The viscosity-concentration relationship for this case, as determined in chapter 3 is :

$$\mu = e^{R(1-c)}\left(1 + D_e{}^2 V^2\right)^{(1-c)(n-1)/2}, \tag{A.13}$$

where the parameter R is as defined by equation (3.64). The above equation at base state becomes :

$$\bar{\mu} = e^{R(1-\bar{c})}\left(1 + D_e{}^2\right)^{(1-\bar{c})(n-1)/2}. \tag{A.14}$$

When the above equation is differentiated with respect to $\bar{c}$, we get :

$$\frac{1}{\bar{\mu}}\frac{d\bar{\mu}}{d\bar{c}} = -R - \frac{n-1}{2}\ln(1 + D_e{}^2). \tag{A.15}$$

Taking the log of equation (A.13) and introducing small perturbations from base state gives :

$$\ln(\bar{\mu} + \mu') = R(1-\bar{c}-c') + \frac{n-1}{2}(1-\bar{c}-c')\ln\left[1 + D_e{}^2(\bar{V}^2 + V^{2'})\right]. \tag{A.16}$$

Linearizing and simplifying in a manner similar to the previous case of a non-Newtonian fluid displacing Newtonian fluid, we obtain :

$$\frac{\mu'}{\bar{\mu}} = -Rc' + \left(\frac{n-1}{2}\right)\left(\frac{2D_e{}^2}{1 + D_e{}^2}\right)(1-\bar{c})u' - \left(\frac{n-1}{2}\right)c'\ln(1 + D_e{}^2). \tag{A.17}$$

By differentiating equation (A.17) twice with respect to y and z respectively, we get :

$$\frac{1}{\bar{\mu}}\frac{\partial^2\mu'}{\partial y^2} = C\frac{\partial^2 c'}{\partial y^2} + B(1-\bar{c})\frac{\partial^2 u'}{\partial y^2}, \tag{A.18}$$

and

$$\frac{1}{\bar{\mu}}\frac{\partial^2\mu'}{\partial z^2} = C\frac{\partial^2 c'}{\partial z^2} + B(1-\bar{c})\frac{\partial^2 u'}{\partial z^2}, \tag{A.19}$$

where B is as defined earlier by equation (A.10), and C is given as :

$$C = -\left[R + \frac{n-1}{2}\ln(1+D_e^{\,2})\right]. \tag{A.20}$$

After substituting above equations (A.18) and (A.19) into equation (4.29), and expanding the velocity perturbations into Fourier components, we get :

$$\frac{\partial^2\phi}{\partial x^2} + C\frac{\partial \bar{c}}{\partial x}(x,t)\frac{\partial \phi}{\partial x} - k^2\phi\left(1 + B(1-\bar{c})\right) = Ck^2\psi\,. \tag{A.21}$$

Applying QSSA at time t_0, and substituting for coefficients from equation (4.35), we obtain :

$$\left(\frac{d^2}{dx^2} + C\frac{d\bar{c}}{dx}(x,t_0)\frac{d}{dx} - k^2\left(1 + B(1-\bar{c})\right)\right)\phi = Ck^2\psi\,. \tag{A.22}$$

The above equation is the second linearized differential equation for the case of a Newtonian fluid displacing a non-Newtonian fluid. It is easy to check that for n = 1 or De = 0, the above Eq. (A.22) reduces to Eq. (4.38) for the case of a Newtonian fluid displacing another Newtonian fluid.

APPENDIX B

COMPUTER PROGRAMS

B.1 Fast Hartley Transform (FHT)

```
/******** Fast Hartley transform in one dimension ********************/

void fht1d(int isn, int p, double *f)
{
        int *alloc_1d_int(int n1);
        void free_1d_int(int *i);
        double *alloc_1d_double(int n1);
        void free_1d_double(double *d);

        int p0, n, n1, n2, n3, n4, n5, n6, n7, i, istep, j, jstep;
        int Nless1, Nover4, Pless1, Pover2, RootN, *powr2, *strut;
        int maxp, nmodes, ntrig, nstruct;
        double HalfSec, tmp1, tmp2, tmp3, tmp4;
        double *sins, *tans;
// parameters
        maxp=10, nmodes = (int)pow(2,maxp), ntrig = nmodes/4;
        nstruct = (int)pow(2,(maxp-maxp/2));
// memory allocation
        sins = alloc_1d_double(ntrig+1);
        tans = alloc_1d_double(ntrig+1);
        powr2 = alloc_1d_int(maxp+1);
```

```
        strut = alloc_1d_int(nstruct+1);
// If p==1 calculate DHT and return
        if(p==1){
                tmp1=f[0] + f[1];
                f[1]=f[0] - f[1];
                f[0]=tmp1;
                n=2;
        }
        else {
                if(p!=1) {
                        Nover4=(int)pow(2,p-2);
                        n=4*Nover4;
                        Nless1=n-1;
                        Pless1=p-1;
                        powr2[0]=1;
                        for(i=0; i<=p-1; i++)
                                powr2[i+1]=powr2[i]+powr2[i];
                        sins[Nover4]=1.0;
                        if(p==3)
                                sins[1]=sin(PI/4.0);
                        else if(p>3){
                                for(i=1; i<=3; i++)
                                        sins[i*Nover4/4]=sin(i*PI/8);
                                HalfSec=1.0/(2.0*cos(PI/16));
                                n1=p-5;
                                for(i=n1; i>=0; i--){
                                        tmp1=0.0;
                                        for(j=powr2[i];j<=Nover4-powr2[i];
j+=powr2[i+1]){
```

```
                    n2=j+powr2[i];
                    sins[j]=HalfSec*(sins[n2]+tmp1);
                    tmp1=sins[n2];
                }
                HalfSec=1.0/sqrt(2.+1./HalfSec);
            }
        }
        for(j=1; j<=Nover4-1; j++)
            tans[j]=(1.-sins[Nover4-j])/sins[j];
        tans[Nover4]=1.0;
        Pover2=p/2;
        RootN=powr2[Pover2];
        Pover2=p-Pover2;
        if(p==4) {
            strut[1]=2;
            strut[2]=1;
            strut[3]=3;
        }
        else if(p==5 || p==6) {
            strut[1]=4;
            strut[2]=2;
            strut[3]=6;
            strut[4]=1;
            strut[5]=5;
            strut[6]=3;
            strut[7]=7;
        }
        else {
            strut[0]=0;
```

```
                strut[1]=1;
                for(i=2; i<=Pover2; i++){
                        for(j=0; j<=powr2[i-1]-1; j++){
                                strut[j]=strut[j]+strut[j];
                                strut[j+powr2[i-1]]=strut[j]+1;
                        }
                }
        }
}

if(p==2) {
        tmp1=f[1];
        f[1]=f[2];
        f[2]=tmp1;
}
else if(p==3){
        tmp1=f[1];
        f[1]=f[4];
        f[4]=tmp1;
        tmp1=f[3];
        f[3]=f[6];
        f[6]=tmp1;
}
else {
        for(i=1; i<=RootN-1; i++){
                n1=RootN*strut[i];
                n2=i;
                n3=n1;
                tmp1=f[n2];
```

```
                f[n2]=f[n3];
                f[n3]=tmp1;
                for(j=1; j<=strut[i]-1; j++){
                        n2=n2+RootN;
                        n3=n1+strut[j];
                        tmp1=f[n2];
                        f[n2]=f[n3];
                        f[n3]=tmp1;
                }
        }
}

for(i=0; i<=n-2; i+=2){
        tmp1=f[i]+f[i+1];
        tmp2=f[i]-f[i+1];
        f[i]=tmp1;
        f[i+1]=tmp2;
}
for(i=0; i<=n-4; i+=4){
        tmp1=f[i]+f[i+2];
        tmp2=f[i+1]+f[i+3];
        tmp3=f[i]-f[i+2];
        tmp4=f[i+1]-f[i+3];
        f[i]=tmp1;
        f[i+1]=tmp2;
        f[i+2]=tmp3;
        f[i+3]=tmp4;
}
n1=Pless1;
```

```
n2=4;
for(n7=2; n7<=Pless1; n7++){
        istep=n2+n2;
        n1=n1-1;
        jstep=powr2[n1-1];
        for(i=0; i<=Nless1; i+=istep){
                n3=i;
                n4=n3+n2;
                n5=n4-1;
                tmp1=f[n3]+f[n4];
                tmp2=f[n3]-f[n4];
                f[n3]=tmp1;
                f[n4]=tmp2;
                for(j=jstep; j<=Nover4; j+=jstep){
                        n3=n3+1;
                        n4=n3+n2;
                        n6=n5+n2;
                        tmp3=f[n4]+f[n6]*tans[j];
                        tmp1=f[n6]-tmp3*sins[j];
                        tmp2=tmp1*tans[j]+tmp3;
                        tmp4=f[n3]+tmp2;
                        tmp3=f[n3]-tmp2;
                        tmp2=f[n5]-tmp1;
                        tmp1=f[n5]+tmp1;
                        f[n3]=tmp4;
                        f[n4]=tmp3;
                        f[n5]=tmp2;
                        f[n6]=tmp1;
                        n5=n5-1;
```

```
                        }
                        n6=n5+n2;
                }
                n2=istep;
        }
    }
    if(isn==-1){
        for(i=0; i<=n-1; i++)
            f[i]=f[i]/n;
    }

    p0=p;

    free_1d_double(sins);
    free_1d_double(tans);
  free_1d_int(powr2);
    free_1d_int(strut);
}

/************* Two-dimensional Hartley transform ********************/

void fht(double **a, int nnx, int nny, int ndir)
{
    void fht1d(int isn, int p, double *f);
    void vec(double **a, double *b, int nnx, int nny, int n, int m);
    void mat(double *b, double **a, int nnx, int nny, int n, int m);
    double *alloc_1d_double(int n1);
    void free_1d_double(double *d);
    double *a1, exs;
```

```
int i,j,nx,ny;
nx = (int)pow(2,nnx);
ny = (int)pow(2,nny);
a1 = alloc_1d_double(nx);

for(i=0; i<nx; i++){
        vec(a, a1, nnx, nny, i, 1);
        fht1d(1, nny, a1);
        mat(a1, a, nnx, nny, i, 1);
}

for(j=0; j<ny; j++){
        vec(a, a1, nnx, nny, j, 2);
        fht1d(1, nnx, a1);
        mat(a1, a, nnx, nny, j, 2);
}

for(i=1; i<nx/2; i++){
        for(j=1; j<ny/2; j++){
                exs = 0.5*(a[i][j] - a[nx-i][j] - a[i][ny-j] + a[nx-i][ny-j]);
                a[i][j] = a[i][j]-exs;
                a[nx-i][j] = a[nx-i][j]+exs;
                a[i][ny-j] = a[i][ny-j]+exs;
                a[nx-i][ny-j] = a[nx-i][ny-j]-exs;
        }
}

if(ndir==-1){
        for(i=0; i<nx; i++)
```

```
                for(j=0; j<ny; j++)
                        a[i][j] = (1.0/(nx*ny))*a[i][j];
        }
        free_1d_double(a1);
}

// program puts the ith (m=1) column or jth (m=2) row of a in vector b
void vec(double **a, double *b, int nnx, int nny, int n, int m)
{
        int i,j,nx,ny;
        nx = (int)pow(2,nnx);
        ny = (int)pow(2,nny);

        if(m==1){
                for(j=0; j<ny; j++)
                        b[j] = a[n][j];
        }
        else {
                for(i=0; i<nx; i++)
                        b[i] = a[i][n];
        }
}

// program puts back in array a the vector b as ith (m=1) column or jth(m=2) row
void mat(double *b, double **a, int nnx, int nny, int n, int m)
{
        int i,j,nx,ny;
        nx = (int)pow(2,nnx);
        ny = (int)pow(2,nny);
```

```
        if(m==1){
                for(j=0; j<ny; j++)
                        a[n][j] = b[j];
        }
        else {
                for(i=0; i<nx; i++)
                        a[i][n] = b[i];
        }
}

/*****************************************************************/
```